Assessing the Severity and Prognosis in PAH Using Magnetic Resonance Imaging and NT-proBNP

By:

Dr Faisal Abdulwahab Alandejani

A thesis submitted in partial fulfilment of the requirements for the degree of Doctor of Philosophy

Co-supervised by:

Dr Andy J Swift

Prof David G Kiely

The University of Sheffield

Faculty of Medicine

Department of Infection, Immunity and Cardiovascular Sciences

Academic Unit of Radiology

Submission Date: November 2022

Abstract

Pulmonary arterial hypertension (PAH) is a progressive, life-threatening condition characterised by pulmonary vascular resistance and associated with severe outcomes. According to the European Society of Cardiology and European Respiratory Society (ESC/ERS) guidelines, the risk assessment and prognosis of PAH are reliant on multiple investigations, including cardiac magnetic resonance imaging (MRI) and N-terminal prohormone brain natriuretic peptide (NT-proBNP). The overall aim of this body of work was to investigate the clinical benefit of cardiac MRI including artificial intelligence (AI) approaches, and NT-proBNP to assess the right atrium (RA) and right ventricle (RV) for severity assessment and prognosis in PAH. A cardiac MRI-based automated AI analysis of the RA and RV was developed, and the AI failure rate of the model was tested. Repeatability and agreement of contours of automated cardiac MRI analysis of the RA were evaluated. The prognostic significance of AI RV and AI RA area and their utility to risk stratify patients with PAH have been identified and compared with one another. The importance and relationship between automated cardiac MRI and NT-proBNP in PAH have been highlighted. The work has shown that cardiac MRI RV and RA area measurements can be fully automated using AI with a very low failure rate. The variability of AI-derived RA area measurements was lower than manual measurements in a scan-rescan cohort. Manual and automated RA area measurements moderately correlate with invasive haemodynamics. NT-proBNP showed a moderate correlation when compared to automated RV function. Measures of RV function and RA area have prognostic value; nonetheless, only measures of RV function but not ESC/ERS RA area thresholds identify patients at low-risk of 1-year mortality. Finally, the need for further work exploring larger cohorts with NT-proBNP and cardiac MRI measurements to investigate the incremental value of different approaches when assessing the right ventricle has been recommended.

Acknowledgements

First and foremost, I would like to thank Allah almighty for all his blessings and guidance throughout my life. I would also like to thank my joint supervisors, Dr Andy Swift and Prof David Kiely, for their guidance, encouragement and support. I would like to extend my appreciation to Andy, who has provided tremendous advice and necessary insight for the success of this project. His enthusiasm and passion have made my research experience positive even though pursuing a PhD during a pandemic was challenging, and I am grateful for everything he has done.

Additional appreciation is extended to David for his enthusiastic input into the clinical context of this research and to Robin Condliffe, a consultant in the Sheffield Pulmonary Vascular Disease Unit, for his clinical insights and guidance.

Finally, I would like to express my sincere gratitude to my parents, my wife, my two sisters and two brothers for all their help and support throughout my academic life, especially in the past five years.

Table of contents

List of Tables

List of Figures

List of Abbreviations

Abbreviation	Definition
6MWD	6-minute walking distance
ACVRL1	Activin receptor-like type 1
AI	Artificial intelligence
ASPIRE	Assessing the Spectrum of Pulmonary hypertension Identified at a REferral centre
AUC	Area under the curve
AVG	Average
BMPR2	Bone morphogenetic protein receptor 2
BNP	Brain natriuretic peptide
BSA	Body surface area
bSSFP	Balanced steady-state free precession
CAV1	Caveolin 1
CCB	Calcium channel blocker
CHD	Congenital heart disease
CI	Cardiac index
CNN	Convolutional neural network
CO	Cardiac output
COMPERA	Comparative, Prospective Registry of Newly Initiated Therapies for PH
CTD	Connective tissue disease
CTEPH	Chronic thromboembolic pulmonary hypertension
DSC	DICE similarity coefficient
EC	Endothelial cell
ECG	Electrocardiogram
ECHO	Electrocardiogram
ED	End-diastolic
EDV	End diastolic volume
EF	Ejection fraction
ENG	Endoglin
ERA	Endothelin receptor antagonist
ERS	European Respiratory Society
ES	End-systolic
ESC	European Society of Cardiology
ESV	End systolic volume
ET	Endothelin
FPHN	French Pulmonary Hypertension Network
GTP	Guanosine triphosphatases
HIV	Human immunodeficiency virus
HPAH	Heritable pulmonary arterial hypertension
HR	Heart rate
ICC	Intraclass correlation coefficient
IPAH	Idiopathic pulmonary arterial hypertension
KCNK3	Potassium two-pore-domain channel subfamily K member 3
LA	Left atrial
LOESS	Locally weighted scatterplot smoothing regression analysis

Abbreviation	Definition
LUMC	Leiden University Medical Centre
LV	Left ventricular
LVEDV	Left ventricular end-diastolic volume
LVSV	Left ventricular stroke volume
Max	Maximal
Min	Minimal
mPAP	Mean pulmonary arterial pressure
mRAP	Mean right atrial pressure
MRI	Magnetic resonance imaging
MvO_2	Mixed venous oxygen saturation
NHS	National Health Service
NO	Nitric oxide
NT-proBNP	N-terminal prohormone brain natriuretic peptide
NYHA	New York Heart Association
PA	Pulmonary artery
PACS	Picture archive and communication systems
PAH	Pulmonary arterial hypertension
PAWP	Pulmonary arterial wedge pressure
PDE5	Phosphodiesterase type 5
PGI2	Prostacyclin
PH	Pulmonary hypertension
PVDU	Pulmonary Vascular Disease Unit
PVR	Pulmonary vascular resistance
QC	Quality control
RA	Right atrium/right atrial
RAC	Relative area change
RAEF	Right atrial ejection fraction
RAP	Right atrial pressure
RCA	Reverse classification accuracy
REVEAL	The North American Registry to Evaluate Early and Long-term PAH Disease Management
RHC	Right heart catheterization
ROC	Receiver operating characteristic
RV	Right ventricle/right ventricular
RVEDV	Right ventricular end diastolic volume
RVEF	Right ventricular ejection fraction
RVESV	Right ventricular end systolic volume
RVF	Right ventricular failure
RVM	Right ventricular mass
RVSV	Right ventricular stroke volume
SD	Standard deviation
SMAD9	Sterile Alpha Motif Domain-Containing Protein 9
SMC	Smooth muscle cells
SV	Stroke volume
SvO_2	Mixed venous oxygen saturation
TAPSE	Tricuspid Annular Plane Systolic Excursion
TE	Echo time

Abbreviation	Definition
TR	Repetition time
UK	United Kingdom
US	United States
VE/VCO_2	Ventilatory equivalents for carbon dioxide
VMI	Ventricular Mass Index
VO_2	Oxygen consumption
WHO FC	World Health Organization functional class
WS	Wall stress
WSPH	World Symposium on Pulmonary Hypertension

Synopsis

This body of work looks into the clinical benefit of cardiac magnetic resonance imaging (MRI) including automated approaches, and N-terminal prohormone brain natriuretic peptide (NT-proBNP) to evaluate the right atrium (RA) and right ventricle (RV) for severity assessment and prognosis in patients with pulmonary arterial hypertension (PAH). This section is written to guide the reader through the contents of each chapter. **Chapter 1** provides a background to PAH including cardiac MRI measurements and NT-proBNP. **Chapter 2** states the research questions, aims, objectives and hypotheses of this thesis.

The main methods and materials used throughout the thesis are described in **Chapter 3**. To allow for the main chapters to be read in isolation, the related methods are repeated in the specific methods section of each of the main chapters. The following six main chapters contain data from cohorts of patients with PAH, and several of the main chapters are largely based on papers that have been published (Alandejani et al., 2022a, Alandejani et al., 2022b). Each of the six main chapters includes a separate introduction, methods, results, discussion and conclusion section.

Chapter 4 - The European Society of Cardiology and European Respiratory Society (ESC/ERS) guidelines provide right atrial thresholds and indicate that the RA area thresholds can be applied to cardiac MRI to assess patients with PAH. Due to limited data to support this recommendation, chapter 4 validates the ESC/ERS guideline thresholds of the RA area and identifies optimal approaches, and assesses the relative prognostic significance of RA and RV cardiac MRI parameters.

Chapter 5 - The advent of deep learning may allow more reliable measurement of RA area to improve clinical assessments in PAH. This chapter describes the development of a quantitative

cardiac MRI-based automated artificial intelligence (AI) analysis of the RA and RV in PAH, and determines the AI failure rate of the model in a large clinical registry of patients with PAH.

Chapter 6 - Automation of RA area measurements may result in lower variability; however, the repeatability of automated cardiac MRI RA area metrics in the setting of PAH remains uncertain. This study assesses interstudy repeatability and agreement of contours of a quantitative cardiac MRI-based automated AI analysis of the RA, and evaluates the repeatability of NT-proBNP and 6-minute walk distance in a prospective cohort of patients with PAH.

Chapter 7 - RA area predicts mortality in patients with pulmonary hypertension and is recommended by the ESC/ERS pulmonary hypertension guidelines. Chapter 7 compares the association of manual RA area and AI RA area with invasive haemodynamics, and evaluates the prognostic value of RA area measurements.

Chapter 8 - ESC/ERS guidelines recommend regular risk stratification with the aim of treating patients with PAH to improve or maintain low-risk status (<5% 1-year mortality). This study investigates the relationship between AI RV and AI RA area measurements and their ability to risk stratify patients with PAH, using the reference standard for assessment of cardiac structure and function, by comparing published thresholds for RV metrics (Lewis et al., 2020) with ESC/ERS thresholds for RA area (Galiè et al., 2015, Galiè et al., 2016, Humbert et al., 2022a).

Chapter 9 - NT-proBNP is a non-invasive clinical biomarker and is used to risk assess and manage patients with PAH (Galiè et al., 2016). However, using both cardiac MRI measurements and NT-proBNP together as a bivariate prognostic marker in PAH has not yet been determined. This chapter evaluates the prognostic role of automated cardiac MRI and NT-proBNP simultaneously, and studies their relationship in PAH. **Chapter 10** is the main discussion, limitations and further work.

Chapter 1: Introduction

1.1 Pulmonary Hypertension

The heart and lungs are two of the most important organs in the human body, and the complexity of the interactions between the cardiovascular and pulmonary systems is growing in recognition. The involvement of the cardiovascular system is particularly significant because it is linked to a deteriorated health status and an increased risk of mortality (Han et al., 2007).

Pulmonary hypertension (PH) is a severe condition that affects the arteries of the lungs and is caused by the thickening and narrowing of the small pulmonary arteries. This condition increases the pressure of the pulmonary arteries, which may lead to right ventricular failure (RVF). Clinically, the patient appears with a different range of signs and symptoms; the commonest amongst them is shortness of breath (Kiely et al., 2013). PH affects 1% of the global population and 10% of those over the age of 65 (Hoeper et al., 2016).

To diagnose PH with no underlying heart or lung diseases, right heart catheterization (RHC) is performed. The normal pulmonary artery pressure is between 8 and 20 mm Hg at rest. A diagnosis is made when the mean pulmonary arterial pressure (mPAP) is 25 mm Hg during the rest state (Galiè et al., 2015, Galiè et al., 2016). RHC can also measure cardiac output (CO), pulmonary arterial wedge pressure (PAWP) and pulmonary vascular resistance (PVR). Thus, in order to calculate any of these measurements, the following formula can be used:

$$PVR = \frac{mPAP - PCWP}{CO}$$

Even though there have been significant improvements in the understanding of the disease mechanism and its management, PH is still a life-threatening condition.

In the past, PH had a simple classification of only two groups. The first group was essential after excluding all possible differential diagnosis of PH, and it was called primary pulmonary hypertension. The second group was any risk factors or causes of PH, hence the name secondary pulmonary hypertension (Rich et al., 1987).

More recently, from the pathological features, haemodynamic findings, clinical picture and therapy approach, PH is clinically classified into five main groups. Each group has different prognosis and therapy management (Hurdman et al., 2012).

The main five groups for PH are pulmonary arterial hypertension (PAH), PH due to hypoxia and/or lung diseases, PH due to left heart disease, chronic thromboembolic pulmonary hypertension (CTEPH) and lastly PH due to multifactorial and/or unclear mechanisms (Table 1.1) (Simonneau et al., 2013).

Table 1. 1 Summary of PH classification

Main PH groups
1. Pulmonary arterial hypertension
2. PH due to left heart disease
3. PH due to hypoxia and/or lung diseases
4. Chronic thromboembolic pulmonary hypertension (CTEPH)
5. PH due to multifactorial and/or unclear mechanisms

1.2 Pulmonary Arterial Hypertension

PAH is an uncommon haemodynamic status that has a devastating and poor outcome (Kiely et al., 2013). After eliminating other causes of PH, if a patient has a high mPAP of 25 mmHg or

higher, a PAWP of 15 mmHg or lower and a PVR higher than 3 Woods units, he/she will be diagnosed with PAH (Hoeper et al., 2013). The new recommendation from the sixth world symposium of PH identified >20mmHg as a potential diagnostic threshold (Simonneau et al., 2019).

Idiopathic pulmonary arterial hypertension (IPAH) is due to an unknown cause and is one of the forms of PAH. Other clinical types of PAH are hereditary, drug and toxin-induced or accompanied with other conditions such as congenital heart disease (CHD), human immunodeficiency virus (HIV) infection, portal hypertension, schistosomiasis and connective tissue disease (CTD). Notably, all PAH types are categorised by similar clinical picture, pathological and haemodynamic features (Simonneau et al., 2013).

A retrospective study of 84 PAH patients performed by Kawut et al. (2005) documented race as a risk factor for death including Asian or African-American. The first and third-year survival for this study was 87 percent and 61 percent, respectively (Kawut et al., 2005).

Furthermore, according to a study in 2010, newly diagnosed PAH patients not receiving treatment have more than 40 percent chance of death within 3 years due to an increase in PVR which leads to severe right ventricle (RV) dysfunction (Humbert et al., 2010a).

1.2.1 Idiopathic PAH

Idiopathic PAH is a rapidly progressive condition. Towards the end of the last century, two studies showed a median survival of 1.9 (Fuster et al., 1984) and 2.8 (Dalonzo et al., 1991) years from the diagnosis of IPAH to death and the majority of the deaths were caused by RVF. PAH has several predictors of mortality such as gender, cause of PAH and biochemical, haemodynamic and functional factors (Simonneau et al., 2013, Wensel et al., 2002). Examples for biochemical markers of mortality predictors in patients with PAH are brain natriuretic

peptide (BNP) and N-terminal prohormone brain natriuretic peptide (NT-proBNP) (Fijalkowska et al., 2006).

By the beginning of the 21st century, newer medications such as epoprostenol and bosentan improved the prognosis of IPAH significantly (McLaughlin et al., 2002, Sitbon et al., 2002, McLaughlin et al., 2005). However, some patients fail to respond to this type of therapy, which causes deterioration of the RV function and may lead to death due to RVF. One approach to assist patients who do not respond to this type of treatment is by directly measuring the function and structure of the RV to provide better prognostic data (van Wolferen et al., 2007).

Cardiac MRI can precisely evaluate direct RV measurements such as myocardial mass, and systolic and diastolic volumes (Boxt et al., 1992, Katz et al., 1993). The high reproducibility advantage of cardiac MRI makes it a valuable imaging tool for tracking RV changes with treatment response (Grothues et al., 2004).

1.2.2 PAH Associated with CTD

PAH in association with CTD (PAH-CTD) is the second most common cause of PAH, following idiopathic PAH. Approximately 90% of PAH-CTD cases are related to systemic sclerosis (74%), mixed connective tissue disease (8%) or systemic lupus erythematosus (8%) (Zanatta et al., 2019). PAH is the primary cause of death in systemic sclerosis and has a worse prognosis than idiopathic PAH (Launay et al., 2013). Two studies, one from the United States (Chung et al., 2010) and the other one form the United Kingdom (Condliffe et al., 2009), have explored the clinical characteristics and outcomes of patients with PAH-CTD and found that the estimated 1- and 3-year survival rates of patients with systemic sclerosis-associated PAH were around 80% and 50%, respectively. Patients with PAH-CTD, and particularly those with systemic sclerosis-associated PAH, continue to have a poor prognosis despite the improvement

of functional metrics and survival rate due to current treatment (Ramjug et al., 2017, Kuwana et al., 2020). This demonstrates the importance of investing time and resources to develop improved methods for measuring severity and prognosis in patients with PAH.

1.2.3 PAH Associated with CHD

PAH is a common complication of CHD, especially in patients with systemic-to-pulmonary (left-to-right) shunts. The most advanced form of PAH-CHD is Eisenmenger syndrome (D'Alto and Mahadevan, 2012). Eisenmenger syndrome refers to any untreated congenital heart anomaly with intra-cardiac communication that results in reversal of flow and PAH (Wood, 1958, Beghetti and Galiè, 2009). The progression of PAH in patients with CHD is correlated with increased mortality and severe morbidity (Lowe et al., 2011). In recent decades, significant advancements in the diagnosis and management of CHD have led to a substantial rise in the number of patients with CHD who survive into adulthood (Diller and Gatzoulis, 2007). This expanding group of adult patients with PAH-CHD challenges physicians with many issues related to managing cardiac and non-cardiac comorbidities. In addition, while recent and encouraging data are developing, mortality remains relatively high (Pascall and Tulloh, 2018). Therefore, new prognostic indicators are required to evaluate severity, prognosis and therapy response in patients with PAH.

1.2.4 Molecular Basis of PAH

There are several molecular mechanisms that are involved in PAH pathology: these include endothelial cell (EC) dysfunction, smooth muscle cells (SMC) and fibroblast activation and the interaction between cells in the vasculature (Morrell et al., 2009). As a result, these mechanisms play an important role in the pulmonary circulation of patients with PAH and lead to vascular remodelling. These vascular abnormalities are summarised in Figure 1.1 and include

muscularization of peripheral arteries, medial hypertrophy of muscular arteries, neointima formation and endothelial channel formation (Rabinovitch, 2012).

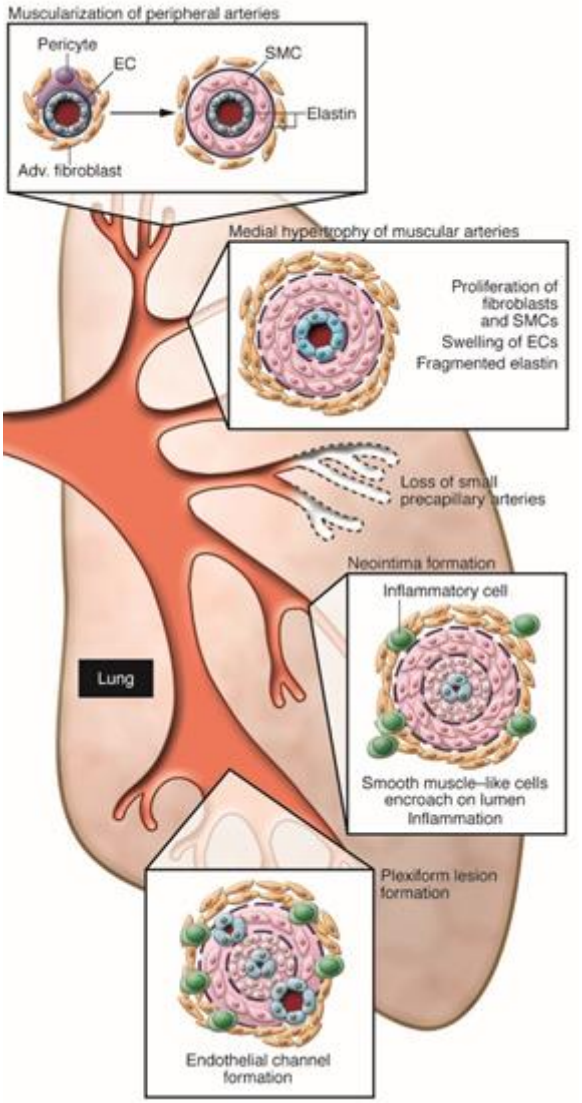

Figure 1. 1 Vascular abnormalities in patients with PAH

Reproduced with permission (Rabinovitch, 2012).

ECs are significantly involved in the regulation of vascular function; on a molecular level, Rho guanosine triphosphatases (GTPases) play a major role in their dysfunction, affecting EC permeability, proliferation, migration and apoptosis. Rho GTPases also directly affect the signalling pathways which are involved in the thrombolytic role of ECs: this explains thrombus formation in small pulmonary arteries that can cause PAH. Other molecular markers of EC dysfunction in PAH include the reduction of nitric oxide (NO) and prostacyclin (PGI_2) production together with increased levels of vasoconstrictors. NO is a vasodilator and its decreased levels in patients may correlate with lower expression of endothelial NO synthase or its inhibition. Again, Rho GTPases are thought to be involved in these processes. However, this is not the only mechanism causing vasoconstriction: voltage-gated K^+ channels are also involved. In PAH patients, these channels can often be defective, causing an increase in Ca^{2+} levels in cells and therefore inducing vasoconstriction (Yuan et al., 1998).

PGI_2 is a growth inhibitor which indirectly inhibits the proliferation of SMCs; however, PAH patients tend to have lower PGI_2 which can contribute to SMCs proliferation. Another molecular mechanism for the proliferation of SMCs may be the upregulation of transient receptor potential channels whose genes are expressed on SMCs. The interaction between pulmonary ECs and SMCs is another important factor in the proliferation of SMCs. This is believed to be the result of EC dysfunction which may, in turn, induce SMCs proliferation and therefore contribute to the vascular remodelling typical of PAH patients (Morrell et al., 2009).

Moreover, PAH, especially hereditary pulmonary arterial hypertension (HPAH), can be caused by genetic mutations: bone morphogenetic protein receptor 2 (*BMPR2*) is one of the major gene mutations responsible for more than 70 percent of genetic or heritable PAH (Deng et al., 2000). Other less common mutated genes have also been found to cause HPAH such as endoglin (*ENG*), Sterile Alpha Motif Domain-Containing Protein 9 (*SMAD9*), activin receptor-

like type 1 (*ACVRL1*), potassium two-pore-domain channel subfamily K member 3 (*KCNK3*) and caveolin 1 (*CAV1*) (Soubrier et al., 2013).

1.3 Therapy in PAH

The development of PAH is often very complex at the molecular level, with different pathways affected. This is reflected in the type and mode of action of drugs that are available for treatment. Currently, the three main classes of drugs include endothelin receptor antagonists, prostanoids and phosphodiesterase type 5 (PDE5) inhibitors (Humbert and Ghofrani, 2016).

1.3.1 Endothelin Receptor Antagonists

There are two types of endothelin receptors, endothelin receptor A and B which are expressed on SMCs in the vasculature. In PAH patients, SMCs proliferation and vasoconstriction are both increased, especially due to endothelin 1 (ET-1). Although with slightly different modes of action, bosentan, macitentan and ambrisentan all work to block ET receptors, therefore preventing the downstream effects of ET-1 (Galiè et al., 2015, Galiè et al., 2016).

1.3.2 Prostanoids

Patients with PAH are found to have reduced levels of the vasodilator prostacyclin (PGI_2). Prostanoid drugs work as substitutes of prostacyclin, therefore inducing vasodilation. These include epoprostenol, iloprost, beraprost, treprostinil and selexipag (Galiè et al., 2015, Galiè et al., 2016).

1.3.3 Phosphodiesterase-5 Inhibitors

Phosphodiesterase type 5 (PDE5) is found to be upregulated in patients with PAH; this results in vasoconstriction due to PDE5-mediated degradation of cGMP (Wharton et al., 2005, Corbin

et al., 2005). cGMP is essential in the signalling pathway for vasodilation; therefore, by blocking PDE5, cGMP will not be hydrolysed. These drugs include sildenafil and tadalafil (Humbert and Ghofrani, 2016). Therefore, it is crucial for physicians to carefully diagnose patients with pulmonary hypertension to ensure that the patient receives the best treatment available. This minimises the risk of misdiagnosis and insensitivity to treatment.

1.4 Treatment Approaches in PAH

In 2003, the 3rd World Symposium on Pulmonary Hypertension (WSPH) presented a therapy plan for PAH that includes drugs targeting the endothelin, prostaglandin, and nitric oxide pathways (Galiè et al., 2004). In the meanwhile, no drugs targeting other pathways have been approved. The development observed in the medical therapy of patients with PAH over the past 20 years is linked to the evolution and testing of new drugs and strategies for combination therapy, as well as the escalation of treatments based on systematic evaluation of clinical response (Galiè et al., 2015, Galiè et al., 2016). A revised treatment algorithm has been proposed by the sixth WSPH (Figure 1.2).

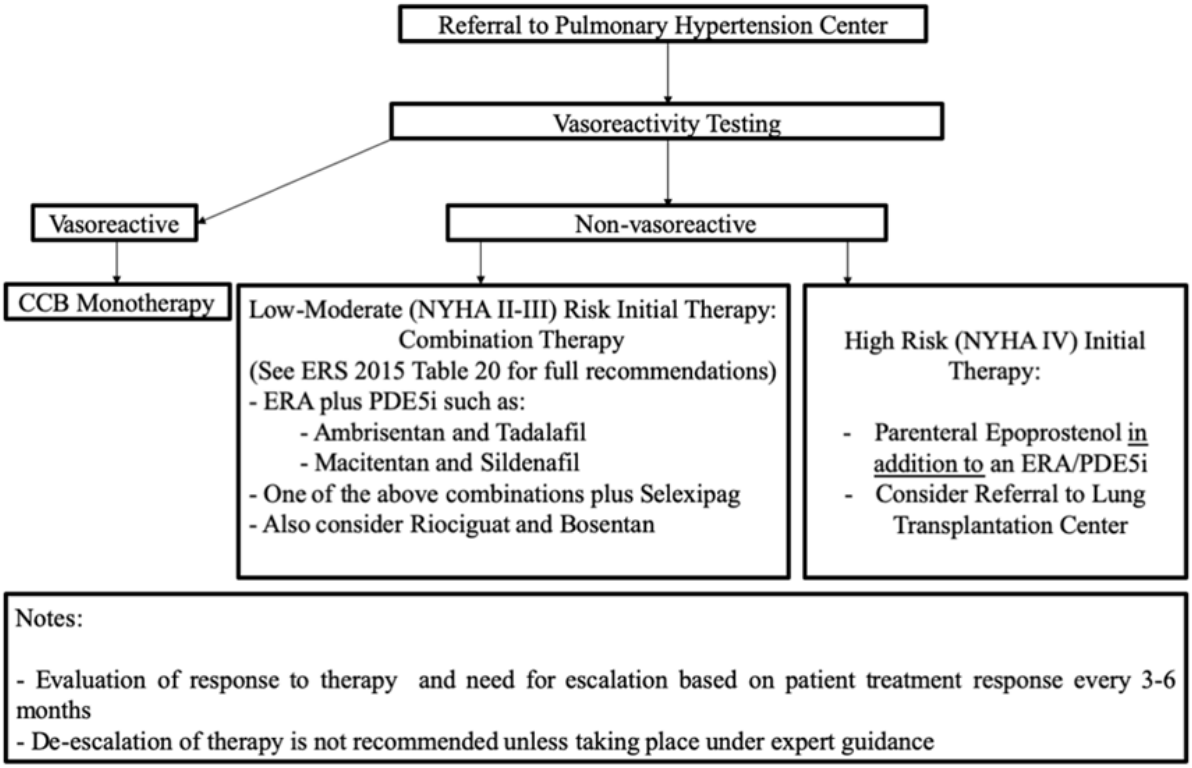

Figure 1. 2 Proposed algorithm for treatment of PAH based on 6th World Symposium on PAH

PAH = pulmonary arterial hypertension: CCB = calcium channel blocker; ERA = endothelin receptor antagonist; NYHA = New York Heart Association; PDE5i = phosphodiesterase inhibitor. Reproduced with permission (Condon et al., 2019).

Only in patients with IPAH, HPAH, and PAH associated with drug and toxin use should acute vasoreactivity testing be undertaken to predict responsiveness to calcium channel blockers (CCBs). Initial oral combination therapy with an endothelin receptor antagonist (ERA) and a phosphodiesterase type 5 inhibitor (PDE5i) should be administered to non-responders to acute vasoreactivity tests who are at low or intermediate risk whereas at high risk, initial combination therapy including intravenous prostacyclin analogues are recommended (Hassoun et al., 2015, Sitbon et al., 2016). On the basis of evidence, dual-combination therapy is advised including macitentan and sildenafil (Pulido et al., 2013), riociguat and bosentan (Ghofrani et al., 2013), and selexipag and ERA and/or PDE5i (Sitbon et al., 2015).

Transitioning from one PAH-specific treatment to another might be considered by physicians for a variety of reasons, including compliance with treatment or convenience and improvement of the side-effect profile. In addition, transitions are recommended for patients who are not meeting their treatment goals in order to escalate therapy and improve their situation (Galiè et al., 2019).

1.5 Cardiac Biomarkers: BNP and NT-proBNP

BNP is a biological molecule secreted from cardiac cells, in particular the ventricles, influenced by the change of blood pressure in the heart such conditions are PAH and heart failure (Bay et al., 2003). There are two forms of this hormone; the first, NT-proBNP which is an inactive prohormone and the second is an active hormone called BNP. The concentration of NT-proBNP circulating in the plasma is higher than the active BNP hormone, and is distinguished by a longer half-life (Alibay et al., 2004). When the RV significantly expands, NT-proBNP levels increase due to an increase in the RV wall stress.

The relationship between RV dysfunction and plasma BNP lies under their association with disease severity in patients with PAH. Worsening RV function has been shown to increase plasma BNP levels (Nagaya et al., 1998, Leuchte et al., 2004). Nagaya et al. (2000) conducted a prospective study and enrolled 53 follow-up patients with idiopathic PAH to evaluate the prognostic impact of BNP. Results showed high plasma BNP levels at baseline and continued to increase throughout the follow-up period (3 months), and indicated that high BNP levels is a strong independent prognostic biomarker of mortality in patients with idiopathic PAH.

Another prospective study was performed by Fijalkowska et al. (2006) to assess the prognostic significance of NT-proBNP in patients with PH. Results indicated that NT-proBNP has a prognostic value of poor outcome in both PH and idiopathic PAH. This shows consistency with

Nagaya et al. (1998) study which showed that RV dysfunction could be predicted by BNP in patients with long-lasting PH. The advantages of cardiac biomarkers are reproducible and easy to evaluate.

According to the European Society of Cardiology and European Respiratory Society (ESC/ERS) guidelines, NT-proBNP is currently used as part of the risk assessment tool for PAH (Galiè et al., 2015, Galiè et al., 2016). However, more data and research are needed for this non-invasive method to assist in evaluating and following up patients with PAH.

1.6 RV Pathophysiology

In a healthy individual, the RV is roughly triangular in shape and trabecular in structure, which differs from the typically compacted myocardium of the LV. The tricuspid valve connects an inlet part to the right atrium and an outlet part that communicates to the pulmonary valve (Galea et al., 2013).

A study by Kawut et al. (2012) in a population of individuals without clinical heart diseases showed that RV pathology results in a high risk of heart failure or may lead to death. This indicates that RV morphological changes are considered as one of the important characteristics of heart failure alongside other diseases of the lungs or the LV. There are some factors that affect the RV morphology such as the race, age and gender of the patient (Ventetuolo et al., 2011, Kawut et al., 2011, Chahal et al., 2010).

Studies have indicated that RV volumes and function are good predictors of mortality in PAH (van Wolferen et al., 2007, Baggen et al., 2016, Swift et al., 2017). Echocardiography, computed tomography (CT) and cardiac MRI are non-invasive methods to evaluate RV volumes. In contrast, RHC is an invasive method used to insert a catheter guided through the

jugular, radial or femoral vein to finally reach the heart and pulmonary arteries to measure, for example, right ventricular ejection fraction (dos Santos et al., 2002).

End systolic volume (ESV) and end diastolic volume (EDV) are two types of blood volumes in both the right and left ventricles that estimate basic ventricular function. ESV means the ventricles are entirely contracted, and the blood volume in the ventricles is at its lowest. While EDV is completely the opposite, it means the ventricles are fully relaxed and contain maximal blood volume at that period (Bellofiore and Chesler, 2013).

Stroke volume (SV) is subtracting EDV from ESV as shown in the following formula:

$$SV = EDV - ESV$$

Additionally, SV is the amount of blood volume pumped from the ventricle each time the heart contracts.

From SV definition, the CO is the amount of blood volume ejected out of the heart per minute. The sum of heartbeats in one minute is the heart rate (HR). This means SV and HR are directly proportional to CO. The formula for this is as the following:

$$CO = SV \times HR$$

Ejection fraction (EF) is an additional vital measurement for evaluating the RV function. EF is SV divided by EDV, whereas SV as mentioned above, is EDV minus ESV. Shown in the following formula:

$$EF = \frac{EDV - ESV}{EDV} = \frac{SV}{EDV}$$

In the last 20 years, it has been found that RV ejection fraction (RVEF) and RV volumes in PAH patients are related to risk of death (Kawut et al., 2005, van Wolferen et al., 2007).

A study was performed by (Campo et al., 2011) to investigate the outcome of 90 patients with PAH admitted between 2000 and 2009 at Johns Hopkins Hospital and its affiliate Johns Hopkins Bayview Medical Centre. More than half of these hospitalisations were due to right heart failure which represents the major cause of admission with 56 percent in this study. Among the patients with right heart failure, 14 percent died before hospital discharge. The 1-year mortality after discharge for all PAH inpatients was 35 percent. This shows that one of the main roots of morbidity and mortality in PAH is RV failure.

Despite the general appearance of the right and left ventricles showing similarities, there are some differences. The LV is covered and enfolded by the RV chamber. The RV chamber is typically a crescent-shaped chamber on the short axis, whereas the LV is circular on the short axis. The challenge of evaluating surface areas and volumes of both ventricles arises from the compound shape of the chambers. Hence 2D images are insufficient to explain the anatomy. Therefore full volumetric coverage is recommended for RV volume analysis (Bellofiore and Chesler, 2013).

High compliance and low hydraulic impedance are characteristics of the pulmonary vascular bed. As a result, the pressure produced by the RV is lower than the LV, which, according to Laplace's law, corresponds to an RV free wall thickness of 3–5 mm (Taverne et al., 2021, Basford, 2002). The Law of Laplace is shown in the formula below.

$$P = \frac{2 \times WS \times T}{r}$$

Whereas P stands for pressure, WS for wall stress, r for radius and T for wall thickness.

High pulmonary pressures can negatively affect the heart by decreasing RV function to an extent beyond myocardium adaptation. This, consequently, increases RV dilatation and

diastolic pressure. This simply explains the mechanism of the main cause of death in PAH, right heart failure (Dalonzo et al., 1991).

From Frank-Starling Law (Kobirumaki-Shimozawa et al., 2014), myocyte stretching and contractility of the heart play a major role in cardiac hemodynamics. The idea behind the Frank-Starling mechanism is when the volume of the ventricle increases for any reason, it will stretch the myocyte. As a result, this will increase SV and ultimately increase contractility; therefore, CO increases (Holubarsch et al., 1996). As previously stated about CO, it is directly proportional to stroke volume.

One of the reasons for an increase in ventricle filling (preload) would be upright physical exercise. The action of the lower extremity muscles will force and increase venous return. This will increase EDV and consequently improve SV. All this shows the functional significance of the Frank-Starling mechanism and the adaptive intrinsic myocardium features (Weil et al., 1998). In addition, some hormones such as angiotensin I and II can also regulate CO along with neural mechanisms (Holubarsch et al., 1993, Eschenhagen, 1993).

1.7 Imaging Assessment of the Right Ventricle in PH

1.7.1 Echocardiography

The initial imaging tool to assess the RV is transthoracic echocardiography (ECHO). ECHO allows the estimation of RV systolic pressure by measuring the tricuspid regurgitant jet velocity in addition to an estimation of right atrial pressure. Transthoracic ECHO is the current routine non-invasive imaging screening tool for the detection of PH (Galiè et al., 2015, Galiè et al., 2016).

However, due to the RV anterior position in the rib cage, irregular shape and thin wall the trans-thoracic echocardiography is less capable than MRI to fully evaluate RV size and function (Buechel and Mertens, 2012, Puchalski et al., 2007). Evaluation of RV strain can be made using echocardiography in PH; typically, a speckle tracking approach is used (Li et al., 2016, Meris et al., 2010).

1.7.2 Cardiac Magnetic Resonance Imaging

Cardiac MRI is a non-invasive tool that uses radio frequency pulses and strong magnetic fields to electronically view the heart and its surrounding organs and blood vessels on an unsophisticated screen.

Balanced steady-state free precession (bSSFP) has replaced gradient echo cardiac imaging. bSSFP is a gradient echo imaging adaptation that balances gradient pulses to eliminate gradient moment at each repetition time (TR), improving signal and blood to myocardial contrast resolution. Therefore, the image contrast is the signal intensity of the square root of T2/ T1, not T2 or T1 weighted. Thus, a very bright signal is achieved when T1 and T2 are similar, such as fat and liquid, and a very low signal is achieved with tissues having long T1 and short T2, namely muscle, offering excellent blood to myocardial contrast. In addition, steady-state sequences are useful for cardiac imaging due to their short repetition times and imaging times. However, off-resonance and field inhomogeneity artefacts make bSSFP imaging difficult. Images have dark stripes whenever the local off-resonance frequency is multiples of 1/TR. In order to shift the black stripes outside of the field of view, the repetition times should be as short as possible (Bieri and Scheffler, 2013).

Cardiac gating imaging uses an electric trigger sent to the magnetic resonance scanner to indicate the heart rate of the patient. Typically, the R component of the QRS complex on the

electrocardiogram (ECG) is utilized as the trigger. The R wave from the ECG trace triggers a predefined voltage threshold once each cardiac cycle. Ventricular contraction is initiated by the electrical impulse of the QRS complex. End-diastole can be represented by the R wave due to the delay between electrical and mechanical systole. Over multiple cardiac cycles, cine cardiac imaging can capture data for each of the 20 cardiac cycle phases. This method is referred to as segmented k-space acquisition (Nacif et al., 2012).

Cardiac MRI is the non-invasive gold standard imaging tool for volume and functional assessment of the RV. Cardiac MRI offers high-quality non-invasive volume measurements of the RV when compared to echocardiography. Geometric assumptions are not required when measuring the RV with MRI, which improves the accuracy (Bellofiore and Chesler, 2013). Cardiac MRI does not include ionizing radiation and the inter- and intraobserver reproducibility is high (Mooij et al., 2008).

Some limitations of cardiac MRI include accessibility, patient acceptance and expense (Kawut et al., 2012). Distinguishing the RV from the right atrium in the short axis plane is a challenge in some cases (Bonnemains et al., 2012). This is due to the complex nature of the tricuspid valve and that it is situated in a more apical location than the mitral valve. The right atrioventricular valve consists of 3 leaflets (anterior, posterior and septal leaflet), annulus, chordae tendinae and papillary muscles (Rodes-Cabau et al., 2016).

Cardiac MRI offers a complete assessment of RV function quantification and anatomical delineation (Galea et al., 2013). It has a number of different unique advantages that outstand other non-invasive tools. Cardiac MRI utilises non-toxic agents for contrast, and produces three-dimensional and high-resolution images. Pitfalls, on the other hand, include the necessity for expertise, time-consuming analysis and unsuitability with infusion pumps or pacemakers (Benza et al., 2008). Table 1.2 summarises the advantages and disadvantages of cardiac MRI.

Table 1. 2 Advantages and disadvantages of cardiac MRI

Advantages	Disadvantages
Accurate	Expensive
Predict PAH	Limited availability
Non-invasive tool	Time-consuming
High-resolution, three-dimensional images	Significant technical support and expertise
Uses non-toxic contrast agents	Incompatible with pacemakers
No ionising radiation	Incompatible with infusion pumps
No geometrical assumptions	Difficulty with breath holding

However, from the importance of RV in PAH, the advantages of cardiac MRI may conceal the downsides for the purpose of enhancing patient monitoring and improving therapy administration (Peacock and Vonk Noordegraaf, 2013).

1.7.2.1 Prognosis

Cardiac MRI delivers information on a variety of characteristics related to prognosis and risk evaluation. One of the important prognostic cardiac MRI measurements is RVEF. RVEF at baseline is a more reliable predictor of mortality than PVR (van de Veerdonk et al., 2011). Right ventricular end diastolic volume (RVEDV) and Left ventricular end diastolic volume (LVEDV) are independent predictors of prognosis in IPAH, with decreased values being associated with an increased risk of mortality (Mauritz et al., 2012). Right ventricular stroke volume (RVSV) is another measurement of right ventricular function and a predictive metric. A low RVSV is substantially linked with mortality at both baseline and follow-up (Campo et al., 2010). Cardiac MRI RVSV measurement correlates well with 6-min walk distance (6MWT) distances in patients with PAH (van Wolferen et al., 2011).

In addition, cardiac MRI can evaluate secondary cardiac abnormalities associated with PH, such as right ventricular dilation (Goerne et al., 2018). Right ventricular hypertrophy results from increased and prolonged afterload in PH, which leads to an increase in right ventricular mass (RVM). In patients with IPAH, a RVM index greater than 59 g/m^2 is associated with an increased risk of mortality (van Wolferen et al., 2007). Furthermore, cardiac output in phase contrast cardiac MRI has been demonstrated to be an independent predictor of prognosis, with slow flow in the main pulmonary artery being associated with a poor prognosis and mortality (Swift et al., 2014b). It has been established that pulmonary artery area change and relative area change are good predictors of adverse outcome in PH (Swift et al., 2012a).

1.7.2.2 Follow-up

Cardiac MRI is an ideal modality for assessing treatment response since it is highly repeatable, non-ionizing, and non-invasive (Kiely et al., 2019). Recent research suggests that cardiac MRI may be more valuable than RHC due to its capacity to offer a full evaluation of both the right ventricle and the pulmonary artery; as a result, an accurate assessment of disease progression is provided (Abolmaali et al., 2007, García-Alvarez et al., 2011). In bosentan (Chin et al., 2008) and sildenafil (Michelakis et al., 2003) trials, the ability of cardiac MRI to reliably measure right ventricular size, mass, and function has been used in endpoints. Moreover, the large prospective EURO-MRI study demonstrated that changes in MRI-derived RVEF and cardiac index correlated with changes in mortality and World Health Organization functional class; and that cardiac MRI variables obtained at baseline and follow-up provide reliable information regarding patient response to vasodilator therapy (Peacock et al., 2014).

1.8 Cardiac MRI and PAH

Previously, it has been shown that RV volumes and RVEF could predict the outcome of patients with PAH while applying cardiac MRI (Swift et al., 2014a, van de Veerdonk et al., 2011).

A study of 233 PH patients was done by (Swift et al., 2012b) to assess the diagnostic accuracy of different cardiac MRI measurements. Ventricular mass index (VMI) had the strongest correlation with RHC mPAP and the highest diagnostic accuracy when compared to echocardiography. Therefore, the study suggested applying VMI and other measurements such as right heart functional parameters and late gadolinium enhancement, as an alternative routine evaluating and diagnostic measurements for PH.

Another cardiac MRI study by (Swift et al., 2017) recruited and followed up 576 patients with PAH for a duration of 3 and a half years to evaluate the prognostic value of numerous cardiac MRI measurements in predicting mortality. Almost 40 percent died during this study, and it showed that cardiac MRI measurements such as right ventricular end systolic volume index (RVESVi) and pulmonary artery relative area change could play an independent significant role in the clinical value of PAH mortality (Figure 1.3).

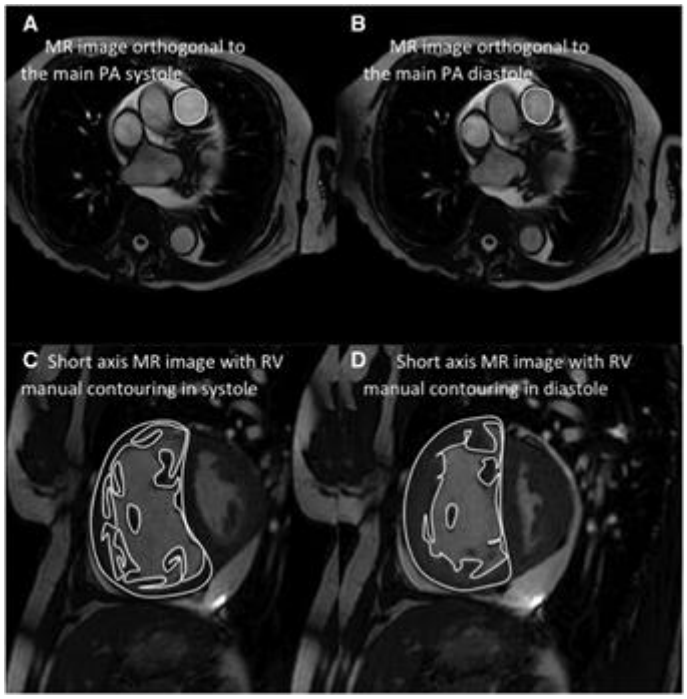

Figure 1. 3 Pulmonary artery (PA) relative area change and RV measurements

A) Shows the maximal PA area whereas **B)** shows the minimal PA area
C) Shows the right ventricle at end diastole and **D)** shows the right ventricle at end systole
Relative area change was calculated as follows: (maximal RA area − minimal RA area)/maximal RA area. Reproduced with permission (Swift et al., 2017).

A prognostic meta-analysis study produced by Baggen et al. (2016) delivered evidence by completing a summary of all described cardiac MRI findings, which can clinically predict poor outcome in patients with PAH. A total of 538 patients from eight different studies included and examined 21 cardiac MRI findings. Results at baseline and follow-up showed RVEF (P = 0.003) is the strongest predictor of mortality in patients with PAH. Additionally, a decrease in LV EDV and an increase in RV volumes could as well predict mortality. Searching for prognostic cardiac MRI measurements that can predict mortality in patients with PAH will help in preventing the deterioration of the condition and prolong life expectancy for patients. This shows the importance of identifying reliable and prognostic cardiac MRI parameters.

Cardiac MRI is considered a well-advanced imaging modality, and it is still expeditiously developing in analysing heart and lung diseases. Semi-automated or automated computer

methods also have been developing in the past decades to analyse cine magnetic resonance images. Currently, the standard measurement for LV function is cine MRI which is commonly applied in cardiovascular MRI investigation (Jerosch-Herold and Kwong, 2008, de Roos and Higgins, 2014). Quantitative measurements of LV function are driven by multi-section short-axis cine imaging that can cover the entire LV (Figure 1.4).

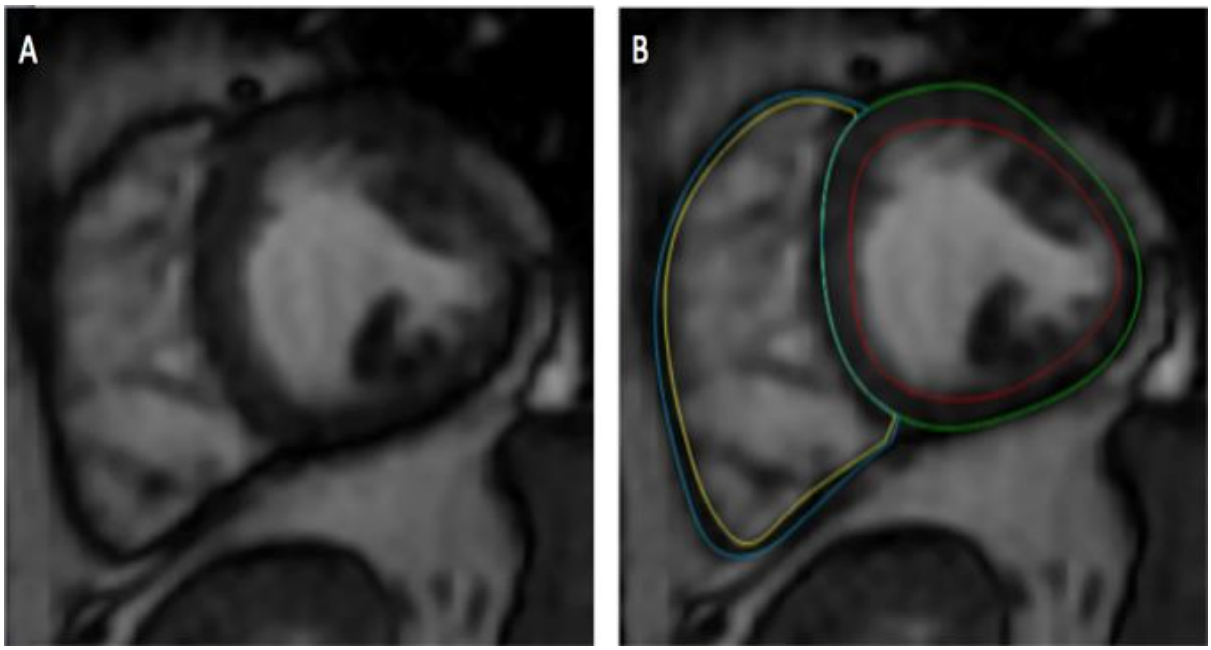

Figure 1. 4 Right and left ventricles on short-axis imaging

A) Short-axis view before myocardium tracing
B) After tracing, yellow and blue represents right ventricle, and red and green represents left ventricle

Quantifying LV function: (1) needs a well-experienced and educated observer that can accurately review various individual images and apply manual segmentation, and (2) is relatively time-consuming (Sardanelli et al., 2008). Identifying the LV border of the myocardium is the definition of LV segmentation. LV detection (distinguishing the presence of LV) and LV segmentation are two steps involved in the practical analysis of LV

quantification. The majority of automated or semi-automated methods depend on individual images or inadequate training sets. Relying on the local edges and shape models of LV, automated methods also try to localize the LV border (Suinesiaputra et al., 2015). Interestingly, deep learning techniques are rapidly developing in relation to automated image analysis (Dreyer and Geis, 2017).

A study done by (Tao et al., 2019) aimed to assess and improve a deep learning–based method to reach automatic LV segmentation and detection of the myocardium by using cine magnetic resonance images. This study was performed on a diverse cohort of patients with cardiovascular disease from various centres, and the cine MRI data was obtained by several magnetic resonance machines from numerous vendors. This showed that providing a deep learning-based method with a multi-centre and multi-vendor data set that is highly variable will attain an accurate and fully automated cine MRI analysis.

1.9 Cardiac MRI and Cardiac Biomarkers

Although cardiac MRI is the gold standard tool for the RV in PAH, in some situations, it is beyond the bounds of possibility to utilise it. For instance, feelings of claustrophobia and discomfort are significant problems for several MRI users. Therefore, a substitute independent non-invasive method would be clinically helpful in adult and paediatric patients (Lohani et al., 2015).

A study done by (Gan et al., 2006) evaluated naïve and follow-up patients with PH by NT-proBNP and cardiac MRI. They found that cardiac MRI measurements such as RV function and structure can be evaluated by changes in NT-proBNP levels. In addition, high levels of NT-proBNP correlate with severe RV failure. After that, a different study (Blyth et al., 2007) investigated the relationship between NT-proBNP and cardiac MRI-derived measurements

(RV volumes and systolic function). It showed that RV systolic dysfunction in a patient with PAH could be predicted by an independent and non-invasive cardiac biomarker (NT-proBNP); therefore, NT-proBNP could be a useful substitute for cardiac MRI.

Van de Veerdonk (2017) studied the difference between the effects of combination therapy and monotherapy and found a reduction in NT-proBNP levels in both groups, although the combination therapy group showed a greater reduction. All patients at baseline and after 1-year follow-up were also subjected to cardiac MRI and RHC. The results of this study showed that NT-proBNP levels could potentially be used to assess patients with PAH because the reduction in NT-proBNP levels after initially receiving combination therapy was also accompanied by better clinical outcomes such as improvement in RV wall stress.

In 2017, a study by (Baillie et al., 2017a) measured the average pulmonary arterial blood flow velocity (meanPAvel) using phase-contrast cardiac MRI in patients with PAH during both rest and standardised intravenous adenosine infusion to evaluate cardiopulmonary reserve and its relation to PAH in an innovative non-invasive fashion. They found that, at peak hyperemia, cardiopulmonary reserve had an excellent correlation with meanPAvel. Thus, they concluded that this method is achievable, simple and safe.

The same group conducted a different study (Baillie et al., 2017b) to assess this new non-invasive method by studying the relationship between meanPAvel (rest and hyperemic) and PAH prognostic markers including cardiac MRI-derived RVEF and RVESVi and cardiac biomarker (NT-proBNP) at baseline and after six months follow-up. There was an initial significant correlation between meanPAvel and RVESVi as well as RVEF at peak hyperemia, and these same measurements at peak hyperemia also shared a significant change over time. Additionally, NT-proBNP and meanPAvel indicated a statistically significant relationship in change overtime during peak hyperemia. However, the cardiac biomarker did not show any

correlation with meanPAvel on either hyperemia or resting state. This could be due to several limitations in the study. A sample size of 20 patients was not representative of all PAH patients, and 6 out of the total patients were at high risk of developing PAH, but their diagnosis was not confirmed. Previous articles (Andreassen et al., 2006, Leuchte et al., 2007, Mauritz et al., 2011) revealed a relationship between NT-proBNP levels and mortality in PAH over time. Therefore there might have been a statistical anomaly in (Baillie et al., 2017b) study that explains why a relationship between meanPAvel (rest and hyperemic) and PAH prognostic markers was not found.

1.10 Risk stratification in PAH

Prognostic evaluation and identification of patients at risk upon diagnosis and during follow-up to choose the appropriate treatment in a timely manner are essential for ensuring the best outcome. Clinical assessment is an important component in evaluating patients with PAH, as it includes vital information on disease severity, improvement, deterioration, or stability. Furthermore, various baseline and follow-up variables, including clinical, functional, exercise, non-invasive, and invasive variables, have been used independently or together in formulas or calculators to predict prognosis over time (Galiè et al., 2019).

The development of risk equations and risk scores has benefited from the use of registries. These registries include the PH connection equation (Thenappan et al., 2010, Thenappan et al., 2012), the Scottish composite score (Lee et al., 2012), the French Pulmonary Hypertension Network (FPHN) registry risk equation (Humbert et al., 2010a, Humbert et al., 2010b), the US Registry to Evaluate Early and Long-term PAH Disease Management (REVEAL) risk equation (Benza et al., 2010) and risk score (Benza et al., 2012, Benza et al., 2015), and the 2015 ESC/ERS PH guidelines risk table (Galiè et al., 2015, Galiè et al., 2016).

Using numerous established risk stratification tools, the clinical status and prognosis of patients with PAH can be determined. According to the ESC/ERS risk assessment in PAH, patients at 1-year mortality are assigned to low-, intermediate-, or high-risk groups based on a combination of clinical, functional, exercise, biochemical, imaging, and hemodynamic variables with known prognostic importance (Table 1.3). The majority of these variables and cut-off values proposed are based on expert opinion (Galiè et al., 2015, Galiè et al., 2016, Humbert et al., 2022a).

Table 1. 3 ESC/ERS risk assessment in PAH

Determinants of prognosis (estimated 1-year mortality)	**Low risk <5%**	**Intermediate risk 5-10%**	**High risk >10%**
Clinical signs of right heart failure	Absent	Absent	Present
Progression of symptoms	No	Slow	Rapid
Syncope	No	Occasional syncope	Repeated syncope
WHO functional class	I, II	III	IV
6MWD	>440 m	165–440 m	<165 m
Cardiopulmonary exercise testing	Peak VO_2 >15ml/min/kg (>65% pred.) VE/VCO_2 slope <36	Peak VO_2 11–15 ml/min/kg (35–65% pred.) VE/VCO_2 slope 36–44.9	Peak VO_2 <11 ml/min/kg (<35% pred.) VE/VCO_2 slope ≥45
NT-proBNP plasma levels	BNP <50 ng/l NT-Pro BNP <300 ng/l	BNP 50-300 ng/l NT-Pro BNP 300-1400 ng/l	BNP >300 ng/l NT-Pro BNP >1400 ng/l
Imaging (echocardiography, cardiac MRI)	RA area < 18 cm^2 No pericardial effusion	RA area 18-26 cm^2 No or minimal, pericardial effusion	RA area >26 cm^2 Pericardial effusion
Haemodynamics	RAP <8 mmHg CI ≥2.5 l/min/m^2 SvO_2 >65%	RAP 8–14 mmHg CI 2.0–2.4 l/min/m^2 SvO_2 60–65%	RAP >14 mmHg CI <2.0 l/min/m^2 SvO_2 <60%

Definition of abbreviations: ESC/ERS = European Society of Cardiology and European Respiratory Society; PAH = pulmonary arterial hypertension; WHO = World Health Organization; 6MWD = 6-minute walking distance; VO_2 = oxygen consumption; pred. = predicted; VE/VCO_2 = ventilatory equivalents for carbon dioxide; BNP = brain natriuretic peptide; NT-proBNP = N-terminal prohormone brain natriuretic peptide; MRI = magnetic resonance imaging; RA = right atrial; RAP = right atrial pressure; CI = cardiac index; SvO_2 = mixed venous oxygen saturation. Reproduced with permission (Galiè et al., 2016).

The ESC/ERS risk assessment tool has been validated at diagnosis and during follow-up in three registries: the French PH Registry (Boucly et al., 2017), the Comparative, Prospective Registry of Newly Initiated Therapies for PH (COMPERA) (Hoeper et al., 2017), and the Swedish Pulmonary Arterial Hypertension Registry (Kylhammar et al., 2018). All three registries proved the value of achieving a low-risk profile.

In addition, validation cohorts from the US showed that the REVEAL 2.0 risk score calculator and an abridged version (REVEAL Lite 2), as well as the equation of the French registry, were accurate and well-calibrated, confirming its generalizability (Benza et al., 2019, Benza et al., 2021, Humbert et al., 2010a). In 2022, the comprehensive ESC/ERS risk assessment table for PAH was updated and included cardiac MRI variables such as RVEF, RVESVi and stroke volume index (Humbert et al., 2022a, Humbert et al., 2022b).

Chapter 2: Research Questions, Aims, Objectives and Hypotheses

2.1 Research questions

This PhD thesis sought to address the following important questions:

- What is the role of cardiac MRI RA and RV parameters in prognostic evaluation of patients with PAH?
- Can a quantitative cardiac MRI-based automated artificial intelligence (AI) analysis be used to measure RA and RV in PAH?
- How reproducible are automated cardiac MRI analysis of the RA and surrogate markers of disease severity in PAH?
- How do manual and automated cardiac MRI RA measurements relate to invasively derived haemodynamic indices?
- Can the reference standard for assessment of cardiac structure and function of AI RV and AI RA be used to risk stratify patients with PAH?
- What is the role of automated cardiac MRI and NT-proBNP in prognostic evaluation of patients with PAH?

2.2 Aims

The aim of this body of work was to evaluate severity and prognosis of PAH using manual and automatic cardiac MRI measurements along with NT-proBNP.

2.3 Objectives

- To evaluate the prognostic importance of manual RA and RV parameters measured by cardiac MRI. This objective was achieved during the first year of my PhD and was measured by (1) assessing the likelihood of 1-year mortality of RA and RV measurements using univariate binary logistic regression, (2) testing the prognostic significance of RA area thresholds using Kaplan-Meier analysis, (3) assessing the prognostic significance of RA area predictors of mortality with area under the curve using receiver operating characteristic analysis, and (4) identifying optimal thresholds for low, intermediate, and high-risk patients using locally weighted scatterplot smoothing regression analysis.
- To develop a quantitative cardiac MRI-based automated AI analysis of the RA and RV in a large cohort of patients with heart failure and PAH. This objective was achieved during the second year of my PhD and was measured by (1) determining the failure rate of the model in a large clinical registry, and (2) assessing the inter-rater reliability of the two observers grading of segmentation quality as satisfactory, suboptimal or failure using Cohen's kappa testing in a subcohort.
- To evaluate interstudy repeatability and agreement of contours of a quantitative cardiac MRI-based automated AI analysis of the RA and evaluate the repeatability of surrogate markers of disease severity in PAH such as NT-proBNP. This objective was achieved during the second year of my PhD and was measured by assessing the repeatability of manual and AI metrics using intraclass correlation coefficients and Bland–Altman plots.
- To compare the association of manual RA area and AI RA area with invasive haemodynamics, and evaluate manual and automated RA measurements as predictors of mortality. This objective was achieved during the third year of my PhD and was

measured by (1) comparing RHC measurements to RA area measurements using Pearson's correlation coefficient, and (2) assessing the accuracy of RA measurements to predict RA thresholds performed using receiver operating characteristic analysis.

- To compare AI RV and AI RA area measurements and their utility to risk stratify patients with PAH, using the reference standard for assessment of cardiac structure and function. This objective was achieved during the third year of my PhD and was measured by (1) comparing published thresholds for RV metrics with 2015 ESC/ERS thresholds for RA area using bar chart figures, (2) testing the prognostic significance of RA area and RV thresholds using Kaplan-Meier analysis, and (3) assessing predictors of 1-year mortality using binary logistic regression analysis.
- To evaluate the prognostic role of automated cardiac MRI and NT-proBNP together in PAH. This objective was achieved during the third year of my PhD and was measured by (1) assessing the prognostic value of cardiac MRI parameters and NT-proBNP levels using univariate Cox regression hazard ratios, and (2) comparing continuous log10 (NT-proBNP) to continuous cardiac MRI parameters using Pearson's correlation coefficient analysis.

2.4 Hypotheses

- Manual cardiac MRI-derived RA and RV measurements have prognostic value independent in patients with PAH.
- Cardiac MRI RA and RV measurements can be fully automated using AI with a low failure.
- Automated cardiac MRI RA and NT-proBNP parameters are highly repeatable.
- Manual and automated cardiac MRI RA measurements estimate invasive haemodynamics at RHC.
- Automated cardiac MRI RV and RA metrics have prognostic value and can risk stratify patients with PAH.
- NTpro-BNP has prognostic value independently of cardiac MRI measurements.

Chapter 3: Materials & Methods

This chapter describes the methods used throughout the thesis. In the following chapters, each chapter describes study-specific methods. The related methods are repeated in the chapter-specific methods section to allow the following chapters to be read in isolation.

3.1 The ASPIRE PH MRI Database

Sheffield is one of the main tertiary referral centres for pulmonary hypertension in adults in the United Kingdom. The Sheffield Pulmonary Vascular Disease Unit (PVDU) is one of Europe's largest Pulmonary Hypertension treatment centres, with a referral population of over 15 million patients. In 2016/17, the Sheffield PVDU evaluated over 2300 patients and received over 800 new referrals (Sheffield Academic Directorate of Respiratory Medicine, 2014). From January 2008 to October 2019, all patients who had cardiac MRI at the Sheffield PVDU were included into an anonymized database. Each patient was assigned a unique identifier.

For statistical analysis, the anonymised data was subsequently transferred to Excel and SPSS formats. These were then combined to build a database containing incident cardiac MRI data, the nearest right heart catheter, N-terminal prohormone brain natriuretic peptide test, and exercise test data, as well as diagnostic and demographic information. A similar strategy was used to identify the scan closest to the 1-year follow-up. The local ethics committee provided ethical approval for this retrospective investigation, and written consent was waived (ASPIRE, ref: c06/Q2308/8).

3.2 Inclusion and Exclusion Criteria

The inclusion criteria required subjects diagnosed with PAH (Group 1 pulmonary hypertension), including idiopathic PAH, heritable PAH, and PAH in association with connective tissue disease, congenital heart disease, portal hypertension, human

immunodeficiency virus infection, and drugs and toxins. PAH was defined by the features of right heart catheterization (RHC) with a cut-off point of mean pulmonary arterial pressure (mPAP) ≥ 25 mmHg and pulmonary arterial wedge pressure (PAWP) ≤ 15 mmHg (Galiè et al., 2015, Galiè et al., 2016). Patients with a history of certain conditions such as contraindication to cardiac MRI, allergy to contrast medium, hepatitis B, C, HIV or pregnancy were excluded.

3.3 Image Acquisition

Cardiac MRI studies of 1.5T (HDx, General Electric Healthcare, Chicago, Illinois, USA) and 1.5T (Ingenia, Philips Healthcare, Best, the Netherlands) were included. Moreover, Cardiac MRI studies were performed using an 8-channel cardiac coil on a whole-body scanner at 1.5T HDx (General Electric Healthcare) (Lewis et al., 2020). Cine cardiac MRI acquisitions were made using a balanced steady state free precession (bSSFP) sequence. Following planning sequences, 4-chamber cine images were acquired. A stack of short axis images was acquired covering apex to base. Slice thickness and number of cardiac phases were 8 mm with 20 phases. The cardiac MRI protocol of multisection short-axis cine images has been previously explained (Alabed et al., 2022).

Other cardiac MRI studies were performed on a 1.5 T system (Ingenia, Philips Healthcare) equipped with a 28-channel flexible torso coil and digitization of the cardiac MRI signal in the receiver coil. Vertical long-axis, horizontal long-axis, 3-chamber (left ventricular (LV) outflow tract-views), and the LV volume contiguous short axis stack cine imaging were defined using survey. All cines were acquired with a bSSFP, single-slice breath-hold sequence. Typical parameters for bSSFP cine were as follows: SENSE factor 2, flip angle 60°, echo time (TE) 1.5 ms, TR 3 ms, field of view 320–420 mm according to patient size, slice thickness 8 mm and 30 phases per cardiac cycle.

3.4 Image Analysis

3.4.1 Manual Measurements

Image analysis was performed on GE Reportcard software with the observer blinded to the patient clinical information, cardiac catheter parameters and outcome data. Right ventricular endocardial and epicardial surfaces were manually traced from the stack of short-axis cine images to obtain right ventricular end diastolic volume (RVEDV) and right ventricular end systolic volume (RVESV). Based on RVEDV and RVESV, right ventricular ejection fraction (RVEF) was calculated.

Right atrial area at systole (maximal area) and diastole (minimal area) were manually traced on 4 chamber views. Pulmonary veins were manually excluded during contouring. Maximum RA area and minimal RA area were measured, and RA relative area change (RAC) was defined as follows:

$$RA\ RAC\ = \frac{maximal\ RA\ area - minimal\ RA\ area}{maximal\ RA\ area}$$

3.4.2 Training Measurements for Artificial Intelligence Development

Four observers, SA, FA, KK and AJS (with 2, 3, 13 and 11 years of cardiac MRI experience, respectively) manually drew LV and RV and atrial contours in 4-chamber cine cardiac MRI views on all cardiac phases for the training cohort. All contours were drawn with observers blinded to the patient's clinical information. All manual contours were reviewed by an expert cardiac MRI reader (AJS). Biventricular endocardial and epicardial surfaces were also manually traced from the stack of short-axis cine images to obtain RV volumetric and functional measurements as previously described (Alabed et al., 2022). MASS software

(research version 2020; Leiden University Medical Center, Leiden, the Netherlands) was used for the manual contouring for developing the artificial intelligence algorithm.

3.5 Artificial Intelligence Development

Cardiac MRI studies including a random selection of patients from different cohorts were used for deep learning training of 4-chamber contours. The training process was performed in two stages. We trained two CNN models with different numbers of manually annotated 4-chamber view images in the training set. The validation set and test set used were the same for both of the CNN models. Since no hyper parameter tuning was performed in the current experiments, a relatively small validation set of 6 subjects (180 images) was deemed sufficient to confirm model convergence during training and to confirm that the models did not suffer from overfitting. The test set consisting of 20 cases was used to compare the model performance of the initial model with the final model. Following this strategy, we maximised the number of studies available for training. The initial model was trained on a combination of Philips (Leeds/LUMC, n = 80) and GE (Sheffield, n = 184) data (total n = 264). The contours used for training were all generated without the use of a CNN. For the final model, 183 additional Sheffield GE scans were added. The contours for these additional cases were generated by reviewing and editing the contours generated using the base model. On average, 50% of the contours generated by the initial model were manually edited for this set of cases. These cases were separate from the test cohorts.

The CNNs used for the experiments had an UNET-like architecture with 16 convolutional layers including residual learning units and were implemented using Python and TensorFlow. Input images were resampled to a fixed pixel spacing of 1 mm and cropped to a 256×256 image matrix size and zero filled when required. During training, data augmentation was performed on the fly by creating new training samples by randomly rotating, flipping, shifting

and modifying image intensities of the original images. A total of 447 manually annotated 4-chamber cine series were used for training, corresponding to 10,045 images. The AI model development and training process of short-axis cine images have been previously explained (Alabed et al., 2022). A detailed description of artificial intelligence development can be found in chapter 5, sub-section 5.2.4.

3.6 Statistical analysis

3.6.1 Data Presentation and Normality Test

Continuous variables are presented as proportions and mean ± standard deviation, and categorical data are displayed as absolute values. Normal distribution was assessed by visual inspection of histograms and/or using the Shapiro–Wilk test.

3.6.2 Relationships between Cardiac MRI, NT-proBNP and RHC Measurements

Locally weighted scatterplot smoothing (LOESS) regression is a nonparametric technique that makes use of local weighted regression to fit a smooth curve through points in a scatter plot. LOESS analysis was carried out using RStudio (version 1.2.5033, RStudio, Boston, Massachusetts, USA). LOESS curves can highlight trends and cycles in data that may be challenging to model using a parametric curve. LOESS regression analysis was carried out to observe the relationship between RA area measurements and 1-year mortality, and to identify optimal thresholds for low, intermediate, and high-risk patients. Pearson's correlation coefficient was used to assess the strength of the relationships between continuous variables.

3.6.3 Diagnostic Accuracy

In clinical research, receiver operating characteristic (ROC) analysis measures the discrimination accuracy of medical diagnostic tests (or systems) between two patient states.

Therefore, ROC analysis was used to assess prognostic significance of RA area predictors of mortality with the area under the curve (AUC). AUC less than or equal to 0.5 indicates no value. The closer the area is to 1.0, the greater the predictive accuracy and significance of the test.

3.6.4 Regression Analysis

Linear regression analysis was used to estimate the relationship between continuous log10 (NT-proBNP) and continuous cardiac MRI parameters that showed a strong correlation with continuous log10 (NT-proBNP). A Scatter plot was constructed for percentage predicted right ventricular end-systolic volume index versus continuous log10 (NT-proBNP).

3.6.5 Prognosis

Binary logistic regression was used to assess predictors of 1-year mortality. Kaplan-Meier analysis assessed the prognostic value of RA area measurements using ESC/ERS thresholds. Groups were compared using the log-rank (Mantel-Cox) test. The interval from evaluation with MRI and RHC until all-cause death or census was regarded as the follow-up period. The prognostic value of demographic, MRI and NT-proBNP were also assessed using univariate Cox proportional hazards regression analysis. The results are Hazard ratios (HR) which can be described as the risk of adverse outcome of one population of patients versus another.

3.6.6 Agreement Statistics

Bland–Altman plots were used to assess the repeatability of cardiac MRI measurements (Bland and Altman, 1986). The bias, standard deviation and 95% limits of the agreement have been presented. In addition, reproducibility was assessed using intraclass correlation coefficient (ICC) analysis, assuming a normal distribution of continuous data (Mooij et al., 2008). The

ICC represents agreements between two or more observers or method evaluations for the same subjects. ICC is superior to a correlation coefficient for the assessment of consensus between observers, as it determines the scale of the variable and not just the relationship. Furthermore, inter-rater reliability of the two observers' grading of segmentation quality as satisfactory, suboptimal or failure was assessed using Cohen's kappa testing.

3.6.7 Software

Statistical analysis was carried out using SPSS (version 26, Statistical Package for the Social Sciences, International Business Machines, Inc., Armonk, New York, USA) and RStudio (version 1.2.5033, RStudio, Boston, Massachusetts, USA). GraphPad Prism (version 9.1.0, GraphPad Software, San Diego, California, USA) software was used for data presentation. A p-value < 0.05 was considered statistically significant.

Chapter 4: The Prognostic Significance of Manual RA and RV Measurements in PAH

My contribution to this work was in the generation of the idea, image analysis, data collection, statistical analysis, tables, figures and the writing.

4.1 Introduction

Pulmonary arterial hypertension (PAH) is a progressive, life-threatening condition that is characterised by pulmonary vascular resistance and associated with devastating consequences due to remodelling of the distal pulmonary arteries which can eventually result in right heart failure and premature death (Galiè et al., 2015, Galiè et al., 2016, Kiely et al., 2013). This rare condition has an average survival of less than three years without treatment (Dalonzo et al., 1991). However, 5-year survival is beyond 60% in patients with idiopathic PAH receiving pulmonary vascular therapy (Thenappan et al., 2010, Ling et al., 2012). Pulmonary vascular therapies target three well-known pathways with well-established treatments in clinical practice: phosphodiesterase type 5 inhibitors, endothelin receptor antagonists and prostanoids (Galiè and Ghofrani, 2013). Although most existing therapies are expensive and have adverse effects, predicting and assessing the severity of this serious condition aids in therapy response evaluation. This has directed scholars to search for non-invasive prognostic markers to assess treatment response in PAH.

Therapy assessment as a result drives to enhance the management plan for patients with PAH in terms of medications as well as listing for transplantation (Lythgoe et al., 2016, Khan and Rich, 2015). An important part when assessing PAH severity and prognosis is to obtain the precise measurement of right ventricular (RV) function (Lewis et al., 2020, Swift et al., 2017, Baggen et al., 2016, Swift et al., 2014b, van de Veerdonk et al., 2011, van Wolferen et al., 2007).

Based on a comprehensive risk assessment and prognostic evaluation of several modifiable variables including clinical worsening signs, the European Society of Cardiology and European Respiratory Society (ESC/ERS) guidelines stratified patients with PAH into three groups: low-risk (<5%), intermediate-risk (5-10%) and high-risk (>10%) mortality at 1-year. These modified variables and cut-off values which are mainly based on expert opinion may serve as a prognostic marker and help drive therapeutic decisions (Galiè et al., 2015, Galiè et al., 2016, Lewis et al., 2020).

Right atrial (RA) area is a well-established imaging measurement that has been shown to have prognostic significance in PAH (Raymond et al., 2002). Typically the RA is measured at the maximal area (ventricular systole); however, studies that have indicated alternative atrial measurements may be more prognostic (Darsaklis et al., 2016). The ESC/ERS guidelines provide RA thresholds indicative of low, intermediate and high risk based on RA size, and indicate that the RA area thresholds can be applied to both echocardiography and cardiac magnetic resonance imaging (MRI). There is limited data to support these thresholds, particularly on cardiac MRI, and there is a need to validate the thresholds in clinical registries to confirm or refute their prognostic significance and identify the optimal approach to the measurement of the RA. The aim of this study was to validate the ESC/ERS guideline thresholds of the RA and identify optimal approaches.

4.2 Methods

4.2.1 Patients

Consecutive patients with PAH underwent at least two cardiac MRI studies, baseline and follow-up, which took place between April 2012 and March 2017. The interval period between the first and second scans was a maximal of 2 years with a mean of 1 year and a standard

deviation of 5 months. All patients were referred from the ASPIRE registry, after completing a standard systematic diagnostic assessment as previously reported (Hurdman et al., 2012, Johns et al., 2019). The inclusion criteria required subjects diagnosed with PAH (Group 1 pulmonary hypertension), including idiopathic pulmonary arterial hypertension (IPAH), connective tissue disease (CTD), and PAH associated with portal hypertension, human immunodeficiency viruses (HIV), or drugs and toxins. PAH was defined by the features of right heart catheterization (RHC) with a cut-off point of mean pulmonary arterial pressure (mPAP) $\geq$ 25 mmHg and pulmonary arterial wedge pressure (PAWP) $\leq$ 15 mmHg (Galiè et al., 2015, Galiè et al., 2016). Patients with a history of certain conditions such as contraindication to cardiac MRI, allergy to contrast medium, hepatitis B, C, HIV or pregnancy were excluded.

4.2.2 Cardiac MRI Acquisition

All cardiac MRI studies were completed using an 8 channel cardiac coil on a whole body scanner at 1.5T GE HDx (GE healthcare, Milwaukee, USA). Short axis cine imaging was acquired using a cardiac gated multi slice balanced steady state free precession (SSFP) sequence (20 frames/cardiac cycle; slice thickness 8 mm; field of view 48; matrix 256 x 256; band width 125 kHz/pixel; repetition time/echo time TR/TE, 3.7/1.6 ms). Standard CINE cardiac views were performed including 4 chamber and right heart and left heart long axis views. In the short-axis plane, images were acquired having 8 mm slice thickness with an inter-slice gap of 2 mm. These images covered both ventricles (right and left) from the base to the apex. The smallest cavity area was regarded to be the end-systole. However, the R-wave triggered acquisition of the largest volume's first cine phase was taken to be the end-diastole. The plane phase contrast imaging was performed in an orthogonal manner on the main pulmonary trunk. The parameters of the phase contrast imaging were given as indicated here: repetition time, TR 5.6 ms; echo time, TE 2.7 ms; slice thickness, 10 mm; field of view, 48 cm,

bandwidth, 62.5 kHz; matrix, 256 3128; 20 reconstructed cardiac phases; and velocity encoding of flow, 150 cm/s. When performing this, all patients were in the supine position with a surface coil as well as retrospective electrocardiographic (ECG) gating.

4.2.3 Cardiac MRI Image Analysis

Baseline and follow-up MRI-derived measurements were recorded, and image analysis was performed on GE Reportcard software with the observer blinded to the patient clinical information, cardiac catheter parameters and outcome data. Right ventricular endocardial and epicardial surfaces were manually traced from the stack of short-axis cine images to obtain right ventricular end diastolic volume (RVEDV) and right ventricular end systolic volume (RVESV). Based on RVEDV and RVESV, right ventricular ejection fraction (RVEF) was calculated.

Right atrial area at systole (maximal area) and diastole (minimal area) were manually traced on 4 chamber views (Figure 4.1). Pulmonary veins were manually excluded during contouring. Maximum RA area and minimal RA area were measured, and RA relative area change (RAC) was defined as follows:

$$RA\ RAC\ = \frac{maximal\ RA\ area - minimal\ RA\ area}{maximal\ RA\ area}$$

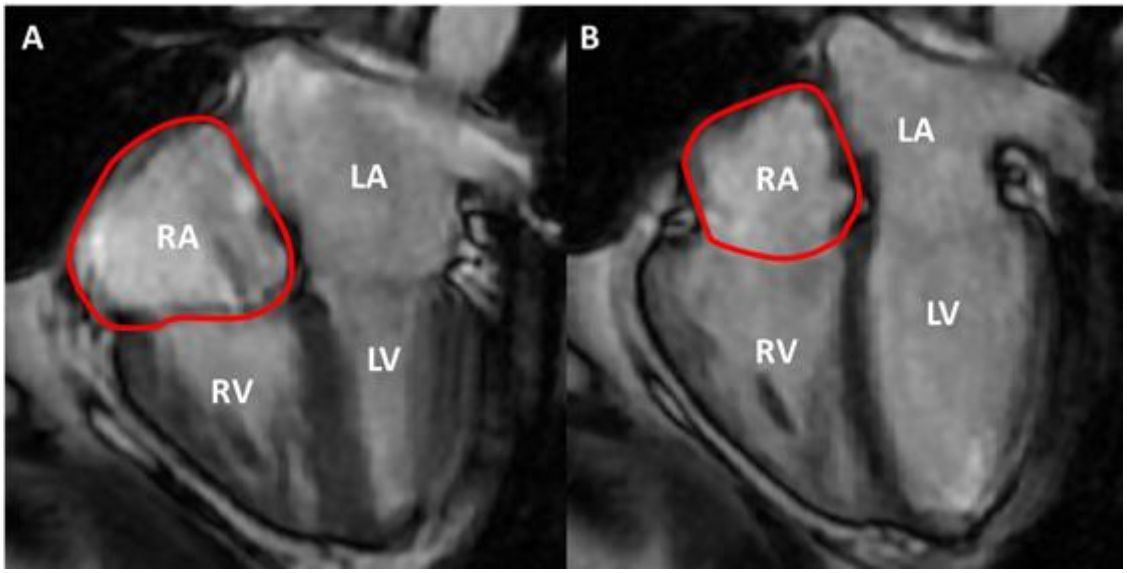

Figure 4. 1 RA area measurement

Four-chamber cardiac MRI for the measurement of (A) maximal RA area (ventricle systole) and (B) minimal RA area (ventricular diastole). MRI = magnetic resonance imaging; RA = right atrial.

4.2.4 Right Heart Catheterization

When performing the right heart catheterization, a balloon-tipped 7.5F thermodilution catheter is used (Becton-Dickson, Franklin, NJ). This operation (right heart catheterization) is usually executed using a Swan-Ganz Catheter via the internal jugular vein. Cardiac output was determined by thermodilution technique. Pulmonary vascular resistance (PVR) was measured by this equation: PVR = (mPAP – PAWP)/cardiac output. After multiprofessional assessment, the diagnostic classification form of PAH was obtained using the standard criteria (Hurdman et al., 2012). This data was generated previously by Swift et al (2017).

4.2.5 Statistical Analysis

The interval from evaluation with MRI until all-cause death or census date was considered as the follow-up period. The census was performed on 20th February 2019. Data for continuous variables are displayed as mean ± standard deviation (SD), and categorical data are presented

as absolute values. Histograms for continuous variables were visually inspected for normality. All right ventricle volumetric and right atrial area parameters were adjusted for body surface area (BSA) and recorded as index variables.

To assess the likelihood of 1-year mortality of all right ventricle volumetric and right atrial area measurements the univariate odds ratio was calculated for both scaled and unscaled MRI metrics. Scaled univariate binary logistic regression data are presented as a forest plot graph.

Variable scaling was performed to allow a direct comparison of odds ratios of all cardiac MRI continuous variables by dividing individual values by the SD of the variable. The odds ratio was scaled to better understand the magnitude of the effect being measured. The scaled odds ratio can help to better interpret the effect size of the predictor variable on the outcome variable.

The units for the odds ratio depend on the units of the predictor variables used in the logistic regression model. When the predictor variable is a continuous variable, the odds ratio represents the change in the odds of the outcome variable associated with a one-unit increase in the predictor variable. When the predictor variable is a continuous variable that has been scalded, the odds ratio is interpreted as the change in the odds of the outcome variable associated with a one-SD increase in the predictor variable.

Locally weighted scatterplot smoothing (LOESS) regression analysis was carried out to observe the relationship between RA area measurements and 1-year mortality, and to identify optimal thresholds for low, intermediate, and high-risk patients.

Kaplan-Meier analysis was performed to test the prognostic significance of RA area thresholds. Groups were compared using the log-rank (Mantel-Cox) test.

Receiver operating characteristic (ROC) analysis was used to assess prognostic significance of RA area predictors of mortality with area under the curve (AUC), data presented at 1-year mortality.

Statistical analysis was performed using SPSS 25 (SPSS, Chicago, IL) and for presentation of the data GraphPad Prism 8 (GraphPad Software, San Diego, CA) software was used. A P value less than 0.05 was considered statistically significant.

4.3 Results

4.3.1 Patients

A total of 226 patients with PAH were identified. The study group involved 130 patients with IPAH; 77 patients with pulmonary arterial hypertension associated with connective tissue disease (PAH-CTD); and 19 patients with PAH associated with portal hypertension, HIV, or drugs and toxins. Table 4.1 shows the demographics, PAH subtype percentage and right heart catheterization data for all patients, both alive and deceased, in terms of overall mortality. The majority of patients were female (72%), IPAH (57.3%) and had a mean age of 53 years. Cardiac MRI RA area and RV volumetric measurements for all patients, alive and dead at 1-year mortality, are shown in Table 4.2.

Table 4. 1 Baseline Demographics

	All patients (n=226)	Alive (n=154)	Dead (n=72)
Demographics			
Age, yr	53 ± 15.8	49.6 ± 15.6	60.2 ± 13.6
Sex, F/M (F %)	163/63 (72)	119/35 (77)	44/28 (61)
WHO FC I/II/III/IV	1/12/187/25	1/10/128/14	0/2/59/11
PAH subtype, *n* (%)			
IPAH	57.3%	62.3%	47.2%
CTD	33.9%	30.5%	41.7%
Other (portal, HIV, and drugs)	8.4%	7.1%	11.1%
Haemodynamics			
mRAP, mm Hg	10 ± 5	10 ± 5	11 ± 6
mPAP, mm Hg	49 ± 14	50 ± 14	47 ± 12
PAWP, mm Hg	10 ± 3	11 ± 3	10 ± 3
Cardiac index, L/min/m^2	3 ± 1	3 ± 1	3 ± 1
PVR, dynes/m^2	714 ± 424	744 ± 472	652 ± 297
MvO_2, %	64 ± 9	65 ± 9	63 ± 9

Definition of abbreviations: WHO FC = world health organisation functional class; PAH = pulmonary arterial hypertension; IPAH = idiopathic pulmonary arterial hypertension; PAH-CTD = pulmonary arterial hypertension associated with connective tissue disease; mRAP = mean right atrial pressure; mPAP = mean pulmonary arterial pressure; PAWP = pulmonary arterial wedge pressure; CI = cardiac index; PVR = pulmonary vascular resistance; SvO_2 = mixed venous oxygen saturation. Apart from gender, WHO FC, and PAH subtypes, values are presented as mean and standard deviation.

Table 4. 2 Cardiac MRI measurements

Metrics	All patients (n=226)	Alive (n=206)	Dead (n=20)
Right atrial and right ventricle at baseline			
Max RA area (cm^2)	24 ± 9	24 ± 9	25 ± 9
Max RA area index (cm^2/m^2)	14 ± 5	14 ± 5	14 ± 5
Min RA area (cm^2)	18 ± 9	17 ± 9	20 ± 9
Min RA area index (cm^2/m^2)	10 ± 5	10 ± 5	11 ± 5
RA RAC (%)	30 ± 13	31 ± 13	22 ± 10
RVESV (ml)	55 ± 28	54 ± 28	67 ± 31
RVESV index (ml/m^2)	32 ± 17	30 ± 16	41 ± 25
RVEDV (ml)	159 ± 62	157 ± 62	173 ± 57
RVEDV index (ml/m^2)	88 ± 33	87 ± 32	99 ± 32
RVEF (%)	40 ± 13	40 ± 13	34 ± 12
Right atrial and right ventricle at follow-up			
Max RA area (cm^2)	23 ± 9	23 ± 9	28 ± 10
Max RA area index (cm^2/m^2)	13 ± 5	13 ± 5	15 ± 5
Min RA area (cm^2)	16 ± 9	15 ± 8	21 ± 10
Min RA area index (cm^2/m^2)	9 ± 5	9 ± 5	11 ± 5
RA RAC (%)	33 ± 12	34 ± 11	26 ± 11
RVESV (ml)	54 ± 33	53 ± 33	70 ± 32
RVESV index (ml/m^2)	28 ± 15	27 ± 15	40 ± 18
RVEDV (ml)	158 ± 63	155 ± 62	186 ± 65
RVEDV index (ml/m^2)	87 ± 34	85 ± 33	104 ± 34
RVEF (%)	44 ± 13	45 ± 12	35 ± 14
Right atrial at change			
Max RA area (%)	-12 ± 35	-12 ± 35	4 ± 34
Min RA area (%)	-19 ± 51	-20 ± 51	-7 ± 54
RA RAC (%)	- 49 ± 646	-52 ± 676	-16 ± 112

Definition of abbreviations: MRI = magnetic resonance imaging; RA = right atrial; max = maximal; min = minimal; RAC = relative area change; RVESV = right ventricular end systolic volume; RVEDV = right ventricular end diastolic volume; RVEF = right ventricular ejection fraction. Values are presented as mean and standard deviation.

4.3.2 One-Year Mortality

During the entire period of this study, an outcome of 72 patients (31.7%) died overall, and 20 patients (8.8%) died at 1-year mortality. Table 4.3 presents the univariate odds ratio data of the binary logistic regression analysis for RA areas and RV volumes measurements at 1-year mortality. At follow-up, cardiac MRI metrics of maximal RA area (P = 0.032), minimal RA area (P = 0.015) and minimal RA area index (P = 0.023) increase the likelihood of 1-year mortality at univariate logistic regression analysis. A reduction in RA RAC at baseline (P = 0.009) and at follow-up (P = 0.015) increases the probability of 1-year mortality. This means that a reduction in RA RAC at two time points (baseline and follow-up MRI) was associated with an increased probability of 1-year mortality.

Table 4. 3 Univariate analysis at 1-year mortality in the full cohort

Metrics	Univariate Odds Ratio	Scaled Univariate Odds Ratio	*P* value
Right Atrial and right ventricle at baseline			
Max RA area (cm^2)	1.000 (1.000–1.001)	1.072 (0.646–1.779)	0.787
Max RA area index (cm^2/m^2)	1.000 (0.999–1.001)	1.116 (0.677–1.841)	0.667
Min RA area (cm^2)	1.000 (1.000–1.001)	1.328 (0.832–2.120)	0.234
Min RA area index (cm^2/m^2)	1.001 (1.000–1.002)	1.352 (0.851–2.148)	0.202
RA RAC (%)	0.003 (0.000–0.236)	0.480 (0.277–0.833)	0.009
RVESV (ml)	1.014 (1.000–1.028)	1.479 (1.001–2.186)	0.049
RVESV index (ml/m^2)	1.027 (1.005–1.048)	1.581 (1.097–2.280)	0.014
RVEDV (ml)	1.004 (0.997–1.010)	1.250 (0.822–1.901)	0.297
RVEDV index (ml/m^2)	1.010 (0.998–1.022)	1.375 (0.923–2.049)	0.117
RVEF (%)	0.966 (0.932–1.001)	0.628 (0.391–1.010)	0.055
Right atrial and right ventricle at follow-up			
Max RA area (cm^2)	1.001 (1.000–1.001)	1.668 (1.044–2.665)	0.032
Max RA area index (cm^2/m^2)	1.001 (1.000–1.002)	1.584 (0.996–2.519)	0.052
Min RA area (cm^2)	1.001 (1.000–1.001)	1.694 (1.107–2.594)	0.015
Min RA area index (cm^2/m^2)	1.001 (1.000–1.002)	1.648 (1.071–2.536)	0.023
RA RAC (%)	0.004 (0.000–0.352)	0.533 (0.320–0.886)	0.015
RVESV (ml)	1.011 (1.000–1.022)	1.450 (1.013–2.075)	0.042
RVESV index (ml/m^2)	1.040 (1.015–1.066)	1.835 (1.261–2.669)	0.001
RVEDV (ml)	1.007 (1.000–1.014)	1.537 (1.021–2.314)	0.039
RVEDV index (ml/m^2)	1.013 (1.002–1.025)	1.559 (1.062–2.288)	0.023
RVEF (%)	0.940 (0.906–0.976)	0.453 (0.280–0.734)	0.001
Right atrial at change			
Max RA area change (%)	1.019 (0.998–1.041)	1.946 (0.937–4.045)	0.074
Min RA area change (%)	1.006 (0.994–1.019)	1.378 (0.721–2.633)	0.332
RA RAC change (%)	1.000 (0.999–1.001)	1.094 (0.459–2.608)	0.840

Definition of abbreviations: RA = right atrial; max = maximal; min = minimal; RAC = relative area change; RVESV = right ventricular end systolic volume; RVEDV = right ventricular end diastolic volume; RVEF = right ventricular ejection fraction. Data in parentheses are 95% confidence intervals.

For the right ventricle cardiac MRI metrics, at baseline, an increase in RVESV (P = 0.049) and RVESV index (P = 0.014) increases 1-year mortality at univariate logistic regression analysis. In addition, at follow-up, an increase in RVESV (P = 0.042), RVESV index (P = 0.001), RVEDV (P = 0.039), RVEDV index (P = 0.023) and a decrease in RVEF (P = 0.001) increases 1-year mortality at univariate logistic regression analysis. No other measurements in this study showed a statistically significant relationship with mortality at 1-year. Figure 4.2 demonstrates the odds ratio in a forest plot with 95% confidence interval (CI) for each variable.

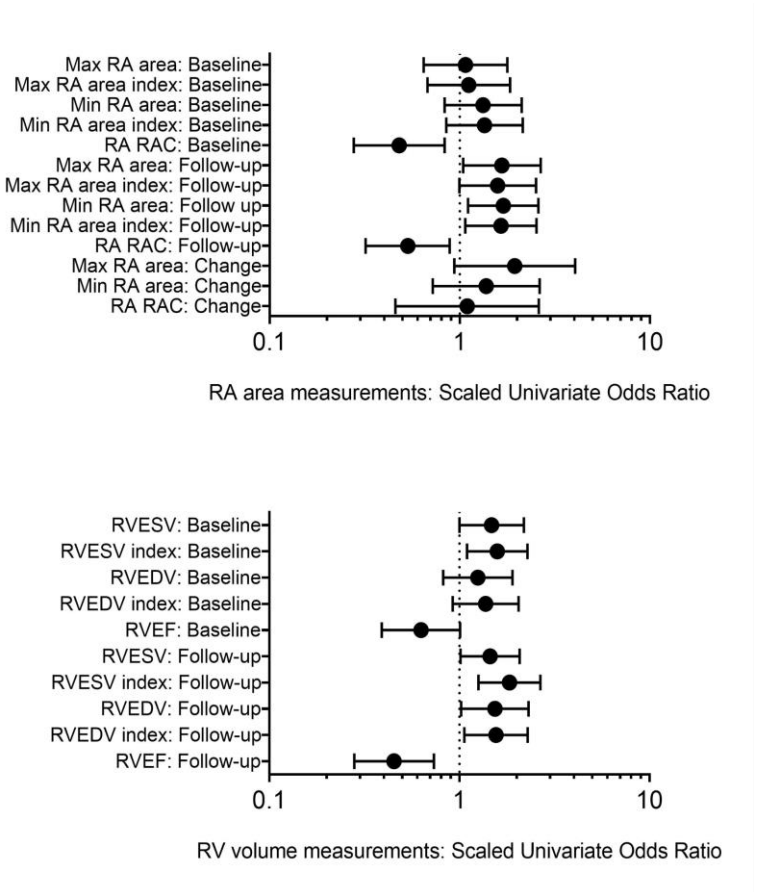

Figure 4. 2 Forest plot of RA area and RV volumes

Showing scaled univariate odds ratio with 95% confidence interval at 1-year mortality of RA area measurements (top) at baseline MRI, follow-up MRI and change between baseline and follow-up MRI, and RV volume measurements (bottom) at baseline MRI and follow-up MRI. RA = right atrial; max = maximal; min = minimal; RAC = relative area change; RV = right ventricle; EF = ejection fraction; ESV = end systolic volume; EDV = end diastolic volume.

Figure 4.3 shows Kaplan-Meier plots at baseline and follow-up for maximal RA area thresholds based on ESC/ERS guidelines which are split into three groups (low-risk, intermediate-risk and high-risk). The cut-off point for maximal RA area thresholds based on ESC/ERS guidelines is less than 18 cm^2 for low-risk (<5%); between 18 and 26 cm^2 for intermediate-risk (5–10%); and greater than 26 cm^2 for high-risk (>10%). Stratification of maximal RA area at follow-up (Log Rank = 13.82, P = 0.001) out of these thresholds showed greater survival curves than at baseline. This means that patients at follow-up showed a higher likelihood of mortality over time compared to when they were first observed (baseline MRI)

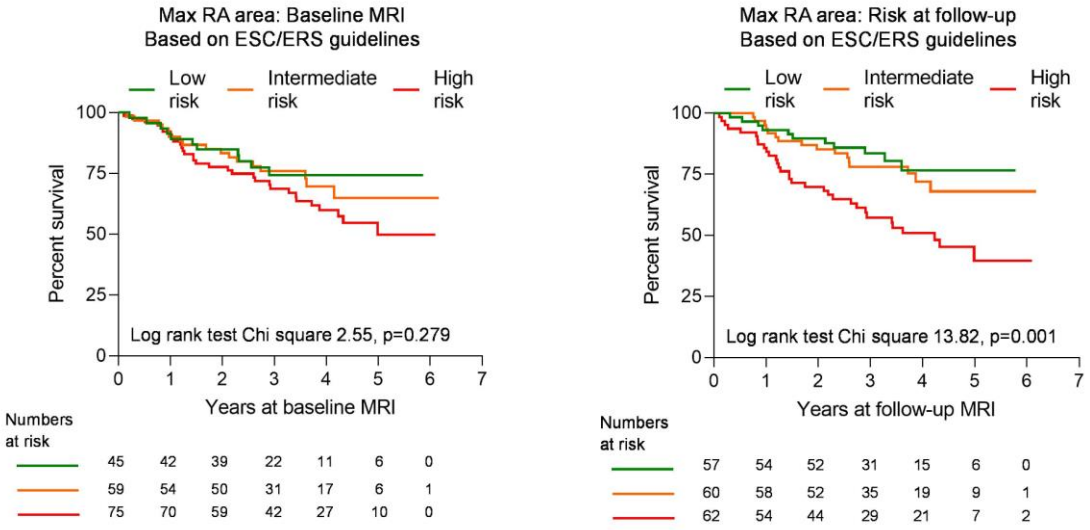

Figure 4. 3 Kaplan–Meier survival curves for max RA area thresholds based on ESC/ERS

Showing three risk groups (low, intermediate and high) at baseline (left) and at follow-up (right). Numbers at risk are presented below each plot. MRI = magnetic resonance imaging; RA = right atrial; max = maximal; ESC/ERS = European Society of Cardiology and European Respiratory Society.

Figure 4.4 shows Kaplan-Meier plots for maximal RA area, minimal RA area and RA RAC thresholds, respectively, based on LOESS analysis which splits into three groups (low-risk, intermediate-risk and high-risk) at 3 points: baseline, follow-up and change.

During the follow-up period, maximal RA area, minimal RA area and RA RAC LOESS analysis thresholds all showed well-stratified splits than baseline and change on Kaplan-Meier survival curves with a Log Rank of 13.96, 19.49 and 15.15 and a P-value of 0.001, less than 0.0001 and 0.001 respectively. In this study, minimal RA area at follow-up showed the most stratified RA area risk groups

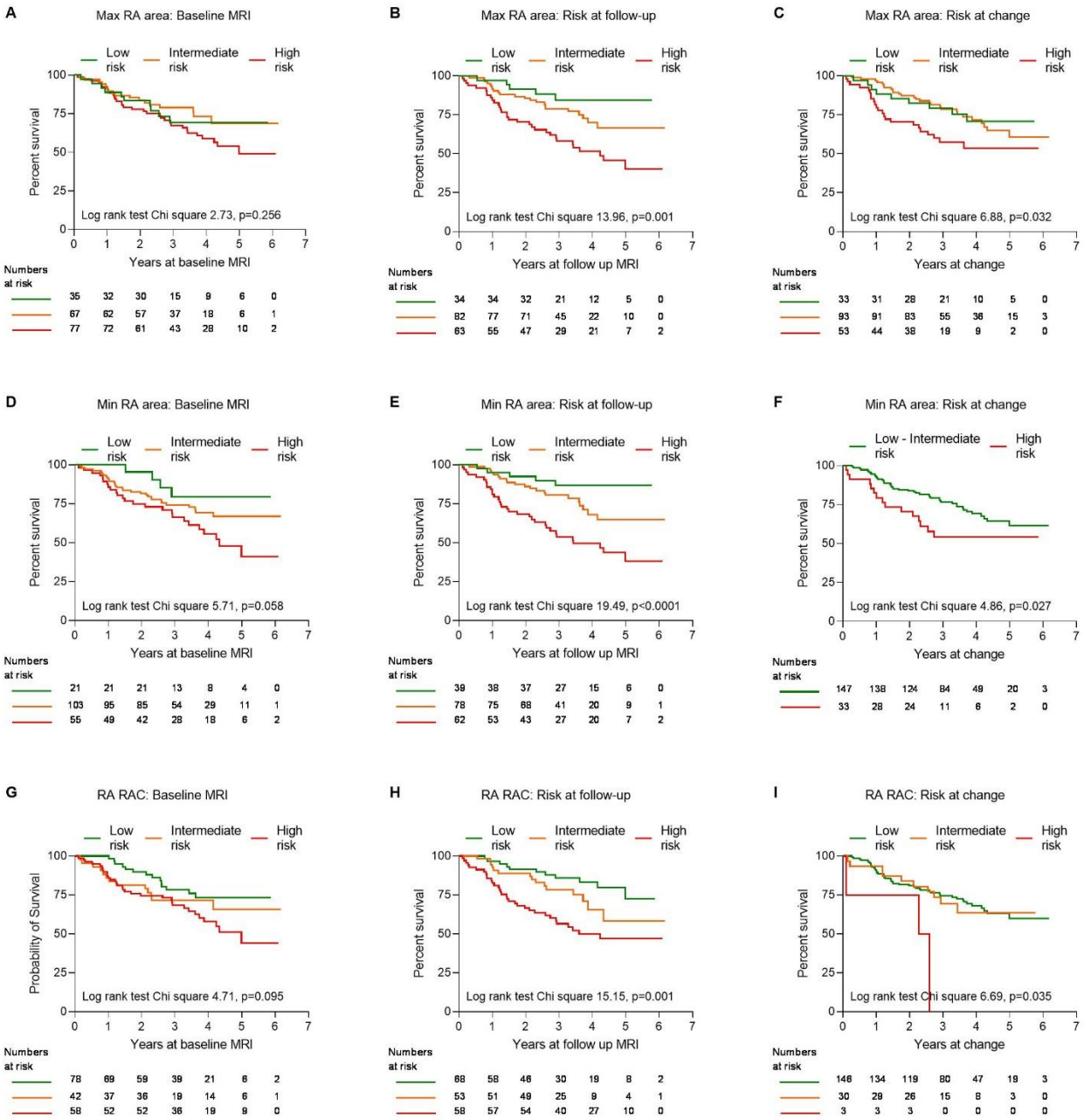

Figure 4. 4 Kaplan–Meier survival curves for RA area measurements based on LOESS analysis

Max RA area at baseline MRI (A), max RA area at follow-up MRI (B), change between baseline and follow-up MRI for max RA area (C), min RA area at baseline MRI (D), min RA area at follow-up MRI (E), change between baseline and follow-up MRI for min RA area (F), RA RAC at baseline MRI (G), RA RAC at follow-up MRI (H), and change between baseline and follow-up MRI for RA RAC (I). Numbers at risk are presented below each plot. MRI = magnetic resonance imaging; RA = right atrial; max = maximal; min = minimal: RAC= relative area change.

For ROC analysis, an AUC value greater than 0.6 is considered a proper explanatory mortality predictor. In the full cohort of PAH patients at follow-up, minimal RA area, maximal RA area and RA RAC showed an AUC of 0.714, 0.686 and 0.672 respectively (Figure 4.5).

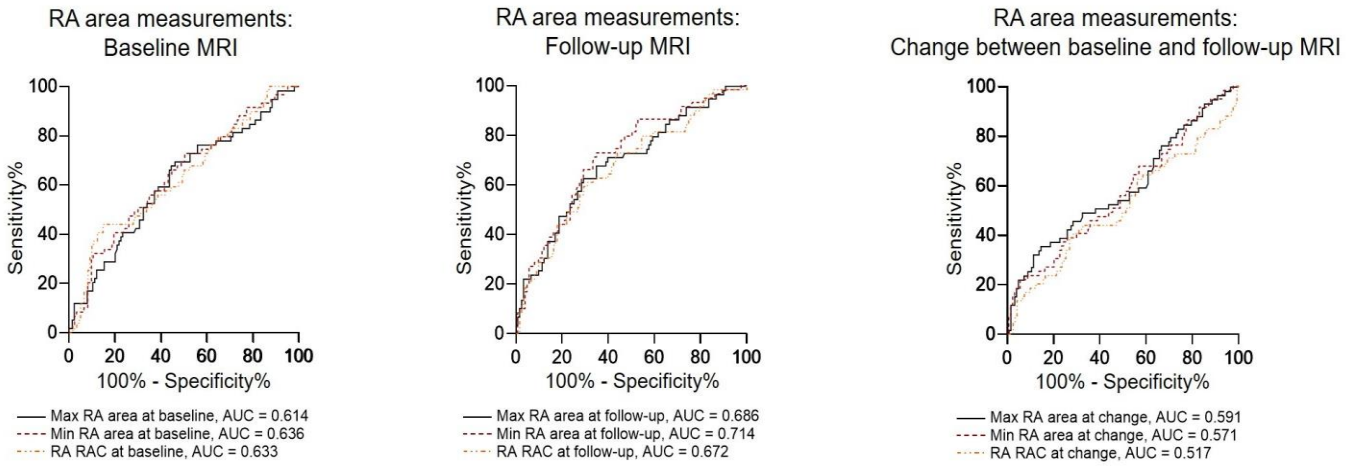

Figure 4. 5 Receiver operating curves of RA area measurements

Showing AUC of max RA area, min RA area and RA RAC based on LOESS analysis at 3 time points; baseline MRI (left), follow-up MRI (middle) and change between baseline and follow-up MRI (right). AUC = area under the curve; RA = right atrial; max = maximal; min = minimal; RAC = relative area change.

4.4 Discussion

4.4.1 Summary of results

There is a need to test the effectiveness of the ESC/ERS guideline thresholds of the RA area to enhance and confirm their use for prognosis and treatment response in PAH. To our knowledge, this is the first cardiac MRI study that has evaluated the ESC/ERS guideline thresholds of the RA area at baseline and follow-up. The findings from this study validate the ESC/ERS guideline thresholds of the RA and suggest that, at follow-up, minimal RA area is potentially a stronger predictor of mortality than maximal RA area and RAC in patients with PAH. In this cohort, all follow-up LOESS-derived thresholds including minimal RA, maximal RA and RAC showed good mortality stratification with some differences; however, this was not the case at baseline or at change in cardiac MRI metrics.

To date, there are no studies that demonstrate the prognostic importance of minimal RA area thresholds in PAH. On the other hand, our data suggest that, at follow-up, minimal RA area LOESS-derived thresholds are more prognostic and identify thresholds of <10 cm^2 for low-risk, 10–17 cm^2 for intermediate-risk, and >17 cm^2 for high-risk. Maximum RA area LOESS-derived thresholds show similar survival curves when compared to ESC/ERS guidelines, especially at follow-up period shown in Figure 2.7. Follow-up maximal RA area LOESS-derived thresholds are shown to be <16 cm^2, 16–26 cm^2 and >26 cm^2 for low, intermediate, and high risk, respectively. Despite the fact that RA area is typically measured at the maximal area, research has shown that RA RAC can be more prognostic than other atrial measurements (Darsaklis et al., 2016). Our LOESS-derived thresholds for RA RAC at follow-up was <30% for low-risk, 30-38% for intermediate-risk, and >38% for high-risk.

4.4.2 Adjustment for BSA

There is uncertainty as to the best approach to measure RA area. From the literature, we know that the RA is commonly adjusted for BSA (Maceira et al., 2013), but the ESC/ERS guidelines do not adjust for BSA, and we do not know what is the optimal approach overall. RA parameters have not been widely studied using cardiac MRI, and in particular, not many studies have adjusted for independent factors such as age, gender and BSA, but few studies on RA reference values have been published (Mohiaddin and Hasegawa, 1995, Anderson et al., 2005, Sievers et al., 2007). A study of 120 patients underwent cardiac MRI for clinical reasons and showed that the RA area indexed for BSA was the most independent indicator for RA enlargement (Maceira et al., 2013). However, index RA area parameters in our data showed less significant results.

4.4.3 Relationship between RA size and RV function

Right atrial area and pressure mirror RV function, and the contraction of the RA accounts for one-third of the normal RV output (Gaynor et al., 2005b). From the thin wall and oval nature of the RA, a marginally high RV pressure will cause stretching and enlargement of the RA as a compensatory mechanism for RV overload (Gaynor et al., 2005a). Reduced contractility, remodelling and hypertrophy of the RA presents as a clinical picture in chronic PAH (Cioffi et al., 2007). Hence, an increase in RA area and pressure indicates early signs of diastolic RV dysfunction and is strongly associated with severe outcomes and risk of mortality in PAH (Raymond et al., 2002, Bustamante-Labarta et al., 2002, Cogswell et al., 2014). Atrial remodelling is precisely measured by atrial volume; however, this is not commonly used in today's clinical practice. Cardiac MRI can accurately measure RV dimensions (Maceira et al., 2013), has a high prognostic value in PAH (Swift et al., 2017) and is the gold standard for measuring RV mass, volume and function including RVEF, which is a well-known prognostic

marker (Swift et al., 2012b, Swift et al., 2014a, Driessen et al., 2014, Grothues et al., 2004, Vonk-Noordegraaf and Souza, 2012, van de Veerdonk et al., 2011, van Wolferen et al., 2007). A recent study compared RA area and RVEF with other established prognostic markers in PAH using cardiac MRI and showed that RA area and RVEF have a significant association with clinical prognosis (Mello et al., 2019). In our present study, RVESV index and RVEF, at follow-up, both have a strong relationship with 1-year mortality.

4.4.4 Multiple prognostic markers

One of the observed measurements in the ESC/ERS guidelines for risk assessment is the RA area. However, multiple variables evaluation of other prognostic factors is recommended to help with risk and therapy assessment (Galiè et al., 2015, Galiè et al., 2016, Humbert et al., 2022a). The North American Registry to Evaluate Early and Long-term PAH Disease Management (REVEAL) produced a quantitative equation and simplified risk score for predicting survival at 1-year mortality. Mortality risk predictors of PAH were included such as WHO FC, demographics, haemodynamic and echocardiographic measurements and other factors (Benza et al., 2012, Benza et al., 2010). In 2015, a collaborative analysis independently validated the French registry risk equation and the simplified REVEAL risk score and suggested that both (equation and risk score) are prognostic in different PAH populations (Raina and Humbert, 2016). It is important for future research to consider that different variables may have different risk groups and that the treatment decisions should be guided by the comprehensive risk assessment of individual patients.

4.5 Limitations and Future Work

This research has raised several questions in need of further investigation. The study did not evaluate the use of cardiac MRI-derived RV mass, right atrial volume and reservoir function

(reservoir, conduit, and contractile functions) which have been previously indicated prognostic value in patients with PAH (Swift et al., 2017) and in patients with clinically worsening pulmonary hypertension (Sato et al., 2015, Sato et al., 2013). This would be a fruitful area for further work.

RA area measured in the apical four-chamber view by echocardiography has shown to be a highly reliable parameter and plays an important role in risk stratification and follow-up assessment in patients with pulmonary hypertension (Rudski et al., 2010, Galiè et al., 2015, Galiè et al., 2016). In addition, advancement in cardiac MRI has warranted reproducible and precise assessment of RA area and function (Jarvinen et al., 1996, Jarvinen et al., 1994). This study was limited by the absence of reproducibility analysis. A natural progression of this work would be to test for inter-observer and intra-observer reliability to show the consistency of our data.

Since this study was conducted in a retrospective fashion and all of the patients were previously diagnosed with PAH, it was not possible to exclude selection bias. Ideally, prospective studies involving a large number of patients are needed in order to confirm and validate the findings of this study. Therefore, further studies are required to help us establish a greater degree of accuracy on the RA area risk stratification at 1-year mortality and to elucidate the potential of cardiac MRI to assess severity and treatment response in PAH.

4.6 Conclusion

This study validates the ESC/ERS guideline thresholds of the RA and suggests that follow-up minimal RA area is a stronger predictor of mortality than maximal RA area and RAC in patients with PAH. All follow-up LOESS-derived thresholds including minimal RA, maximal RA and

RAC showed good mortality stratification. In addition, follow-up RVESV index and follow-up RVEF both have a strong relationship with 1-year mortality.

The results of this study could potentially have clinical implications for the management of patients with PAH. By identifying which measures of RA and RV function are most predictive of mortality, clinicians may be able to better assess the severity of a patient's condition and tailor their treatment accordingly.

Chapter 5: Radiological Quality Control of Automated RA and RV Measurements

This chapter is mainly based on a published paper for which I was the first author (Alandejani et al., 2022a). My contribution to this work was in the generation of the idea, image analysis, data collection, statistical analysis, tables, figures and the writing. Co-authors have interpreted the data and assisted in writing the paper. In addition, the result presented in sub-section 5.3.2, paragraph 2 (page 85) is from work by a different researcher (Alabed et al., 2022), which I contributed to the image analysis and right ventricle contouring.

5.1 Introduction

Right atrial (RA) and right ventricle (RV) measurements are often made manually on images viewed on picture archive and communication systems (PACS) or dedicated software packages with potential for observer variability. Image analysis tools differ between packages, and the analysis does take a small but significant amount of time. With the advent of artificial intelligence (AI), deep learning using convolutional neural networks (CNNs), accurate cardiac chamber segmentations are possible (Chen et al., 2020, Tao et al., 2019, Suinesiaputra et al., 2018, Bai et al., 2018, Bernard et al., 2018). Reference ranges for cardiac structure and function in healthy Caucasian adults from the UK Biobank population cohort were described for all four cardiac chambers using cardiac magnetic resonance imaging (MRI) (Petersen et al., 2017).

Automated quality control (QC) in image segmentation was applied to the UK Biobank cardiac MRI study via the reverse classification accuracy (RCA) approach to categorize between successful and failed segmentations. This previous work showed that RCA has the potential for accurate and fully automatic segmentation QC on a per-case basis (Robinson et al., 2019). A deep learning based framework for automated, quality-controlled characterization of cardiac function from cine cardiac MRI has been established, and reference values for cardiac function metrics were automatically derived from the UK Biobank cohort (Ruijsink et al., 2020).

Fully automated cardiac MRI derived biventricular evaluation of function and morphology in a real-world setting has achieved good results without any operator interaction (Backhaus et al., 2019). However, in the case of unseen anatomic variations, such as severe cardiac chamber shape changes and dilatation as in pulmonary artery hypertension (PAH), or significant artefact, then deep learning measurements may fail or be suboptimal (Thrall et al., 2018).

Automation of RA area measurements may assist clinicians in reaching fast and robust clinical decisions. However, there are currently no studies that have automated cardiac MRI RA area metrics in the setting of PAH in which patients have varying degrees of right ventricular failure, and the success/failure rate in clinical populations remains unknown.

The aim of this study was to develop a quantitative cardiac MRI-based automated AI analysis of the RA and RV in a large cohort of patients with heart failure and PAH with varying aetiology and disease severity, and determine the failure rate of the model in a large clinical registry.

5.2 Methods

5.2.1 Study Population

A cohort of 365 subjects with 4-chamber cine images was used for training. This number was felt to be adequate for machine learning training based of prior knowledge (Tao et al., 2019). This included a random selection of cardiac MRI studies from 285 patients in the ASPIRE registry (several ASPIRE follow-up scans were included with a total number of studies of 367). Sixty-six subjects from Leeds, including 29 healthy subjects and 37 patients with myocardial infarction of which 19 were acute and 18 were old. Fourteen healthy subjects from Leiden University Medical Centre (LUMC) were also included. The total number of cardiac MRI studies included in the training cohort of 4-chamber cine images was 447.

The demographics of the Leeds and Leiden subjects have been previously described (Garg et al., 2018, Crandon et al., 2018). To test the model of 4-chamber cine images for quality control and failure rate we included 3795 patients (5756 studies, as follow-up studies were included) from the ASPIRE registry (Figure 5.1). Baseline characteristics of the retrospective training data set (611 studies) and testing data set (5316 studies) of the AI model of short-axis cine images have been previously described (Alabed et al., 2022). Consent was waived for analysis of retrospective cases.

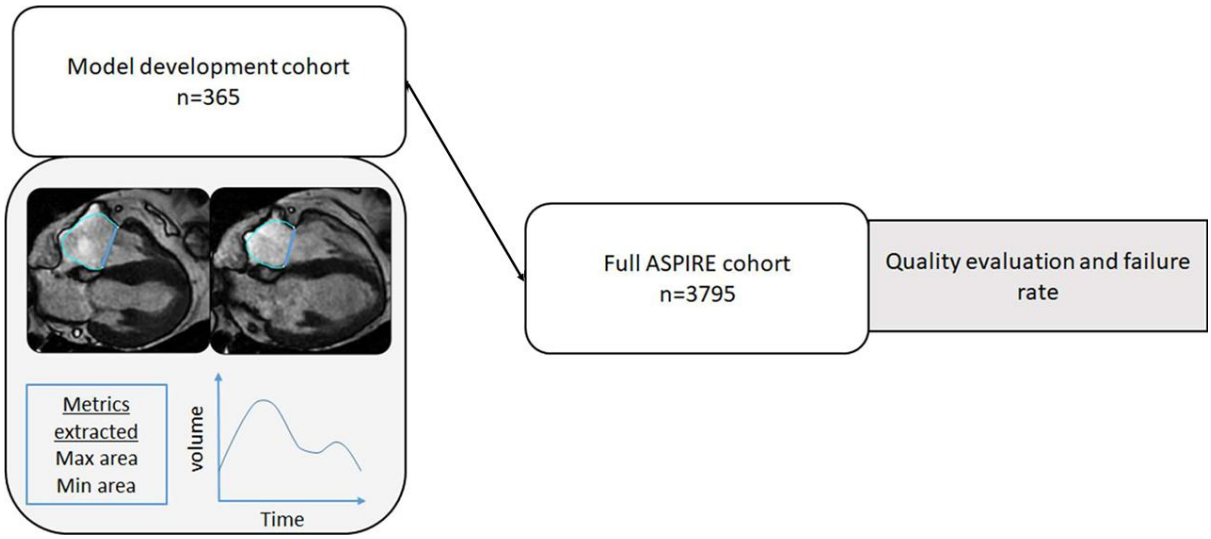

Figure 5. 1 Study flow chart for the training set of 4-chamber cine images

Max = maximal; Min = minimal. Reproduced with permission (Alandejani et al., 2022a).

5.2.2 Cardiac MRI Protocol

The training cohort included 1.5T (HDx, General Electric Healthcare, Chicago, Illinois, USA) and 1.5T (Ingenia, Philips Healthcare, Best, the Netherlands) studies. Cardiac MRI studies in the testing cohort were performed using a whole-body scanner at 1.5T (HDx (General Electric Healthcare) (Lewis et al., 2020). Cine cardiac MRI acquisitions were made using a balanced

steady state free precession (bSSFP) sequence. Following planning sequences, 4-chamber cine images were acquired. A stack of short axis images were acquired covering apex to base. Slice thickness and number of cardiac phases were 8 mm with 20 phases. The cardiac MRI protocol of multisection short-axis cine images has been previously explained (Alabed et al., 2022).

Leeds and Leiden cardiac MRI studies were performed on a 1.5 T system (Ingenia, Philips Healthcare) equipped with a 28-channel flexible torso coil and digitization of the cardiac MRI signal in the receiver coil. Vertical long-axis, horizontal long-axis, 3-chamber (left ventricular (LV) outflow tract-views), and the LV volume contiguous short axis stack cine imaging were defined using survey. All cines were acquired with a bSSFP, single-slice breath-hold sequence. Typical parameters for bSSFP cine were as follows: SENSE factor 2, flip angle 60°, TE 1.5 ms, TR 3 ms, field of view 320–420 mm according to patient size, slice thickness 8 mm and 30 phases per cardiac cycle.

5.2.3 Image Analysis

Four observers, SA, FA, KK and AJS (with 2, 3, 13 and 11 years of cardiac MRI experience, respectively) manually drew LV and RV and atrial contours in 4-chamber cine cardiac MRI views on all cardiac phases for the training cohort. All contours were drawn with observers blinded to the patient's clinical information. All manual contours were reviewed by an expert cardiac MRI reader (AJS). Biventricular endocardial and epicardial surfaces were also manually traced from the stack of short-axis cine images to obtain RV volumetric and functional measurements as previously described (Alabed et al., 2022). MASS software (research version 2020; Leiden University Medical Center, Leiden, the Netherlands) was used for the manual contouring for developing the algorithm).

5.2.4 Deep Learning Training

The AI model development and training process of short-axis cine images have been previously explained (Alabed et al., 2022). Cardiac MRI studies including a random selection of patients from the ASPIRE registry, subjects from Leeds, and from LUMC were used for deep learning training of 4-chamber contours. The training process was performed in two stages. We trained two CNN models with different numbers of manually annotated 4-chamber view images in the training set. The validation set and test set used were the same for both of the CNN models. Since no hyper parameter tuning was performed in the current experiments, a relatively small validation set of 6 subjects (180 images) was deemed sufficient to confirm model convergence during training and to confirm that the models did not suffer from overfitting. The test set consisting of 20 cases was used to compare the model performance of the initial model with the final model. Following this strategy, we maximised the number of studies available for training. The initial model was trained on a combination of Philips (Leeds/LUMC, n = 80) and GE (Sheffield, n = 184) data (total n = 264). The contours used for training were all generated without the use of a CNN. For the final model, 183 additional Sheffield GE scans were added. The contours for these additional cases were generated by reviewing and editing the contours generated using the base model. On average, 50% of the contours generated by the initial model were manually edited for this set of cases. These cases were separate from the test cohorts.

The CNNs used for the experiments had an UNET-like architecture with 16 convolutional layers including residual learning units and were implemented using Python and TensorFlow. Input images were resampled to a fixed pixel spacing of 1 mm and cropped to a 256×256 image matrix size and zero filled when required. During training, data augmentation was performed on the fly by creating new training samples by randomly rotating, flipping, shifting and modifying image intensities of the original images. Modifying image intensities of the

original images refers to adjusting the brightness, contrast, and colour balance of the images. This is done to increase the diversity of the training data and make the model more robust. For example, by increasing or decreasing the brightness, the computer can create images that are lighter or darker than the original, which can help the model recognize objects in different lighting conditions

A total of 447 manually annotated 4-chamber cine series were used for training, corresponding to 10,045 images. Whilst the patient/scan unique identifier is inputted with the image into the CNN. That information is not used in the deep learning, just the image and the paired contour are processed to learn the contouring. For training, the Adam optimizer method was used, the learning rate was selected as 0.001 and cross-entropy was used as loss function. The Adam optimizer is a widely used algorithm for optimising the parameters of a neural network during training. A learning rate of 0.001 was selected, indicating a gradual and careful training process. Cross-entropy was used as the loss function to measure the difference between predicted probabilities and actual probabilities of target class labels, with the goal of minimising this function to improve model accuracy on the training data.

Each training batch included a random selection of 20 images. The number of epochs was set at a fixed number of 50, with all images used once in every epoch. The raw output of the CNNs is a labeled image, with the six possible label values corresponding to either one of the four cardiac cavities, the LV myocardium, or background. For each cardiac label, the largest connected component was extracted and a closed spatially smoothed contour around the extracted region generated. The area of the cardiac cavities was subsequently derived as the area surrounded by the generated contours. All experiments were executed on a standard PC with Intel Core i7 CPU with 64 GB of internal RAM memory equipped with an Nvidia GTX 1080 TI GPU with 12 GB of memory.

5.2.5 Quality Control

All automatically AI-segmented 4-chamber and biventricular contours across all cardiac phases and resultant volume-time curves were evaluated by AJS and scored as satisfactory, suboptimal or failure. In addition, the quality of the image acquisition was assessed for artefacts and slice position errors. The definitions for QC were assigned prior to image review. Satisfactory was defined as either perfect contouring or minor errors that were not thought to affect the volumetric results. Suboptimal was defined as contours with errors deemed significant enough to affect the volumetric results. Failure defined as either absent contours or gross failure of the algorithm to segment the cardiac structures.

5.2.6 Statistical Analysis

Continuous variables are presented as proportions and mean ± standard deviation. Inter-rater reliability of the two observers grading of segmentation quality as satisfactory, suboptimal or failure was assessed using Cohen's kappa testing in a subcohort. Statistical analysis was carried out using SPSS (version 26, Statistical Package for the Social Sciences, International Business Machines, Inc., Armonk, New York, USA), and a *P* value of 0.05 or less was considered statistically significant.

5.3 Results

5.3.1 Patients

The ASPIRE registry in the training model included patients with left heart disease (15%), lung disease (12%), chronic thromboembolic PAH (21%), PAH (29%), other PAH (2%) and non-PAH (21%). The mean and standard deviation (SD) of the main haemodynamics of the ASPIRE registry in the training model is 10.4 ± 6.2 mmHg for mean RAP, 41.0 ± 15.5 mmHg

for mean pulmonary arterial pressure, 13.4 ± 6.0 mmHg for pulmonary arterial wedge pressure, and 561 ± 466 dynes/m^2 for pulmonary vascular resistance. The characteristics of the ASPIRE test set of 4-chamber cine images are presented in Table 5.1.

Table 5. 1 Demographics, MRI and haemodynamics for the ASPIRE test set of 4-ch cine images

	ASPIRE Test Set (*n = 3795*)
Demographics	
Age, yr	62.8 ± 15.3
Sex, F/M (F %)	2355/1440 (62)
BSA (m^2)	1.8 ± 0.2
WHO FC I, *n* (%)	47 (1)
WHO FC II, *n* (%)	441 (12)
WHO FC III, *n* (%)	2743 (77)
WHO FC IV, *n* (%)	336 (10)
Diagnosis, *n* (%)	
Left Heart Disease	611 (16)
Lung Disease	632 (17)
CTEPH	728 (19)
PAH	1040 (28)
Other PH	84 (2)
Other (not PH)	677 (18)
Haemodynamics	
mRAP, mmHg	10.1 ± 6.0
mPAP, mmHg	40.8 ± 14.2
PAWP, mmHg	12.8 ± 5.9
Cardiac output L/min	4.9 ± 1.9
Cardiac index, L/min/m^2	2.7 ±1.0
PVR, dynes/m^2	561.5 ± 418.6
MvO_2, %	65.2 ± 9.3
Cardiac MRI volumetric measurements	
RVESVi, ml/m^2	37.3 ± 27.1
RVEDVi, ml/m^2	62.6 ± 35.5
RVSVi, ml/m^2	25.3 ± 15.4
RVEF, %	44.6 ± 16.1
Cardiac MRI area measurements	
Automatic max RA area, cm^2	25.8 ± 10.6
Automatic min RA area, cm^2	18.5 ± 10.3

Definition of abbreviations: MRI = magnetic resonance imaging; 4-ch = 4-chamber; BSA = body surface area; WHO FC = World Health Organisation functional class; CTEPH = chronic thromboembolic pulmonary hypertension; PAH = pulmonary arterial hypertension; PH = pulmonary hypertension; RHC = right heart catheterization; mRAP = mean right atrial pressure; mPAP = mean pulmonary arterial pressure; PAWP = pulmonary arterial wedge pressure; PVR = pulmonary vascular resistance; MvO_2 = mixed venous oxygen saturation; RVESVi = right ventricular end-systolic volume index; RVEDVi = right ventricular end-diastolic volume index; RVSVi = right ventricular stroke volume index; RVEF = right ventricular ejection fraction; max = maximal; min = minimal; RA = right atrial. Data presented as mean ± standard deviation. Reproduced with permission (Alandejani et al., 2022a).

5.3.2 Quality Control

Of the automatic 4-chamber segmentation of 3795 patients (5756 studies) analysed by the AI model, 16 (0.3%) failed (Figure 5.2A). 108 (1.9%) had suboptimal contours significant enough to be thought to affect the area measurements. In 72/108 patients, the 4-chamber slice was off-plane, with the most frequent error being inclusion of the LV outflow tract and suboptimal view of the RA (Figure 5.2B). In 36/108 severe image artefact, typically breathing artefact or poor cardiac gating led to suboptimal RA contours. In a randomly selected subcohort of 1018 studies, the scoring of satisfactory, suboptimal and failure showed excellent agreement between observer 1 and observer 2, with a high kappa statistic of 0.84.

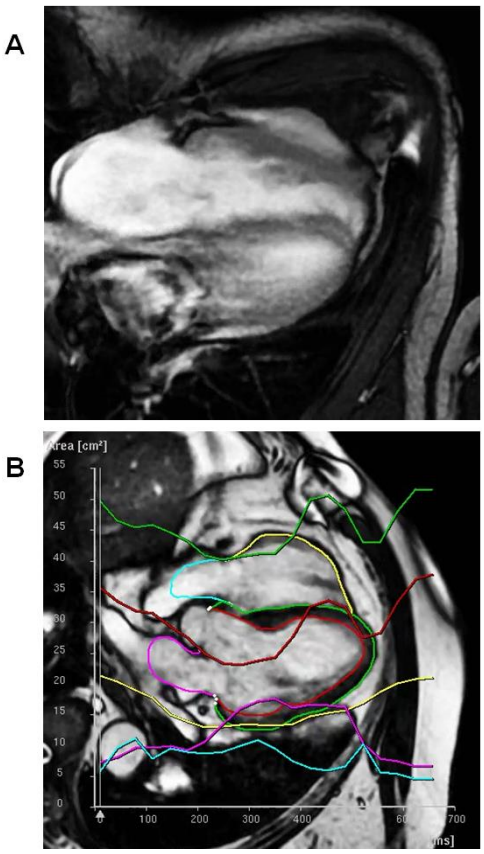

Figure 5. 2 Examples of failed and suboptimal AI 4-chamber segmentations

(A) Major failure because of missing/failed contours. (B) Minor failure mainly because of inclusion of the LV outflow tract and suboptimal view of the RA. The turquoise, violet, red, and yellow circles indicate the RA endocardial, LA endocardial, LV endocardial, and RV endocardial contours, respectively. AI = artificial intelligence; RA = right atrial; LA = left atrial; LV = left ventricle; RV = right ventricle.

The overall failure rate of the automatic short-axis segmentation was 1.0% (53 of 5316 studies). This was mainly caused by congenital heart diseases such as ventricular septal defect (Figure 3A) or technical issues and artefacts affecting image quality. Other segmentation errors mostly affecting the heart apex (Figure 5.3B) were considered minor failures (1.7%, 91 of 5316 studies).

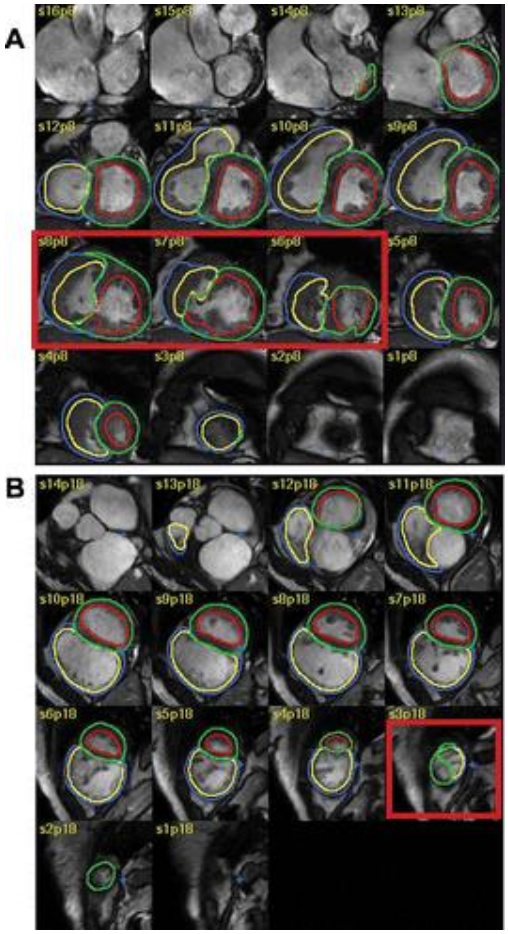

Figure 5. 3 Examples of failed and suboptimal AI short-axis segmentations

(A) Major failure because of congenital heart disease causing the LV contours to extend into the right ventricle (RV; red box). (B) Minor failure at the apex where the RV was incorrectly labelled as LV (red box). The red, green, yellow, and blue circles indicate the LV endocardial, LV epicardial, RV endocardial, and RV epicardial contours, respectively. AI = artificial intelligence; LV = left ventricle; RV = right ventricle. Reproduced with permission (Alabed et al., 2022).

5.4 Discussion

This study shows that cardiac MRI RA area and RV volumetric measurements can be fully automated using AI with a very low failure rate in a large clinical cohort with varying RA and RV size, and deformity. This study shows that fully automated Al-based contouring of the RA and RV has a very low AI failure rate of 2.2% and 2.7%, respectively, in a large clinical population of patients with varying degrees of breathlessness, exercise limitation and aetiology of cardiac and pulmonary disease. The main reasons for failure were ventricular septal defect, and severe artefact, in particular poor cardiac gating, image noise and acquisition issues such as poor slice positioning of the 4-chamber slice, the latter the most common scenario. Such images cannot yield accurate RA area or RV volumetric measurements by an observer or AI.

Using cardiac MRI, reference ranges for cardiac structure and function in healthy adults were previously described for all four cardiac chambers (Petersen et al., 2017). Automation of the QC process can potentially assist in validating AI algorithms. The potential for accurate and fully automatic segmentation QC has been demonstrated and applied to the UK Biobank cardiac MRI study using the RCA approach (Robinson et al., 2019). Reference values for cardiac function metrics were automatically derived from the UK Biobank, and a deep learning based framework for automated, quality-controlled characterization of cardiac function from cine cardiac MRI has been confirmed (Ruijsink et al., 2020). Although, we advocate the use of observer review in the QC process to maintain oversight of the segmented contours.

5.5 Limitations and Future Work

This is a single centre clinical testing of an AI algorithm developed in a multi-vendor multicentre cohort, with the clinical testing in the setting of a tertiary referral centre for patients with PAH. The imaging appearances and patient populations are likely representatives of other

PAH referral centres. The algorithm was generated in a multicentre setting, with single centre testing. Multicentre testing would be the next step to determine wider applicability of the algorithm. The current approach uses manual QC which is advantageous from a regulatory standpoint and maintains expert oversight of the AI. Future work to automate QC is of interest; however, we consider manual review an important component of the system. To enhance the accuracy of the model, failed AI segmentation will be regularly recognised and combined in future training rounds. Furthermore, future work will include evaluation of the utility of such automatic QC approaches in clinical populations.

5.6 Conclusion

In this study, we have developed and tested an AI model to fully automate cardiac MRI RA area and RV volumetric measurements; the AI model has a low failure rate in a diverse population of suspected pulmonary hypertension.

Chapter 6: Agreement and Repeatability of Manual and Automatic RA Measurements

This chapter is mainly based on a published paper for which I was the first author (Alandejani et al., 2022a). My contribution to this work was in the generation of the idea, image analysis, data collection, statistical analysis, tables, figures and the writing. Co-authors have interpreted the data and assisted in writing the paper.

6.1 Introduction

Accurate and repeatable measurements of cardiac chamber size and function are important for patient management (Kiely et al., 2019). A number of studies have revealed the prognostic significance of cardiac magnetic resonance imaging (MRI) measurements in various cardiopulmonary diseases such as cardiomyopathies, pulmonary arterial hypertension (PAH), heart failure and ischaemic heart disease (Klem et al., 2011, Mordi et al., 2015, Swift et al., 2017, Rodriguez-Palomares et al., 2019, Alabed et al., 2020). RA size and function measured by cardiac MRI can predict mortality (Ivanov et al., 2017, Sato et al., 2015, Sallach et al., 2009) and the European Society of Cardiology (ESC) and European Respiratory Society (ERS) guidelines advocate the use of maximal (systolic) right atrial (RA) area, 6-minute walk distance (6MWD) and N-terminal prohormone brain natriuretic peptide (NT-proBNP) for stratification of PAH patients (Galiè et al., 2015, Galiè et al., 2016, Humbert et al., 2022a).

Cardiac MRI can track changes occurring in the heart by direct visualisation and repeatable volumetric analysis of RV morphology and function, an advantage over existing methods. Fully automated cardiac MRI-derived biventricular evaluation of function and morphology in a real-world setting has achieved good results without any operator interaction (Backhaus et al., 2019). Automation of RA area measurements may result in lower variability; however, the repeatability of automated cardiac MRI RA area metrics in the setting of PAH remains unknown. The aim of this study was to (i) evaluate interstudy repeatability and agreement of contours of a quantitative cardiac MRI-based automated artificial intelligence (AI) analysis of

the RA, and (ii) evaluate the repeatability of surrogate markers of disease severity in PAH such as 6MWD and NT-proBNP in a prospective cohort of patients with PAH.

6.2 Methods

6.2.1 Study Population

This study included 36 patients with cardiac MRI studies for prospective repeatability testing from the RESPIRE study (ClinicalTrials.gov Identifier: NCT03841344) (Swift et al., 2021). Patients were diagnosed with Group 1 pulmonary arterial hypertension, including IPAH, heritable and CTD, and PAH associated with portal hypertension; mean pulmonary arterial pressure ≥ 25 mmHg and pulmonary arterial wedge pressure ≤ 15 mmHg. Prospectively recruited patients provided written informed consent.

6.2.2 Cardiac MRI Protocol

The RESPIRE prospective cohort consisted of GE studies (Swift et al., 2021). Cardiac MRI studies were performed using a whole-body scanner at 1.5T (HDx (General Electric Healthcare) (Lewis et al., 2020). Cine cardiac MRI acquisitions were made using a balanced steady state free precession (bSSFP) sequence. Following planning sequences, 4-chamber cine images were acquired. A stack of short axis images were acquired covering apex to base. Slice thickness and number of cardiac phases were 8 mm with 20 phases.

6.2.3 Image Analysis

Four observers, SA, FA, KK and AJS (with 2, 3, 13 and 11 years of cardiac MRI experience, respectively) manually drew LV and RV and atrial contours in 4-chamber cine cardiac MRI views on all cardiac phases for the training and testing cohorts. All contours were drawn with observers blinded to the patient's clinical information. All manual contours were reviewed by

an expert cardiac MRI reader (AJS). RV endocardial and epicardial surfaces were also manually traced from the stack of short-axis cine images to obtain RV volumetric and functional measurements as previously described (Alabed et al., 2022). MASS software (research version 2020; Leiden University Medical Center, Leiden, the Netherlands) was used for the manual contouring for developing the algorithm and repeatability testing).

6.2.4 Deep Learning Training

Cardiac MRI studies including a random selection of patients from the ASPIRE registry, subjects from Leeds, and from Leiden University Medical Centre were used for deep learning training. The deep learning training process as described in chapter 5, sub-section 5.2.4.

6.2.5 Repeatability and Agreement of the Deep Learning Contours

To evaluate inter-study agreement, two cardiac MRI scans were performed on the same day in two separate sittings as part of the RESPIRE study (Swift et al., 2021) for AI and manual measurements. In addition, interobserver agreement assessments, manual (AS) vs manual (FA), AI vs (AJS) and AI versus (FA) were made. Agreement of the machine learning contouring model was evaluated by DSC. The DICE similarity for all cardiac cavities was computed in the 20 subjects in the test set. This was both for the baseline model as well as the final model.

6.2.6 Repeatability of Walk Test and NT-proBNP

A field walk test (6MWD) was performed by a fully qualified respiratory physiologist, and the walk test distance was recorded. Blood was taken for NT-proBNP prior to the walk test where possible. NT-proBNP analysis was performed on patient plasma samples using the Luminex

100/200 multiplex analyser utilising the cardiovascular marker kit (HCVD1MAG-67K Millipore).

A blood draw and a 6-minute walk distance test were carried out in the morning. These investigations were repeated in the afternoon in the same way and in the same order. Patients were to refrain from exercise, caffeinated drinks and alcohol between investigations. The 6MWD and NT-ProBNP of tests 1 and 2 were individually compared for agreement.

6.2.7 Statistical Analysis

Continuous variables are presented as proportions and mean ± standard deviations. Intraclass correlation coefficients and Bland–Altman plots were used to assess the repeatability of manual and AI cardiac MRI metrics. Statistical analysis was carried out using SPSS (version 26, Statistical Package for the Social Sciences, International Business Machines, Inc., Armonk, New York, USA) and RStudio (version 1.2.5033, RStudio, Boston, Massachusetts, USA), and p-value of 0.05 was considered statistically significant. For data presentation, GraphPad Prism (version 9.1.0, GraphPad Software, San Diego, California, USA) software was used.

6.3 Results

6.3.1 Patients

A total of 36 patients with PAH were identified in this study. 60% of patients were diagnosed with either idiopathic PAH or heritable PAH, and 24% were PAH in association with connective tissue disease. Patients had a mean age of 49.5 ± 15.9 years, and 83% were female. Table 6.1 presents the demographic, walk and blood test, cardiac MRI measurements, and right heart catheter data for all patients with PAH.

Table 6. 1 Demographics, haemodynamics, walk and blood test, and MRI measurements

	RESPIRE repeatability (*n = 36*)
Demographics	
Age, yr	49.5 ± 15.9
Sex, F/M (F %)	30/6 (83)
BSA (m^2)	1.9 ± 0.2
WHO FC I, *n* (%)	0 (0)
WHO FC II, *n* (%)	2 (6)
WHO FC III, *n* (%)	30 (83)
WHO FC IV, *n* (%)	4 (11)
Diagnosis, *n* (%)	
PAH	36 (100)
Haemodynamics	
mRAP, mmHg	11 ± 7
mPAP, mmHg	52 ± 13
PAWP, mmHg	10 ± 3
Cardiac output L/min	4.5 ± 1.7
Cardiac index, L/min/m^2	2.5 ± 0.9
PVR, dynes/m^2	899 ± 512
MvO_2, %	65.0 ± 9.1
Walk test	
6MWD (m)	375 ± 167
Blood test	
NT-proBNP	561 ± 648
Cardiac MRI volumetric measurements	
RVESVi, ml/m^2	25.4 ± 9.2
RVEDVi, ml/m^2	63.3 ± 27.6
RVSVi, ml/m^2	37.9 ± 20.7
RVEF, %	43.3 ± 10.0
Cardiac MRI area measurements	
Automatic max RA area, cm^2	22.6 ± 6.3
Manual max RA area, cm^2	22.5 ± 6.3
Automatic min RA area, cm^2	15.0 ± 5.5
Manual min RA area, cm^2	15.3 ± 5.7

Definition of abbreviations: MRI = magnetic resonance imaging; BSA = body surface area; WHO FC = World Health Organisation functional class; CTEPH = chronic thromboembolic pulmonary hypertension; PAH = pulmonary arterial hypertension; PH = pulmonary hypertension; RHC = right heart catheterization; mRAP = mean right atrial pressure; mPAP = mean pulmonary arterial pressure; PAWP = pulmonary arterial wedge pressure; PVR = pulmonary vascular resistance; MvO_2 = mixed venous oxygen saturation; 6MWD = 6-minute walk distance; NT-ProBNP = N-terminal prohormone brain natriuretic peptide; RVESVi = right ventricular end-systolic volume index; RVEDVi = right ventricular end-diastolic volume index; RVSVi = right ventricular stroke volume index; RVEF = right ventricular ejection fraction; max = maximal; min = minimal; RA = right atrial. Data presented as mean ± standard deviation. Reproduced with permission (Alandejani et al., 2022a).

6.3.2 Segmentation Agreement

Manual and automatic AI segmentation were assessed in the same day repeat studies from the prospective RESPIRE study. DSC showed high agreement (Figure 6.1) comparing automatic AI and manual cardiac MRI readers, with a minimal bias towards either reader, validating similarity in the resulting contours. Manual contours made by observer 1 and observer 2 were closely related for both maximal RA area and minimal RA area. The mean and SD DSC metric for observer 1 vs observer 2, AI measurements vs observer 1 and AI measurements vs observer 2 is 92.4 ± 3.5, 91.2 ± 4.5 and 93.2 ± 3.2 for maximal RA area. The mean and SD DSC metric for observer 1 vs observer 2, AI measurements vs observer 1 and AI measurements vs Observer 2 is 89.8 ± 3.9, 87.0 ± 5.8 and 91.8 ± 4.8 for minimal RA area. The DSC for all four cardiac chambers before and after refinement for the 20 subjects in the test set are shown in Table 6.2.

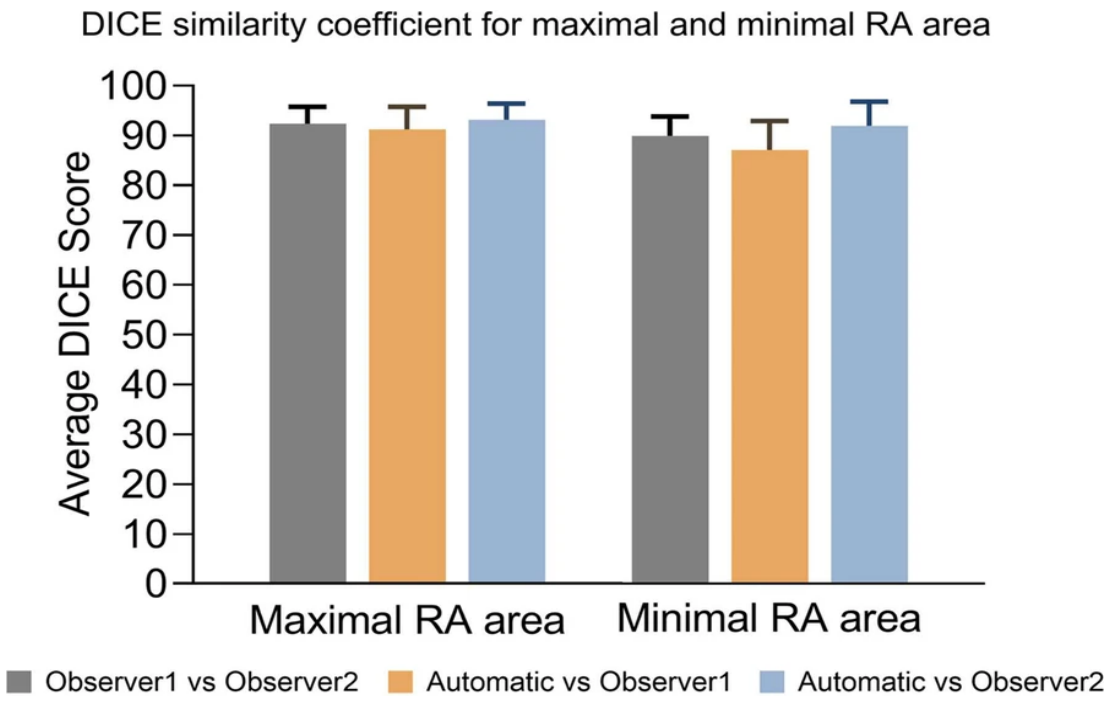

Figure 6. 1 RA measurements and DICE similarity coefficient

Maximal and minimal RA area DICE similarity coefficient results for (i) observer 1 vs observer 2 contour agreement, (ii) automatic vs observer 1 and (iii) automatic vs observer 2. RA = right atrial. Reproduced with permission (Alandejani et al., 2022a).

Table 6. 2 DSC values before and after refinement for all four cardiac chambers area

DICE	Baseline model (SD)		Final model (SD)	
LV Endo ED	93.93	2.58	94.37	2.31
LV Endo ES	89.71	4.26	90.47	3.61
LV Epi ED	93.78	2.52	95.12	1.44
LV Epi ES	92.53	3.50	93.26	2.37
RV Endo ED	91.68	3.66	94.30	2.33
RV Endo ES	88.26	4.59	91.35	3.09
LA Endo ED	91.05	4.45	92.04	3.56
LA Endo ES	86.87	7.75	90.03	4.67
RA Endo ED	92.63	5.84	93.56	3.26
RA Endo ES	92.37	4.82	93.10	3.50
AVG	91.28	4.40	92.76	3.01

Definition of abbreviations: DSC = DICE similarity coefficient; SD = standard deviation; LV = left ventricular; Endo = endocardial; ED = end-diastolic; ES = end-systolic; Epi = epicardial; RV = right ventricular; LA = left atrial; RA = right atrial; AVG = average. Reproduced with permission (Alandejani et al., 2022a).

6.3.3 Repeatability and Agreement Assessment

All AI RA measurements showed higher interstudy (scan-rescan) repeatability ICC 0.91 to 0.95, compared to manual measurements (observer 1 ICC 0.82 to 0.88, observer 2 ICC 0.88 to 0.91). Similar repeatability was also found comparing both observers with AI RA contours compared to observer 1 vs observer 2 ICC 0.96 to 0.98, see Tables 6.3, 6.4. Minimal bias was found for AI RA measurements, Figure 6.2. The 6MWD test had excellent repeatable ICC 0.99, while NT-proBNP was of moderate repeatability 0.72.

Table 6. 3 Scan-rescan variability of automatic and manual cardiac MRI RA measurements

Interstudy (scan-rescan) variability (n = 36)						
	Automatic		Observer 1		Observer 2	
	ICC	95% CI	ICC	95% CI	ICC	95% CI
Max RA area	0.91	0.82, 0.96	0.82	0.65, 0.91	0.88	0.76, 0.94
Min RA area	0.95	0.89, 0.97	0.88	0.75, 0.94	0.91	0.84, 0.96

Definition of abbreviations: AI= artificial intelligence; MRI = magnetic resonance imaging; max = maximal; min = minimal; RA=right atrial. Reproduced with permission (Alandejani et al., 2022a).

Table 6. 4 Interobserver variability of automatic and manual cardiac MRI RA measurements

Interobserver variability (n = 36)						
	Automatic vs Observer 1		Automatic vs Observer 2		Observer 1 vs Observer 2	
	ICC	95% CI	ICC	95% CI	ICC	95% CI
Max RA area	0.99	0.97, 0.99	0.98	0.95, 0.99	0.98	0.94, 0.99
Min RA area	0.99	0.98, 0.99	0.97	0.92, 0.99	0.96	0.95, 0.99

Definition of abbreviations: AI= artificial intelligence; MRI = magnetic resonance imaging; max = maximal; min = minimal; RA=right atrial. Reproduced with permission (Alandejani et al., 2022a).

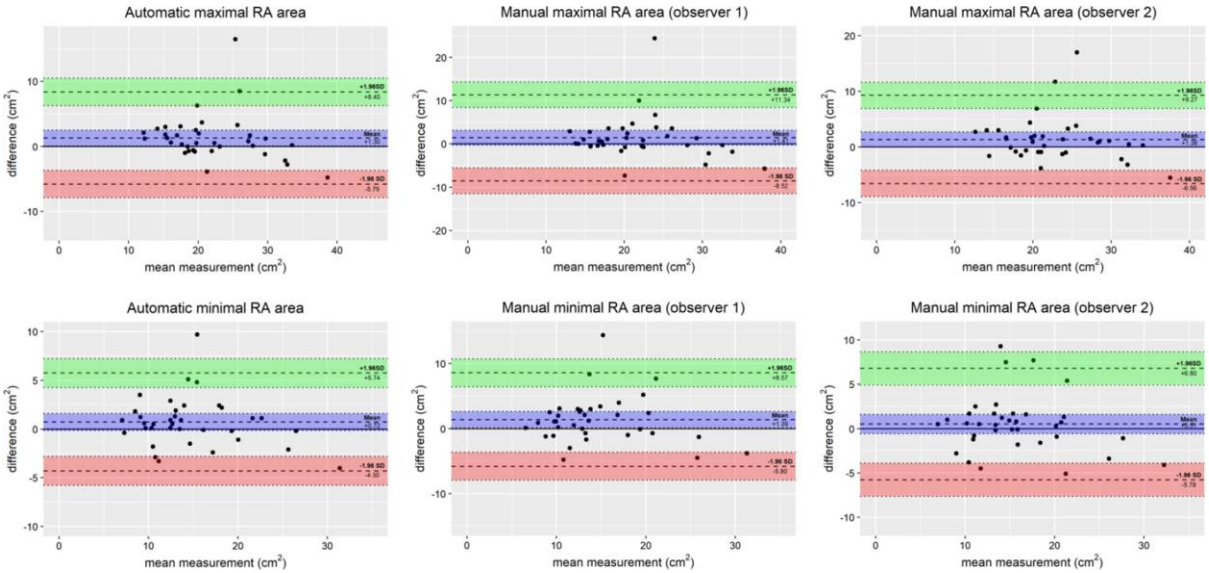

Figure 6. 2 Bland–Altman plots and RA measurements

Bland–Altman plots showing cardiac MRI RA measurements scan-rescan results for (left) deep learning automatic AI measurements, (middle) observer 1 manual measurements, and (right) observer 2 manual measurements. MRI = magnetic resonance imaging; AI = artificial intelligence; RA = right atrial. Reproduced with permission (Alandejani et al., 2022a).

6.4 Discussion

This study shows that both cardiac MRI RA area measurements and walk test data have excellent repeatability in patients with PAH as judged by excellent test-test ICC repeatability, while NT-proBNP was of moderate repeatability. Walk test was highly repeatable with near perfect agreement. NT-proBNP failed to reach the excellent ICC threshold. The variability of AI-derived RA area measurements is lower than manual measurements in a scan-rescan cohort of patients with varying severities of RA size and function, and PAH.

Assessment of interstudy (scan-rescan) repeatability is crucial to evaluate the utility of imaging measurements (Grothues et al., 2004). Interstudy repeatability is especially important for the comparison of automatic AI measurements with manual measurements (Augusto et al., 2021).

We utilised a prospective scan-rescan study with rigorous study design (Swift et al., 2021) and show AI measurements are highly repeatable with marginally higher repeatability than manual measurements. Lower variability has advantages for more precise evaluation of changes in the RA following therapeutic intervention in trials and clinical practice, where treatment decisions are impacted by progressive structural and functional changes in the heart.

6.5 Limitations and Future Work

This is a single centre study of an AI algorithm developed in a multi-vendor multicentre cohort. This study developed an AI model for RA area estimation rather than volume. The rationale was to automate measurements made clinically and consistent with the ESC/ERS guidelines in PAH. Further research regarding the role of RA volume would be worthwhile.

NT-proBNP blood tests were performed in a university laboratory and were not clinical-grade test kits. Therefore further work is to repeat the NT-proBNP samples on trust-grade sample kits in Sheffield Teaching Hospitals NHS Foundation Trust.

The respiratory physiologist was not blinded to 6MWD data of visit 1 at visit 2. Blood tests were analysed in bulk, and visit 1 and visit 2 blood tests were analysed at the same time to limit the possibility of observer bias. One limitation of the study is that the morning versus afternoon sampling may be limited in terms of reproducibility due to interval fluid intake and lunchtime diuretic doses. In addition, the blood tests were analysed in bulk, which may affect the accuracy and precision of the results.

6.6 Conclusion

In this study, we have tested a fully automated AI model and showed that AI cardiac MRI RA area measurements are highly repeatable, and 6MWD showed excellent repeatability whereas NT-proBNP was of moderate repeatability.

Chapter 7: Clinical Testing of Manual vs Automatic RA Area Measurements

This chapter is based on a published paper for which I was the first author (Alandejani et al., 2022a). My contribution to this work was in the generation of the idea, image analysis, data collection, statistical analysis, tables, figures and the writing. Co-authors have interpreted the data and assisted in writing the paper.

7.1 Introduction

Changes in the right atrium (RA) are important to recognise in the evaluation of patients with right ventricular (RV) failure (Austin et al., 2015, Raymond et al., 2002, Roca et al., 2015, Fukuda et al., 2014, Fukuda et al., 2016). Right atrial pressure (RAP) measured at right heart catheterisation is fundamental to the haemodynamic assessment of RV failure (Damman et al., 2009, Drazner et al., 2001) and predicts mortality in patients with pulmonary artery hypertension (PAH) (Lichtblau et al., 2020, Dalonzo et al., 1991).

Automation of RA area measurements may assist clinicians to reach fast and robust clinical decisions. However, there are currently no studies that have automated cardiac magnetic resonance imaging (MRI) RA area metrics in the setting of PAH in which patients have varying degrees of RV failure, and the correlation with invasive haemodynamics and prediction of mortality in clinical populations remains unknown.

As described in Chapter 5 and Chapter 6, we developed a quantitative cardiac MRI-based automated artificial intelligence (AI) analysis of the RA in a large cohort of patients with heart failure and PAH with varying aetiology and disease severity, and (i) determined the failure rate of the model in a large clinical registry and (ii) evaluated interstudy repeatability. The aim of this study was to directly compare the association of manual RA area and AI RA area with invasive haemodynamics and evaluate RA measurements as predictors of mortality.

7.2 Methods

7.2.1 Study Population

The study included 400 patients with cardiac MRI studies for clinical testing from the ASPIRE registry (ASPIRE, ref: c06/Q2308/8). The inclusion criteria require that the patients must have undergone MRI between January 2008 and July 2016 and must have met the haemodynamic criteria for PAH. On the other hand, the exclusion criteria require that patients who could not tolerate MRI were not included in the study. In addition, patients whose MRI images were not of diagnostic quality for analysis were also excluded from the study. This means that only patients who could undergo MRI and whose images were of sufficient quality for analysis were included in the study. Consent was waived for analysis of retrospective cases.

7.2.2 Cardiac MRI Protocol

This cohort consisted of GE studies acquired in a clinical setting in the ASPIRE registry. Cardiac MRI studies in this cohort were performed using a whole-body scanner at 1.5T (HDx (General Electric Healthcare) (Lewis et al., 2020). Cine cardiac MRI acquisitions were made using a balanced steady state free precession (bSSFP) sequence. Following planning sequences, 4-chamber cine images were acquired. A stack of short axis images was acquired covering apex to base. Slice thickness and number of cardiac phases were 8 mm with 20 phases.

7.2.3 Image Analysis

Four observers, SA, FA, KK and AJS (with 2, 3, 13 and 11 years of cardiac MRI experience, respectively) manually drew LV and RV and atrial contours in 4-chamber cine cardiac MRI views on all cardiac phases for the training and testing cohorts. All contours were drawn with observers blinded to the patient's clinical information. All manual contours were reviewed by

an expert cardiac MRI reader (AJS). RV endocardial and epicardial surfaces were also manually traced from the stack of short-axis cine images to obtain RV volumetric and functional measurements as previously described (Alabed et al., 2022). MASS software (research version 2020; Leiden University Medical Center, Leiden, the Netherlands) was used for the manual contouring for developing the algorithm and repeatability testing).

7.2.4 Deep Learning Training

Cardiac MRI studies including a random selection of patients from the ASPIRE registry, subjects from Leeds, and from Leiden University Medical Centre were used for deep learning training. The deep learning training process as described in chapter 5, sub-section 5.2.4.

7.2.5 Association of Cardiac MRI with Invasive Haemodynamics

Correlations with invasive haemodynamics were performed in patients in the ASPIRE registry clinical testing cohort who underwent right heart catheterisation within 48 h of cardiac MRI. The accuracy of RA cardiac MRI measurements to predict ESC/ERS mean RAP low and high-risk thresholds of 8 mmHg and 14 mmHg, respectively, was assessed.

7.2.6 Statistical Analysis

Continuous variables are presented as proportions and mean ± standard deviation. Normal distribution assessed by visual inspection of histograms and using the Shapiro–Wilk test. Pearson's correlation coefficient was used to compare RHC to RA area measurements. Univariate Cox regression Hazard ratios were calculated for AI and manual RA measurements to estimate the prognostic significance. Accuracy of RA measurements to predict RA thresholds performed using receiver operating characteristic analysis. Statistical analysis was carried out using SPSS (version 26, Statistical Package for the Social Sciences, International

Business Machines, Inc., Armonk, New York, USA), and a *P* value of 0.05 or less was considered statistically significant. For data presentation, GraphPad Prism (version 9.1.0, GraphPad Software, San Diego, California, USA) software was used.

7.3 Results

7.3.1 Patients

The characteristics for the clinical testing cohort are presented in Table 7.1. In this cohort, 218 of the 400 patients had died (54.5%) during a mean follow-up period of 1-year.

Table 7. 1 Demographics, MRI and haemodynamics measurements

	Clinical testing (*n = 400*)
Demographics	
Age, yr	55.4 ± 16.4
Sex, F/M (F %)	283/117 (71)
BSA (m^2)	1.8 ± 0.2
WHO FC I, *n* (%)	2 (1)
WHO FC II, *n* (%)	21 (5)
WHO FC III, *n* (%)	338 (85)
WHO FC IV, *n* (%)	36 (9)
Diagnosis, *n* (%)	
PAH	400 (100)
Haemodynamics	
mRAP, mmHg	10.4 ± 6.0
mPAP, mmHg	48.0 ± 13.7
PAWP, mmHg	10.3 ± 2.9
Cardiac output L/min	4.9 ± 1.5
Cardiac index, L/min/m^2	2.8 ± 0.9
PVR, dynes/m^2	720.0 ± 419.4
MvO_2, %	63.5 ± 9.1
Cardiac MRI volumetric measurements	
RVESVi, ml/m^2	46.8 ± 28.2
RVEDVi, ml/m^2	72.7 ± 35.5
RVSVi, ml/m^2	25.9 ± 12.7
RVEF, %	39.1 ± 14.1
Cardiac MRI area measurements	
Automatic max RA area, cm^2	25.5 ± 9.8
Manual max RA area, cm^2	26.0 ± 10.3
Automatic min RA area, cm^2	18.4 ± 9.4
Manual min RA area, cm^2	19.3 ± 10.1

Definition of abbreviations: MRI = magnetic resonance imaging; BSA = body surface area; WHO FC = World Health Organisation functional class; CTEPH = chronic thromboembolic pulmonary hypertension; PAH = pulmonary arterial hypertension; PH = pulmonary hypertension; RHC = right heart catheterization; mRAP = mean right atrial pressure; mPAP = mean pulmonary arterial pressure; PAWP = pulmonary arterial wedge pressure; PVR = pulmonary vascular resistance; MvO_2 = mixed venous oxygen saturation; RVESVi = right ventricular end-systolic volume index; RVEDVi = right ventricular end-diastolic volume index; RVSVi = right ventricular stroke volume index; RVEF = right ventricular ejection fraction; max = maximal; min = minimal; RA = right atrial. Data presented as mean ± standard deviation. Reproduced with permission (Alandejani et al., 2022a).

7.3.2 Clinical Testing Cohort

In the clinical testing cohort (n = 400), RA area measurements made by AI and observers were comparable (Table 7.1). In the clinical testing cohort, both manual and AI maximal RA area predicted overall all-cause mortality with similar predictive values, (hazard ratio 1.02 (95% confidence interval 1.01 to 1.03) and 1.02 (95% confidence interval 1.01 to 1.03) respectively, both $p < 0.01$). Manual and AI minimal RA area also showed a similar predicted mortality hazard ratio of 1.03 (95% confidence interval 1.01 to 1.02) and 1.02 (95% confidence interval 1.01 to 1.03), respectively, both $p < 0.01$.

Of the 400 patients identified for the clinical testing cohort, 212 patients underwent cardiac MRI and right heart catheterization (RHC) within 48-hr. Moderate positive correlations were found between RA area measurements and mean RAP (mRAP) (AI, $r = 0.64$ and manual, $r = 0.57$). Moderate correlations of AI maximal RA area measurements with all invasive haemodynamics were found, see Table 7.2. The strongest correlation was found between minimal RA area and mRAP, $r = 0.66$), see Table 7.3.

Table 7. 2 Pearson correlation for the relation of max RA measurements with RHC parameters

RHC parameters	Manual max RA area (n = 212)		Automatic max RA area (n = 212)	
	r	***p***	**r**	***p***
mRAP	0.57	<0.001	0.64	<0.001
mPAP	0.38	<0.001	0.46	<0.001
Cardiac index	-0.36	<0.001	-0.45	<0.001
PVR	0.36	<0.001	0.47	<0.001
SvO2	-0.41	<0.001	-0.48	<0.001

Definition of abbreviations: RA = right atrial; max = maximal; RHC = right heart catheterization; mRAP = mean right atrial pressure; mPAP = mean pulmonary arterial pressure; PVR = pulmonary vascular resistance; MvO_2 = mixed venous oxygen saturation. Reproduced with permission (Alandejani et al., 2022a).

Table 7. 3 Pearson correlation for the relation of min RA measurements with RHC parameters

RHC parameters	Manual min RA area (n = 212)		Automatic min RA area (n = 212)	
	r	***p***	**r**	***p***
mRAP	0.57	<0.001	0.66	<0.001
mPAP	0.40	<0.001	0.50	<0.001
Cardiac index	-0.39	<0.001	-0.50	<0.001
PVR	0.40	<0.001	0.54	<0.001
SvO2	-0.44	<0.001	-0.55	<0.001

Definition of abbreviations: RA = right atrial; min = minimal; RHC = right heart catheterization; mRAP = mean right atrial pressure; mPAP = mean pulmonary arterial pressure; PVR = pulmonary vascular resistance; MvO_2 = mixed venous oxygen saturation. Reproduced with permission (Alandejani et al., 2022a).

Maximal RA area could accurately predict mRAP low and high ESC/ERS risk thresholds (area under the receiver operating characteristic curve AI = 0.82 vs manual = 0.78 to identify low-risk patients with mRAP ≤ 8 mmHg and AI = 0.87 vs manual = 0.83 to identify high-risk patients with mRAP > 14 mmHg). Minimal RA area had a marginally highest accuracy for prediction of elevated mRAP, the strongest prediction was for mPAP > 14, area under the curve (AUC) 0.90, see Figure 7.1. In comparison with manual measurements, automatic maximal RA area was not more accurate for detection of patients with mRAP > 8 mmHg and mRAP > 14 mmHg, (p = 0.11) and (p = 0.13), respectively. Automatic contouring of minimal RA area trended to suggest higher accuracy for predicting elevated mRAP > 8 mmHg and mRAP > 14 mmHg than manual measurements (p = 0.05) (p = 0.06), respectively; however, these results are not of statistical significance.

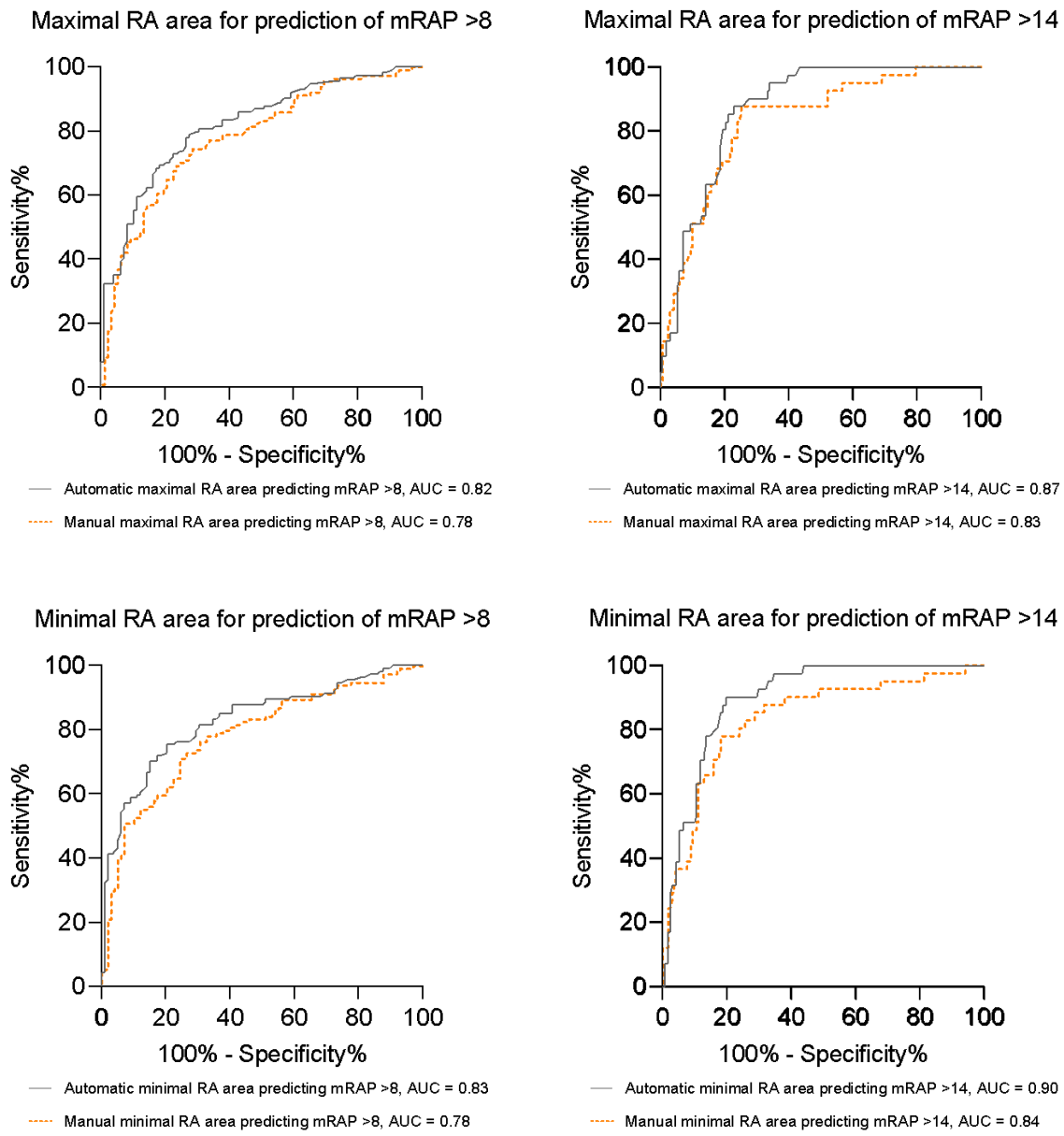

Figure 7. 1 ROC curves and RA area measurements

ROC curves showing the accuracy of RA area measurements to predict mRAP at ESC/ERS guidelines risk thresholds. ROC = receiver operating characteristic; RA = right atrial; mRAP = mean right atrial pressure; ESC/ERS = European Society of Cardiology and European Respiratory Society; AUC = area under the curve. Reproduced with permission (Alandejani et al., 2022a).

7.4 Discussion

RA area measurements moderately correlate with invasive haemodynamics, AI measurements can identify mRAP prognostic thresholds with more confidence than manual measurements, and RA area measurements predict mortality with similar accuracy to manual measurements. The ASPIRE registry includes a wide range of pathology including PAH, left heart failure, lung disease, chronic thromboembolic disease and patients found to have normal invasive haemodynamics. The AI 'seeing' a wider range of pathology is of paramount importance (Chen et al., 2020). This is the first study to compare AI and manual measurements with invasive haemodynamic measurements of RAP.

Here in this diverse population we identify a close correlation of AI RA area measurements with invasive mRAP, this combined with the low scan-rescan variability supports its potential use as a clinical tool. We show that RA area measurements using AI are prognostic to a similar level as manual measurements. Further work to evaluate AI metrics in risk stratification is required, as has been achieved for RV measurements (Lewis et al., 2020). In addition, further work will be to clinically evaluate the range of physiological parameters that can be extracted from the AI segmentations, such as RA strain (Maceira et al., 2016, Xie et al., 2020) and potentially reservoir and conduit function (Truong et al., 2020, Qu et al., 2021). RHC measurements correlated moderately with AI RA measurements, indicating AI metrics may provide physiologically accurate measures of pathophysiological changes in the heart, given their high consistency and repeatability.

7.5 Limitations and Future Work

This is a single centre clinical testing of an AI algorithm developed in a multi-vendor multicentre cohort, with the clinical testing in the setting of a tertiary referral centre for patients

with PAH. The imaging appearances and patient populations are likely representatives of other PAH referral centres.

This study clinically tested an AI model for RA area estimation rather than volume. The rationale was to automate and evaluate measurements made clinically and consistent with the ESC/ERS guidelines in PAH. Further work to develop and clinically test a 3-dimensional or multislice RA volumetric model would be of value and work to extract physiological parameters previously suggested to be important (Sato et al., 2015) may be of benefit in future studies.

7.6 Conclusion

In this study, we have clinically validated an AI model to fully automate cardiac MRI RA area measurements. The data suggest AI-derived RA measurements are moderately related to mean right atrial pressure.

Chapter 8: Imaging and Risk Stratification in Pulmonary Arterial Hypertension: Time to Include Right Ventricular Assessment

This chapter is based on a published paper for which I was the first author (Alandejani et al., 2022b). My contribution to this work was in the generation of the idea, image analysis, data collection, statistical analysis, tables, figures and the writing. Co-authors have interpreted the data and assisted in writing the paper.

8.1 Introduction

Pulmonary arterial hypertension (PAH) is a progressive life-shortening condition. The European Society of Cardiology and European Respiratory Society (ESC/ERS) guidelines stratified patients with PAH into three groups; low-risk (<5%), intermediate-risk (5-10%), and high-risk (>10%) of 1-year mortality (Galiè et al., 2015, Galiè et al., 2016, Humbert et al., 2022a). Variables used in risk assessment include symptoms, exercise capacity, haemodynamics and imaging metrics. In PAH, failure of the right ventricle to cope with increased afterload results in haemodynamic changes with rises in right ventricular (RV) end diastolic pressure and right atrial (RA) pressure. An extensive body of literature has shown that cardiac magnetic resonance imaging (MRI) derived RV measurements are prognostic, predict clinical worsening (van de Veerdonk et al., 2011, Alabed et al., 2020, Goh et al., 2020), are sensitive to treatment effect (Swift et al., 2021) and have utility in risk stratification in PAH (Lewis et al., 2020); however, there are limited data on RA area measurements (Darsaklis et al., 2016, Liu et al., 2020). To our knowledge, no study has assessed the accuracy of RA area thresholds to assess risk of 1-year mortality. This study compares RV and RA area measurements as derived from the artificial intelligence tool and their utility to risk stratify patients with PAH, using the reference standard for assessment of cardiac structure and function, by comparing published thresholds for RV metrics (Lewis et al., 2020) with current ESC/ERS thresholds for RA area (Galiè et al., 2015, Galiè et al., 2016, Humbert et al., 2022a).

8.2 Methods

8.2.1 Patients

Consecutive patients with PAH (idiopathic PAH, heritable PAH, and PAH in association with connective tissue disease, congenital heart disease, portal hypertension, human immunodeficiency virus infection, and drugs and toxins) who underwent cardiac MRI between January 2008 and March 2017 were identified from the ASPIRE registry, after a standardised systematic assessment (Hurdman et al., 2012). Patients were required to have mean pulmonary artery pressure ≥25 mmHg and pulmonary arterial wedge pressure ≤15 mmHg at right heart catheter. Incident treatment naïve patients who underwent a cardiac MRI at baseline and who had a further cardiac MRI after a minimum of 3 months and before 31 March 2017 were included in the follow-up cohort. Ethical approval for this single centre study was obtained (ASPIRE, c06/Q2308/8).

8.2.2 Cardiac MRI Acquisition and Image Analysis

Cardiac magnetic resonance imaging studies were completed using an 8-channel cardiac coil on a whole-body scanner at 1.5T GE HDx (GE Healthcare, Milwaukee, WI, United States), as previously described (Lewis et al., 2020). Image analysis was performed on MASS software (MASS, research version 2020; Leiden University Medical Center, Leiden, Netherlands) with the observer blinded to the patient's clinical information, cardiac catheter parameters and outcome data. RA endocardial, and RV endocardial and epicardial surfaces were identified using artificial intelligence software. RA area, and RV volumetric and functional measurements were obtained from the 4-chamber cine images and the stack of short-axis cine images, respectively. RV trabeculations were included in the blood pool. In addition, RA

endocardial surfaces were manually traced to measure manual maximal RA area at RV end systole. The RA appendage was manually excluded during contouring.

8.2.3 Statistical Analysis

Data for continuous variables are displayed as mean ± standard deviation. Survival data were censored on 30 September 2020. Kaplan–Meier survival curves were evaluated using the log rank (Mantel–Cox) test. Locally weighted scatterplot smoothing (LOESS) regression analysis was performed to understand relationships between variables. Binary logistic regression was used to assess predictors of 1-year mortality. A p-value < 0.05 was considered statistically significant.

8.3 Results

8.3.1 Patients

A total of 311 consecutive treatment-naïve patients were identified, and 121 patients underwent follow-up cardiac MRI at a mean interval of 1.9 ± 1.8 years. The mean age was 56.7 ± 16.1 years, and 72% of patients were female. The majority (82%) had idiopathic/heritable PAH (33%), and PAH in association with connective tissue disease (49%) including 117 patients with systemic sclerosis (38%). Data for demographics, haemodynamics and cardiac MRI metrics at baseline are shown in Table 8.1. The mean interval between the date of diagnosis and baseline cardiac MRI (n = 311) was 1.2 ± 6.5 months, and between the date of diagnosis and follow-up cardiac MRI (n = 121) was 1.8 ± 1.7 years.

Table 8. 1 Baseline demographics, haemodynamics and cardiac MRI Metrics

	Baseline (*n = 311*)	IPAH/HPAH (*n = 101*)	PAH-CTD (*n = 154*)	PAH-CHD (*n = 24*)	PoPH (*n = 22*)	Other PAH (*n = 10*)
Demographics						
Age, yr	56.7 ± 16.1	50.9 ± 17.6	63.2 ± 13.0	48.0 ± 18.1	53.5 ± 11.0	43.3 ± 6.1
Sex, F/M (F %)	223/88 (72)	70/31 (69)	119/35 (77)	20/4 (83)	12/10 (55)	2/8 (20)
WHO FC I, *n* (%)	1 (1)	0 (0)	0 (0)	1 (4)	0 (0)	0 (0)
WHO FC II, *n* (%)	14 (4)	5 (5)	4 (3)	2 (8)	2 (9)	1 (10)
WHO FC III, *n* (%)	261 (84)	76 (75)	137 (89)	20 (87)	19 (86)	9 (90)
WHO FC IV, *n* (%)	34 (11)	20 (20)	13 (8)	0 (0)	1 (5)	0 (0)
PAH subtype, *n* (%)						
IPAH/HPAH	101 (33)					
PAH-CTD	154 (49)					
PAH-CHD	24 (8)					
PoPH	22 (7)					
Other	10 (3)					
Haemodynamics						
mRAP, mm Hg	10 ± 6	12 ± 6	9 ± 6	11 ± 5	11 ± 7	15 ± 8
mPAP, mm Hg	48 ± 14	57 ± 12	41 ± 12	55 ± 8	46 ± 8	52 ± 6
PAWP, mm Hg	10 ± 3	11 ± 3	10 ± 3	11 ± 3	11 ± 3	13 ± 2
Cardiac output L/min	4.8 ± 1.5	4.3 ± 1.3	5.0 ± 1.5	6.0 ± 1.4	5.6 ± 1.7	5.5 ± 0.6
Cardiac index, L/min/m^2	2.7 ± 0.9	2.4 ± 0.8	2.9 ± 0.8	3.0 ± 0.6	3.1 ± 1.6	2.8 ± 0.5
PVR, dynes/m^2	728 ± 420	976 ± 404	596 ± 393	640 ± 214	540 ± 189	593 ± 87
MvO_2, %	63.4 ± 9.2	59.8 ± 8.0	65.1 ± 8.9	73.3 ± 10.9	67.8 ± 7.0	56.8 ± 12.8
Right atrial measurement						
Manual RA area, cm^2	25.6 ± 9.5	27.2 ± 10.2	24.2 ± 8.4	28.3 ± 10.7	24.3 ± 9.7	28.4 ± 11.4
Automatic RA area, cm^2	25.3 ± 9.3	26.5 ± 10.3	24.0 ± 8.5	26.2 ± 8.6	24.7 ± 9.6	31.6 ± 8.9
Automatic right ventricle measurements						
RVESVi, ml/m^2	73.6 ± 34.0	84.9 ± 31.7	63.6 ± 31.4	85.7 ± 43.9	66.7 ± 28.4	100.2 ± 27.5
RVESVi %pred	301.8 ± 141.5	69.5 ± 22.4	75.7 ± 21.6	103.2 ± 63.6	81.0 ± 28.3	76.8 ± 31.3
RVEDVi, ml/m^2	110.8 ± 37.1	119.4 ± 34.7	99.9 ± 33.6	135.9 ± 43.5	107.4 ± 35.1	141.3 ± 38.8
RVSVi, ml/m^2	37.2 ± 13.8	34.5 ± 10.6	36.3 ± 10.2	50.2 ± 28.8	40.8 ± 14.3	41.0 ± 16.8
RVEF, %	35.8 ± 12.8	30.1 ± 9.6	39.2 ± 12.7	38.1 ± 17.6	39.2 ± 12.2	28.8 ± 7.5
RVEF %pred	53.3 ± 18.5	45.6 ± 14.6	57.3 ± 18.3	57.8 ± 25.3	59.0 ± 18.0	44.7 ± 11.4

Definition of abbreviations: MRI = magnetic resonance imaging; WHO FC = World Health Organisation functional class; PAH = pulmonary arterial hypertension; IPAH = idiopathic pulmonary arterial hypertension; HPAH = heritable pulmonary arterial hypertension; PAH-CTD = pulmonary arterial hypertension associated with connective tissue disease; PAH-CHD = pulmonary arterial hypertension associated with congenital heart disease; PoPH = portopulmonary hypertension; mRAP = mean right atrial pressure; mPAP = mean pulmonary arterial pressure; PAWP = pulmonary arterial wedge pressure; PVR = pulmonary vascular resistance; MvO_2 = mixed venous oxygen saturation; RA = right atrial; %pred = percentage predicted for age and sex; RVESVi = right ventricular end-systolic volume index; RVEDVi = right ventricular end-diastolic volume index; RVSVi = right ventricular stroke volume index; RVEF = right ventricular ejection fraction. Data are shown as mean ± standard deviation unless otherwise stated. Adapted with permission (Alandejani et al., 2022b).

8.3.2 Survival

One-year following the baseline cardiac MRI, 29 of 311 incident treatment-naïve patients had died (9.3%). Of 121 patients who underwent repeat cardiac MRI, 13 (10.7%) died within 1-year of follow-up cardiac MRI. Using ESC/ERS RA area risk thresholds for 1-year mortality, both manual and automatic RA area stratified patients into intermediate and high-risk at baseline and follow-up, but was not able to identify a low-risk group either at baseline or at follow-up (Figure 8.1). In contrast, using previously published thresholds (Lewis et al., 2020) for automatic RV measurements, right ventricular end systolic volume index (RVESVi), percentage predicted RVESVi and percentage predicted right ventricular ejection fraction (RVEF) low and high-risk groups were identified at baseline and follow-up. RVEF was able to identify low, intermediate and high-risk patients at baseline and intermediate and high-risk patients at follow-up.

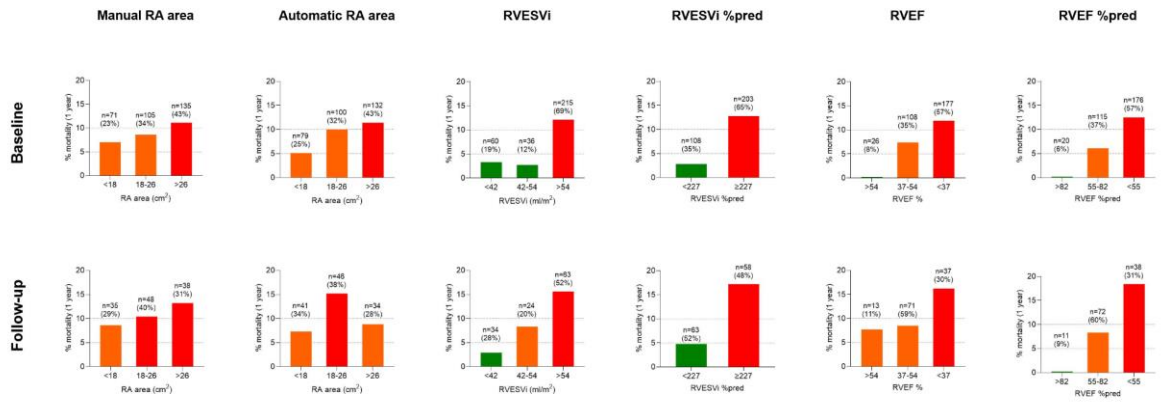

Figure 8. 1 Bar charts displaying cardiac MRI RA area and RV metrics

cardiac MRI RA area thresholds based on ESC/ERS guidelines and RV metrics based on published thresholds, and percentage mortality at 1-year for treatment naïve patients at (top) baseline (n=311) and (bottom) follow-up (n=121). MRI = magnetic resonance imaging; RA = right atrial; ESC/ERS = European Society of Cardiology and European Respiratory Society; RV = right ventricular; %pred = percentage predicted for age and sex; RVESVi = right ventricular end-systolic volume index; RVEF = right ventricular ejection fraction. Adapted with permission (Alandejani et al., 2022b).

Kaplan–Meier analysis showing survival at baseline and follow-up and risk transition at follow-up are shown in Figure 8.2. Baseline patients with manual RA area <18 cm^2 (23% of patients) and 18–26 cm^2 (34% of patients) had 1-year survival of 92.5% and 90.6%, respectively, while patients with manual RA area of >26 cm^2 (43% patients) had 1-year survival of 87.7%. Moreover, baseline patients with percentage predicted RVESVi <227 (35% of patients) had 1-year survival of 97.5%, while patients with percentage predicted RVESVi ≥227 (65% of patients) had 1-year survival of 87.2%. Using manual RA area at follow-up for low risk (29% of patients) and intermediate risk (40% of patients), 1-year survival was 91.3 and 90.1%, respectively, while for high risk (31% patients), 1-year survival was 85.5%. Additionally, using percentage predicted RVESVi at follow-up low risk (52% of patients), 1-year survival was 96.9%, while for high risk (48% patients), 1-year survival was 83.5%.

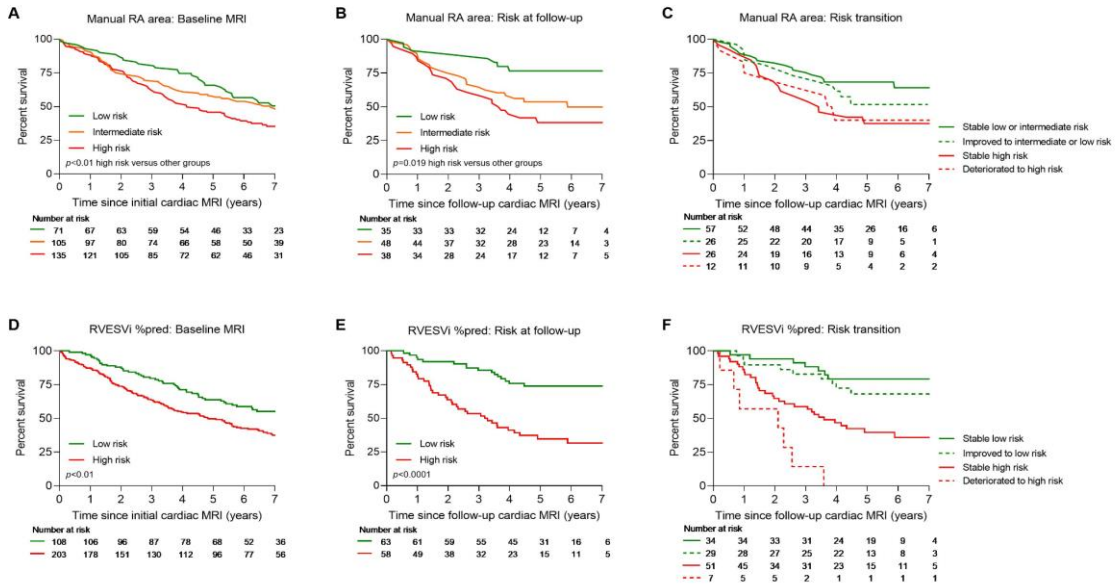

Figure 8. 2 Kaplan–Meier survival curves for RA area measurements

(A–F) Kaplan–Meier survival curves for treatment naïve patients for manual RA area at baseline (A), manual RA area at follow-up cardiac MRI (B), transition of risk between baseline and follow-up cardiac MRI for manual RA area (C), RVESVi %pred at baseline (D), RVESVi %pred at follow-up cardiac MRI (E), transition of risk between baseline and follow-up cardiac MRI for RVESVi %pred (F). MRI = magnetic resonance imaging; RA = right atrial; %pred = percentage predicted for age and sex; RVESVi = right ventricular end-systolic volume index. Adapted with permission (Alandejani et al., 2022b).

A multi-variable binary logistic regression was carried out to assess the effect of age, sex, World Health Organisation functional class, percentage predicted RVESVi, RVEF, and manual RA area on the likelihood of 1-year mortality. It was found that age (Wald = 114.11, $p < 0.01$, odds ratio = 1.07 [95% confidence interval (CI): 1.03, 1.10]) as well as RVEF (Wald = 8.05, $p < 0.01$, odds ratio = 0.95 [95% CI: 0.92, 0.98]), but not manual RA area, were independent predictors of 1-year mortality.

8.4 Discussion

Using cardiac MRI, we have shown that AI measures of RV function and RA area have prognostic value; however, only AI measures of RV function but not ESC/ERS RA area thresholds identify patients at low-risk of 1-year mortality.

The ESC/ERS guidelines recommend that treatment is aimed at achieving and maintaining a low-risk of 1-year mortality (Galiè et al., 2015, Galiè et al., 2016, Humbert et al., 2022a) with patients remaining in an intermediate or high-risk group having significantly higher mortality. Our study using cardiac MRI has shown that although manual and automatic RA measurements can be used to identify intermediate and high-risk patients, the current RA area thresholds do not allow for identification of a low-risk group. Moreover, LOESS analysis shows that the confidence intervals for mortality are large in patients who have a manual measurement of RA area within the normal range (Figure 8.3). Recent publications have highlighted other imaging parameters including measures of RV function that can identify patients at low-risk of 1-year mortality (Alabed et al., 2020, Goh et al., 2020, Lewis et al., 2020). In this study, we have shown that AI RV measurements acquired with inclusion of trabeculations in the blood pool, can also be used to risk stratify patients. Including trabeculations in the blood pool is the most commonly used approach and is less timing consuming as it does not necessitate tracing around trabeculations. A further publication using echocardiography has shown that combining

echocardiographic measures including those that assess RV function (TAPSE, tricuspid regurgitant jet grade and inferior vena cava area), stratified the risk of all-cause mortality in PAH. Inclusion of parameters such as RA area and pericardial effusion did not provide additional prognostic value (Ghio et al., 2020).

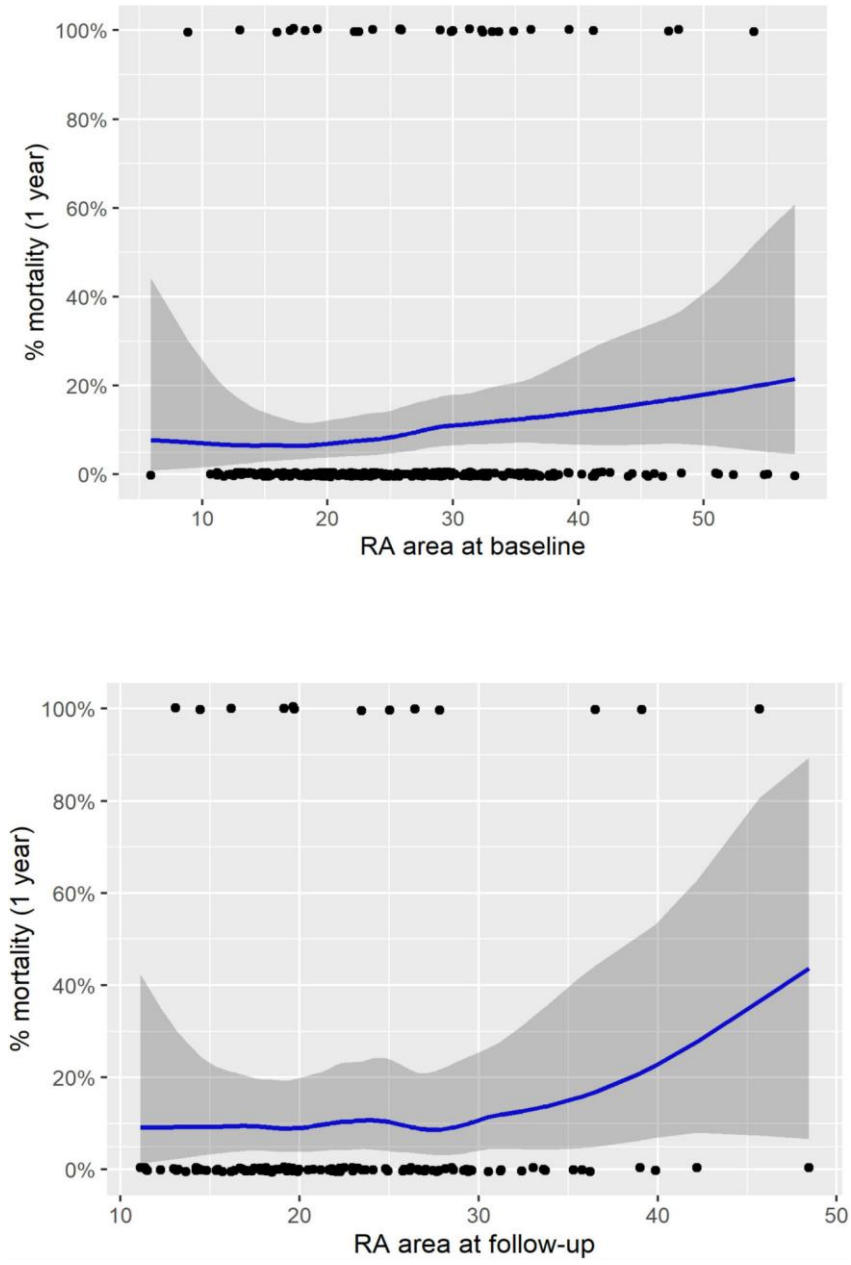

Figure 8. 3 LOESS regression analysis for treatment naïve patients for manual RA area

Manual RA area at baseline (top) and follow-up (bottom). RA = right atrial; LOESS = locally weighted scatterplot smoothing. Reproduced with permission (Alandejani et al., 2022b).

8.5 Limitations and Future Work

This study is limited by its single centre design, nonetheless, it is one of the largest cohorts of patients with PAH to have undergone cardiac MRI. As per ESC/ERS pulmonary hypertension guidelines, we measured RA area. However, we did not evaluate the use of cardiac MRI-derived RV mass, right atrial volume and reservoir function (reservoir, conduit, and contractile functions). Whether other measures of RV mass, and RA volume and/or function provide additional prognostic value requires further study.

In addition, this study does not include a comparison with left ventricular parameters as they are less established in patients with PAH as a prognostic marker, although recent studies have demonstrated that left ventricular parameters have prognostic value (Knight et al., 2015, Alabed et al., 2020, Anton Vonk Noordegraaf et al., 2022) and may have a potential role in the risk stratification of patients with PAH (Lewis et al., 2020).

8.6 Conclusion

In conclusion, this study confirms the prognostic value of AI RA and RV metrics using the reference standard for measures of cardiac structure and function in PAH. However, with respect to risk stratification of PAH, this study highlights the need for guidelines to include measures of RV function rather than relying on RA area alone.

Chapter 9: The Prognostic Role of N-terminal Prohormone Brain Natriuretic Peptide and Cardiac Magnetic Resonance Imaging in Pulmonary Arterial Hypertension

My contribution to this work was in the generation of the idea, image analysis, data collection, statistical analysis, tables, figures and the writing.

9.1 Introduction

Pulmonary arterial hypertension (PAH) is a rare, progressive life-threatening condition which is known to cause endothelial dysfunction and vascular remodelling on branches of the pulmonary arteries, and eventually right ventricular (RV) failure. Two of the main characteristics of PAH at right heart catheterization (RHC) are increased mean pulmonary artery pressure (mPAP) and increased pulmonary vascular resistance (PVR) (Hoeper et al., 2017, Simonneau et al., 2004). The survival of patients with PAH is mainly associated with the progression of RV dysfunction (Kiely et al., 2013). Present-day approaches to evaluate and risk stratify patients depend on assessments of symptoms, haemodynamics, exercise capacity and RV function (Humbert et al., 2022a, Galiè et al., 2019, Benza et al., 2019).

Cardiac magnetic resonance imaging (MRI) is the gold standard test to assess RV function (Swift et al., 2017, Lewis et al., 2020). However, there are a few drawbacks of cardiac MRI as it is expensive, not widely available, some patients feel discomfort during the procedure, and it is contraindicated in patients with internal metallic devices. On the contrary, N-terminal prohormone brain natriuretic peptide (NT-proBNP) is a non-invasive clinical biomarker, a widely available blood test, cost-effective and commonly used in hospitals as an alternative marker of cardiac function (Fu et al., 2018). NT-proBNP is secreted by cardiomyocytes following ventricular stretch and is used as a marker of RV dysfunction (Lador et al., 2014) and is also used to risk assess and manage patients with PAH (Humbert et al., 2022a). However, using both cardiac MRI measurements and NT-proBNP together as a bivariate prognostic marker in PAH has not yet been determined. The aim of this study was to evaluate the prognostic role of cardiac MRI and NT-proBNP simultaneously in patients with PAH.

9.2 Methods

9.2.1 Patients

Consecutive patients with PAH who underwent cardiac MRI and NT-proBNP test between August 2011 and October 2019 were identified from the ASPIRE registry, after a standardised systematic evaluation (Hurdman et al., 2012). Several PAH subtypes included in this study (idiopathic PAH, heritable PAH, PAH in association with connective tissue disease, PAH in association with congenital heart disease, and portopulmonary hypertension). All patients had a right heart catheter and were required to have mean pulmonary artery pressure ≥25 mmHg and pulmonary arterial wedge pressure ≤15 mmHg. Ethical approval for this single centre study was obtained (ASPIRE, c06/Q2308/8).

9.2.2 Cardiac MRI Acquisition

Cardiac MRI studies were performed using a whole-body scanner at 1.5T (Avanto, Siemens Solutions; Signa HDx, GE Healthcare; and Achieva, Philips Healthcare) (Alabed et al., 2022). Cine Cardiac MRI acquisitions were made using a balanced steady state free precession (bSSFP) sequence. Following planning sequences, 4-chamber cine images were acquired. A stack of short axis images was acquired covering apex to base. Slice thickness and number of cardiac phases were 8 mm with 20 phases (Alandejani et al., 2022b).

9.2.3 Image Analysis

Image analysis was performed on MASS software (MASS, research version 2020; Leiden University Medical Center, Leiden, Netherlands) with the observer blinded to the patient's clinical information, cardiac catheter parameters and outcome data. Right atrial (RA) endocardial, and RV endocardial and epicardial surfaces were identified using artificial intelligence software with manual correction as required. RA area, and RV volumetric and

functional measurements were obtained from the 4-chamber cine images and the stack of short-axis cine images, respectively. RV trabeculations were included in the blood pool. The RA appendage was excluded during contouring.

9.2.4 Plasma NT-proBNP Levels

A blood specimen was taken from a peripheral vein whilst the patient was at rest, within an average of 43 days of MRI measurements. NT-proBNP plasma levels were analysed on Luminex 100/200 multiplex analyser utilising the cardiovascular marker kit (HCVD1MAG-67K Millipore).

9.2.5 Right Heart Catheterization

When performing the right heart catheterization, a balloon-tipped 7.5F thermodilution catheter is used (Becton-Dickson, Franklin, NJ). This operation (right heart catheterization) is usually executed using a Swan-Ganz Catheter via the internal jugular vein. Cardiac output was determined by thermodilution technique. PVR was measured by this equation: PVR = (mPAP – PAWP)/cardiac output.

9.2.6 Statistical Analysis

Continuous variables are presented as proportions and mean ± standard deviation. Cardiac MRI volumetric parameters were adjusted for body surface area (BSA) and recorded as index variables. Then, indexed measurements for body surface area were corrected for age and sex, and presented as index percentage predicted. Both cardiac MRI and NT-proBNP measurements were referred to as continuous or categorical variables when needed. Categorical classifications were based on published thresholds (Lewis et al., 2020, Humbert et al., 2022a).

Pearson's correlation coefficient was used to compare continuous log10 (NT-proBNP) to the continuous cardiac MRI parameters. Linear regression analysis was used to estimate the relationship between continuous log10 (NT-proBNP) and continuous cardiac MRI parameters that showed a strong correlation with continuous log10 (NT-proBNP).

Univariate Cox regression hazard ratios were carried out to assess the prognostic value of categorical and continuous cardiac MRI parameters and categorical NT-proBNP levels. Univariate parameters that showed a *P* value of less than 0.2 were entered into the bivariate Cox regression analysis. Survival data were censored on 21 June 2021. Statistical analysis was carried out using SPSS (version 28, Statistical Package for the Social Sciences, International Business Machines, Inc., Armonk, New York, USA). A *P* value less than 0.05 was considered statistically significant.

9.3 Results

9.3.1 Patients

One hundred twenty-one patients were identified with PAH and underwent cardiac MRI and NT-proBNP test. The mean interval between the date of cardiac MRI and NT-proBNP test was 1.4 ± 3.5 months. The mean age was 58.9 ± 15.6 years, and 76% of patients were female. The majority (94%) of patients had PAH in association with connective tissue disease (57%) and idiopathic/heritable PAH (37%). Data for demographics, haemodynamics, NT-proBNP and cardiac MRI metrics are shown in Table 9.1.

Table 9. 1 Baseline demographics, haemodynamics, NT-proBNP and MRI measurements

	Patients with PAH (*n* = 121)	Survivors (*n* = 92)	Nonsurvivors (*n* = 29)
Demographics			
Age, yr	58.9 ± 15.6	56.6 ±15.5	66.4 ± 13.6
Sex, F/M (F %)	92/29 (76)	68/24 (74)	24/5 (83)
WHO FC I, *n* (%)	0 (0)	0 (0)	0 (0)
WHO FC II, *n* (%)	7 (6)	6 (7)	1 (3)
WHO FC III, *n* (%)	107 (89)	81 (88)	26 (90)
WHO FC IV, *n* (%)	6 (5)	4 (5)	2 (7)
PAH subtype, *n* (%)			
IPAH/HPAH	37 (31)	31 (34)	6 (21)
PAH-CTD	57 (47)	38 (41)	19 (66)
PAH-CHD	21 (17)	18 (20)	3 (10)
PoPH	6 (5)	5 (5)	1 (3)
Haemodynamics			
mRAP, mm Hg	8 ± 5	8 ± 5	8 ± 6
mPAP, mm Hg	48 ± 16	49 ± 18	44 ± 12
PAWP, mm Hg	9 ± 3	9 ± 3	8 ± 3
Cardiac output L/min	4.6 ± 1.7	4.6 ± 1.8	4.6 ± 1.6
Cardiac index, L/min/m^2	2.6 ±1.0	2.6 ± 1.1	2.7 ± 1.0
PVR, dynes/m^2	797.5 ± 475.3	825.0 ± 509.1	724.5 ± 66.8
MvO_2, %	66.6 ± 10.16	66.6 ± 11.2	66.8 ± 7.2
NT-proBNP levels			
NT-proBNP	1951.9 ± 3610.0	1313.5 ± 2164.4	3977.0 ± 5919.6
Log10 (NT-proBNP)	2.8 ± 0.7	2.6 ± 0.7	3.1 ± 0.7
Cardiac MRI measurements			
RVESVi	70.5 ± 34.4	69.2 ± 35.6	74.8 ± 30.3
RVESVi %pred	298.5 ±140.9	280.2 ± 131.7	356.6 ± 155.3
RVEDVi	112.2 ± 41.2	111.3 ± 42.7	114.9 ± 36.4
RVEDVi %pred	154.2 ± 54.9	149.7 ± 53.4	168.3 ± 57.9
RVEF	39.1 ± 12.3	40.1 ± 12.3	35.7 ± 11.9
RVEF %pred	57.8 ± 18.4	59.8 ± 18.5	51.6 ± 17.0
LVEDVi	72.5 ± 22.5	73.5 ± 24.0	69.2 ± 16.8
LVEDVi %pred	99.1 ± 29.9	99.4 ± 31.5	98.2 ± 24.6
LVSV	72.5 ± 29.8	73.8 ± 31.7	68.6 ± 22.7
RA area	24.2 ± 9.4	24.2 ± 9.8	24.1 ± 8.2
RAEF	0.5 ± 0.2	0.5 ± 0.2	0.4 ± 0.1

Definition of abbreviations: PAH = pulmonary arterial hypertension; WHO FC = World Health Organisation functional class; IPAH = idiopathic pulmonary arterial hypertension; HPAH = heritable pulmonary arterial hypertension; PAH-CTD = pulmonary arterial hypertension associated with connective tissue disease; PAH-CHD = pulmonary arterial hypertension associated with congenital heart disease; PoPH = portopulmonary hypertension; mRAP = mean right atrial pressure; mPAP = mean pulmonary arterial pressure; PAWP = pulmonary arterial wedge pressure; PVR = pulmonary vascular resistance; MvO_2 = mixed venous oxygen saturation; NTpro-BNP = N-terminal prohormone brain natriuretic peptide; log10 = logarithm with a base equal to 10; MRI = magnetic resonance imaging; %pred = percentage predicted for age and sex; RVESVi = right ventricular end-systolic volume index; RVEDVi = right ventricular end-diastolic volume index; RVEF = right ventricular ejection fraction; LVEDVi = left ventricular end-diastolic volume index; LVSV = left ventricular stroke volume; RA = right atrial; RAEF = right atrial ejection fraction.

9.3.2 Correlations

Strong correlation was found between continuous log10 (NT-proBNP) and continuous percentage predicted right ventricular end systolic volume index (RVESVi) (r = 0.65, *P* < 0.001), see Figure 9.1. Moderate correlations of continuous log10 (NT-proBNP) with continuous left ventricular stroke volume, continuous RA measurements and all continuous RV measurements included in this study, apart from continuous percentage predicted RVESVi, were found. Weak correlation was found between continuous log10 (NT-proBNP) and continuous left ventricular end diastolic volume index (r = -0.26, *P* = 0.003), see Table 9.2.

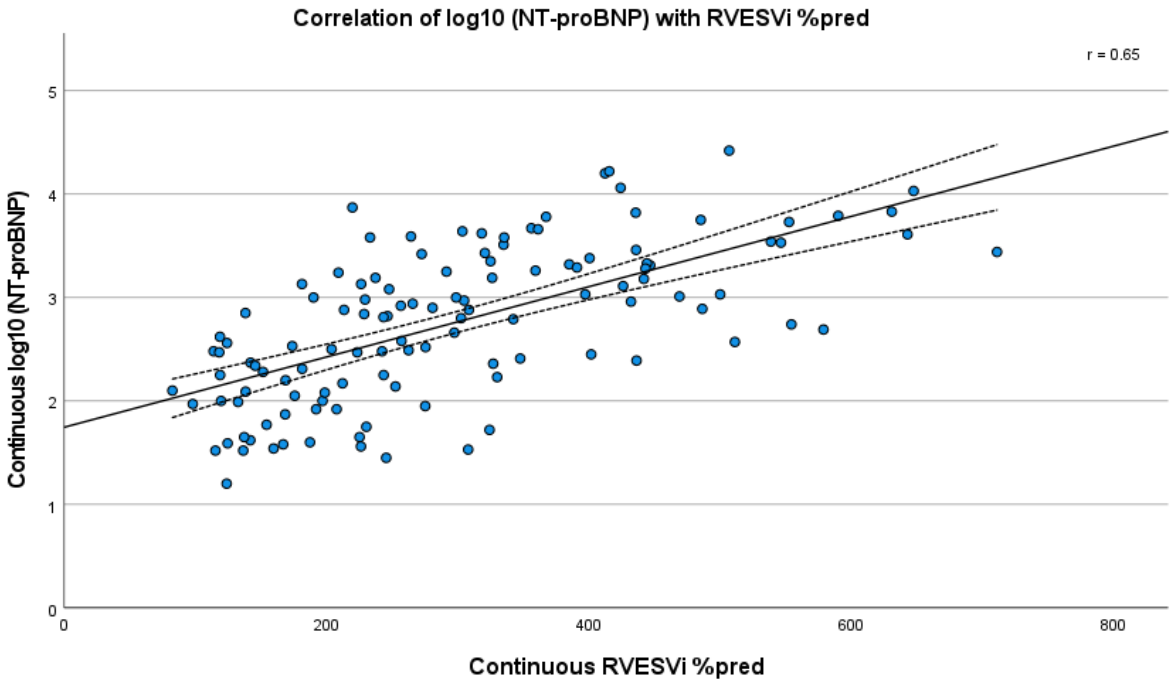

Figure 9. 1 Scatter plot of NTpro-BNP and RV measurement

Showing the relationship of continuous log10 (NTpro-BNP) versus continuous percentage predicted RVESVi. Log10 = logarithm with a base equal to 10; NTpro-BNP = N-terminal prohormone brain natriuretic peptide; %pred = percentage predicted for age and sex; RVESVi = right ventricular end-systolic volume index.

Table 9. 2 Relationships between continuous MRI and continuous log10 (NTpro-BNP)

Cardiac MRI parameters	Log10 (NTpro-BNP) (n = 121)	
	r	***p***
RVESVi	0.53	<0.001
RVESVi %pred	0.65	<0.001
RVEDVi	0.42	<0.001
RVEDVi %pred	0.52	<0.001
RVEF	-0.54	<0.001
RVEF %pred	-0.59	<0.001
LVEDVi	-0.26	0.003
LVEDVi %pred	-0.19	0.041
LVSV	-0.41	<0.001
RA area	0.42	<0.001
RAEF	-0.50	<0.001

Definition of abbreviations: MRI = magnetic resonance imaging; log10 = logarithm with a base equal to 10; NTpro-BNP = N-terminal prohormone brain natriuretic peptide; %pred = percentage predicted for age and sex; RVESVi = right ventricular end-systolic volume index; RVEDVi = right ventricular end-diastolic volume index; RVEF = right ventricular ejection fraction; LVEDVi = left ventricular end-diastolic volume index; LVSV = left ventricular stroke volume; RA = right atrial; RAEF = right atrial ejection fraction.

A simple linear regression was carried out to test if continuous percentage predicted RVESVi significantly predicted continuous log10 (NTpro-BNP). The results of the regression indicated that the model explained 42% of the variance and that the model was significant, $F(1,119) = 86$, $p<.001$. It was found that continuous percentage predicted RVESVi significantly predicted continuous log10 (NTpro-BNP) ($\beta1 = 0.003$, $p<.001$).

9.3.3 Survival

During the mean follow-up period (2.9 years), 29 of 121 (24%) patients died. Categorical NT-proBNP ($P = 0.016$) and continuous percentage predicted right ventricular end diastolic volume index ($P = 0.044$) were associated with adverse outcome at univariate Cox regression analysis. Continuous percentage predicted RVESVi ($P = 0.004$) was the strongest predictor of mortality from univariate Cox regression analysis (Table 9.3 and 9.4).

Table 9. 3 Univariate Cox regression hazard ratios for categorical parameters

Categorical parameters	Overall mortality (29 deaths), *n* = 121	
	Hazard ratio (95% confidence interval)	***P* value**
NT-proBNP	1.175 (1.110–2.763)	0.016
RVESVi	1.392 (0.836–2.319)	0.203
RVESVi %pred	2.062 (0.879–4.841)	0.096
RVEF	1.615 (0.893–2.923)	0.113
RVEF %pred	1.734 (0.913–3.293)	0.093
LVEDVi	0.710 (0.288–1.749)	0.456
LVEDVi %pred	0.796 (0.399–1.591)	0.519
RA area	0.967 (0.625–1.496)	0.880

Definition of abbreviations: MRI = magnetic resonance imaging; NTpro-BNP = N-terminal prohormone brain natriuretic peptide; %pred = percentage predicted for age and sex; RVESVi = right ventricular end-systolic volume index; RVEF = right ventricular ejection fraction; LVEDVi = left ventricular end-diastolic volume index; RA = right atrial.

Table 9. 4 Univariate Cox regression hazard ratios for continuous MRI parameters

Continuous parameters	Overall mortality (29 deaths), *n* = 121	
	Hazard ratio (95% confidence interval)	***P* value**
RVESVi	1.005 (0.994–1.015)	0.378
RVESVi %pred	1.004 (1.001–1006)	0.004
RVEDVi	1.003 (0.994–1.012)	0.486
RVEDVi %pred	1.006 (1.000–1.013)	0.044
RVEF	0.978 (0.950–1.006)	0.125
RVEF %pred	0.981 (0.962–1.000)	0.054
LVEDVi	0.999 (0.981–1.017)	0.874
LVEDVi %pred	1.004 (0.992–1.017)	0.524
LVSV	0.997 (0.983–1.011)	0.643
RA area	0.996 (0.958–1.035)	0.848
RAEF	0.083 (0.005–1.428)	0.086

Definition of abbreviations: MRI = magnetic resonance imaging; %pred = percentage predicted for age and sex; RVESVi = right ventricular end-systolic volume index; RVEDVi = right ventricular end-diastolic volume index; RVEF = right ventricular ejection fraction; LVEDVi = left ventricular end-diastolic volume index; LVSV = left ventricular stroke volume; RA = right atrial; RAEF = right atrial ejection fraction.

Tables 9.5 and 9.6 present the results of bivariate analysis of categorical NTpro-BNP on categorical and continuous covariate predictors of mortality. The prognostic value of categorical NTpro-BNP was not independent of any of the categorical or continuous RV volumetric measurements, or continuous right atrial ejection fraction.

Table 9. 5 Bivariate Cox regression hazard ratios for categorical NT-proBNP vs categorical MRI

Categorical parameters	Hazard ratio of covariate with categorical NT-proBNP	*P* value	Hazard ratio of categorical NT-proBNP with covariate	*P* value
RVESVi %pred	1.081 (0.343–3.406)	0.894	1.702 (0.920–3.150)	0.090
RVEF	1.076 (0.522–2.218)	0.842	1.691 (0.956–2.990)	0.071
RVEF %pred	1.088 (0.482–2.459)	0.838	1.683 (0.928–3.049)	0.086

Definition of abbreviations: MRI = magnetic resonance imaging; NTpro-BNP = N-terminal prohormone brain natriuretic peptide; %pred = percentage predicted for age and sex; RVESVi = right ventricular end-systolic volume index; RVEF = right ventricular ejection fraction.

Table 9. 6 Bivariate Cox regression hazard ratios for categorical NT-proBNP vs continuous MRI

Continuous parameters	Hazard ratio of covariate with categorical NT-proBNP	*P* value	Hazard ratio of categorical NT-proBNP with covariate	*P* value
RVESVi %pred	1.003 (0.999–1.006)	0.107	1.329 (0.748–2.361)	0.332
RVEDVi %pred	1.003 (0.996–1.011)	0.407	1.580 (0.940–2.656)	0.084
RVEF	1.002 (0.965–1.041)	0.910	1.790 (0.987–3.248)	0.055
RVEF %pred	0.995 (0.968–1.002)	0.717	1.623 (0.879–2.996)	0.122
RAEF	0.347 (0.012–9.695)	0.534	1.510 (0.875–2.606)	0.139

Definition of abbreviations: MRI = magnetic resonance imaging; NTpro-BNP = N-terminal prohormone brain natriuretic peptide; %pred = percentage predicted for age and sex; RVESVi = right ventricular end-systolic volume index; RVEDVi = right ventricular end-diastolic volume index; RVEF = right ventricular ejection fraction; RAEF = right atrial ejection fraction.

9.4 Discussion

This study evaluated the prognostic value of cardiac MRI and NT-proBNP simultaneously in patients with PAH. The most obvious findings to emerge from this study are that (i) continuous log10 (NT-proBNP) was found to be most strongly correlated with an established RV function prognostic marker, namely, continuous percentage predicted RVESVi, and (ii) the prognostic value of categorical NTpro-BNP was not independent of any of the categorical or continuous RV volumetric measurements.

Our study shows a strong and significant relationship between continuous log10 (NT-proBNP) and continuous percentage predicted RVESVi in patients with PAH. Forty-two percent of the variance in the dependent variable continuous log10 (NTpro-BNP) is explained by the independent variable continuous percentage predicted RVESVi. In other words, continuous percentage predicted RVESVi significantly predicts continuous log10 (NTpro-BNP) as we have measured both variables by explaining 42% of the variance. This finding supports previous research which observed an association between NT-proBNP and RVESV (Fenster et al., 2014, Blyth et al., 2007).

The results have shown that the strongest predictors of mortality from univariate Cox regression analysis were categorical NT-proBNP and continuous percentage predicted RVESVi. Contrary to expectations, the prognostic value of categorical NTpro-BNP was not independent of the continuous percentage predicted RVESVi at bivariate analysis. These factors may explain the strong correlation between NTpro-BNP and the percentage predicted RVESVi and might suggest an approach where clinicians can either use cardiac MRI measurements or NT-proBNP test to assess and risk stratify patients with PAH. Another possible explanation for this unexpected result is that high concentrations of NT-proBNP can be influenced by other pathologies such as acute/chronic heart failure, anaemia, acute coronary

syndrome, pulmonary embolism, type 2 diabetes mellitus and chronic renal failure (Fu et al., 2018, Santaguida et al., 2014, Nayer et al., 2014, Kiely et al., 2005); however, this study did not control for this.

9.5 Limitations and Future Work

Several limitations to this pilot study need to be acknowledged. First, this study is limited by its single centre design. Second, with a small sample size, caution must be applied, as the findings might not be transferable at this stage. Further work with a larger number of patients is required to establish this work. Third, other factors that elevate NT-proBNP levels must be considered when conducting a research study or clinically assessing patients with PAH (Nishimura et al., 2018, Humbert et al., 2022a). Fourth, the retrospective nature of this study and the time gap between blood specimen collection and MRI measurements may have limitations, as any interval changes in treatment could affect the BNP levels. Future studies on the current topic are therefore recommended.

9.6 Conclusion

Categorical NT-proBNP is strongly related to the continuous percentage predicted RVESVi and has prognostic significance in patients with PAH. This opens up the need for further study to assess the added value of different approaches for the assessment of the right ventricle.

Chapter 10: Discussion, Limitations and Further Work

10.1 Research Design

All cohorts in this PhD thesis are limited by their single referral centre design, even though this thesis includes one of the largest cohorts of patients with PAH who underwent cardiac MRI. In addition, this thesis incorporates a single-centre clinical evaluation of an AI algorithm created in a multi-vendor, multi-centre cohort, with the clinical evaluation taking place in a tertiary referral centre for patients with PAH. Imaging characteristics and patient populations are probably indicative of other PAH referral centres. The AI algorithm was developed in a multicentre setting and tested at a single centre. Multicentre testing would be the next stage in determining the algorithm's applicability to a broad community.

Since the majority of this thesis was completed retrospectively and all patients had already been diagnosed with PAH, selection bias could not be ruled out. Ideally, prospective studies with a substantial number of patients are required to confirm and validate the results of this research. Therefore, more research is required to develop a higher degree of precision in RA area risk stratification at 1-year mortality and to highlight the potential of cardiac MRI for assessing PAH severity.

10.2 Artificial Intelligence and Reproducibility

One of the main goals of this PhD thesis was to develop a quantitative cardiac MRI-based automated artificial intelligence (AI) analysis of the RA in a large cohort of patients with heart failure and PAH of diverse aetiology and disease severity; and to determine the failure rate of the model in a large clinical registry, evaluate interstudy repeatability of the RA and NTpro-BNP, directly compare the association of manual RA area and AI RA area with invasive haemodynamics, and assess RA measurements as predictors of mortality. However, the current AI methodology utilises manual quality control, which is favourable from a regulatory

perspective and preserves expert supervision of the AI. Future developments to automate quality control are promising, but we consider manual review an essential component of the system. In order to improve the accuracy of the model, unsuccessful AI segmentation will be routinely identified and implemented into subsequent training rounds.

The findings from this research make several contributions to the current literature. Cardiac MRI RA area measurements can be fully automated utilising AI with a very low failure rate in a large clinical cohort with varied RA size and deformity. In a scan-rescan cohort of patients with different severities of RA size and function, and PAH, the variability of AI-derived RA area measurements was excellent and lower than manual measurements, while NT-proBNP was of moderate repeatability. Furthermore, the correlation between RA area measurements and invasive haemodynamics was moderate, and AI measurements can identify mRAP prognostic thresholds with greater certainty than manual measurements. In addition, AI RA area measurements predict mortality with similar accuracy to manual measurements. Future research will assess the efficacy of such automatic QC techniques in clinical populations. However, artificial intelligence has downsides: constantly improving algorithms, time-consuming and enormous amounts of data required to train. For example, if you feed a model inaccurate data, it will only produce inaccurate results. To reduce generalisation error and determine broader applicability of the algorithm, multicentre setting and multicentre testing are recommended for future research.

10.3 Prognostic Value and Risk Stratification

An initial objective of this PhD work was to validate the ESC/ERS guideline thresholds of manual RA area and identify optimal approaches. The findings from this study validate the ESC/ERS guideline thresholds of the RA and suggest that, at follow-up, minimal RA area is potentially a stronger predictor of mortality than maximal RA area and RAC in patients with

PAH. In addition, the work of this PhD thesis was designed to compare AI RV and AI RA area measurements and their utility to risk stratify patients with PAH, using the reference standard for assessment of cardiac structure and function. This was performed by comparing published thresholds for RV metrics (Lewis et al., 2020) with ESC/ERS thresholds for RA area (Humbert et al., 2022a, Humbert et al., 2022b). The results of this study confirm the prognostic value of RA and RV metrics using the reference standard for measures of cardiac structure and function in PAH. However, in regard to PAH risk stratification, this study highlights the necessity for guidelines to include RV function measurements in addition to RA area.

According to ESC/ERS pulmonary hypertension guidelines, we mainly measured the RA area. The predictive relevance of cardiac MRI-derived right atrial volume and reservoir function (reservoir, conduit, and contractile functions) in patients with clinically deteriorating pulmonary hypertension has been previously established (Sato et al., 2013, Sato et al., 2015). Further research is required to determine whether alternative measures of RA volume and/or function provide further prognostic value. In addition, this research work presents an AI model for RA area estimation rather than volume estimation. The objective was to automate clinical measurements done in accordance with ESC/ERS guidelines for PAH. Future investigations could benefit from the development and clinical evaluation of a 3-dimensional or multislice RA volumetric model, as well as the extraction of physiological data previously reported to be essential (Sato et al., 2015).

10.4 Cardiac MRI and NT-proBNP

This PhD thesis set out with the aim of evaluating the prognostic role of automated cardiac MRI and NT-proBNP in PAH. The most remarkable findings to arise from this study is that NT-proBNP was found to be most strongly correlated with an established RV function prognostic marker; specifically, percentage predicted RVESVi, and the prognostic value of

NTpro-BNP was not independent of any of the RV volumetric measurements. This necessitates additional research to evaluate the added value of different approaches when assessing the right ventricle.

In addition, the work of this PhD thesis does not include a comparison with left ventricular parameters because they are less established in patients with PAH as a prognostic marker, despite recent studies demonstrating that left ventricular parameters have prognostic value (Knight et al., 2015, Alabed et al., 2020, Anton Vonk Noordegraaf et al., 2022) and may play a role in risk stratification of patients with PAH (Lewis et al., 2020). Further clinical research is needed, and it is essential to understand what is happening with the left ventricle as well. Furthermore, this thesis has not solved how to integrate the information for the right atrial and right ventricle. We would use advanced modelling and dynamic measurements such as strain parameters to analyse cardiac structure and function in future research.

MRI has some disadvantages, including the fact that it is noisy, pricey, limited availability and contraindicated for patients with metallic devices. In addition, feelings of claustrophobia and discomfort are significant problems for several MRI users. Most hospitals have an MRI scanner; however, physicians do not always have access to an MRI scanner to use for pulmonary hypertension. Further work is to compare cardiac MRI against three-dimensional echocardiography (3DE), identify the optimal measurements and investigate the incremental value of MRI over 3DE.

In regards to the serological biomarker, high concentrations of NT-proBNP can be influenced by other pathologies, such as acute/chronic heart failure, anaemia, acute coronary syndrome, pulmonary embolism, type 2 diabetes mellitus, and chronic renal failure (Kiely et al., 2005, Nayer et al., 2014, Santaguida et al., 2014, Fu et al., 2018), but this was not accounted for in this thesis. When performing a research study or clinically evaluating patients with PAH, it is

important to assess the factors that increase NT-proBNP levels (Nishimura et al., 2018, Humbert et al., 2022a, Humbert et al., 2022b). Therefore, further research on this area is recommended. Moreover, NT-proBNP blood tests were carried out in university laboratories using test kits that were not clinical-grade. For future work, the NT-proBNP samples will be repeated using trust-grade sample kits at Sheffield Teaching Hospitals NHS Foundation Trust.

10.5 Conclusions

Using manual and automated cardiac MRI, this work demonstrated that RV function and RA area measurements had predictive significance; however, only RV function measurements, and not the current ESC/ERS RA area thresholds, identify patients with a low risk of 1-year mortality. Furthermore, cardiac MRI RV and RA area measurements can be fully automated using AI with a very low failure rate. In a scan-rescan cohort of patients with PAH, the variability of AI-derived RA area measures was lower than manual measurements. The correlation between manual and automated RA area measurements and invasive hemodynamics is moderate. In addition, NT-proBNP showed a moderate correlation with automated RV function. Recommendations have been made for additional research investigating larger cohorts with NT-proBNP and cardiac MRI measures to determine the added value of alternative techniques for measuring the right ventricle.

Appendix 1: Publications, Presentations and Awards

Published papers directly related to the thesis

Alandejani F, Alabed S, Garg P, Goh ZM, Karunasaagarar K, Sharkey M, Salehi M, Aldabbagh Z, Dwivedi K, Mamalakis M, Metherall P, Uthoff J, Johns C, Rothman A, Condliffe R, Hameed A, Charalampoplous A, Lu H, Plein S, Greenwood JP, Lawrie A, Wild JM, de Koning PJH, Kiely DG, van der Geest R, Swift AJ. Training and clinical testing of artificial intelligence derived right atrial cardiovascular magnetic resonance measurements. J Cardiovasc Magn Reson. 2022 Apr 7;24(1):25. doi: 10.1186/s12968-022-00855-3. PMID: 35387651; PMCID: PMC8988415.

Alandejani F, Hameed A, Tubman E, Alabed S, Shahin Y, Lewis RA, Dwivedi K, Mahmood A, Middleton J, Watson L, Alkhanfar D, Johns CS, Rajaram S, Garg P, Condliffe R, Elliot CA, Thompson AAR, Rothman AMK, Charalampopoulos A, Lawrie A, Wild JM, Swift AJ, Kiely DG. Imaging and Risk Stratification in Pulmonary Arterial Hypertension: Time to Include Right Ventricular Assessment. Front Cardiovasc Med. 2022 Mar 25;9:797561. doi: 10.3389/fcvm.2022.797561. PMID: 35402574; PMCID: PMC8989834.

Alabed S, **Alandejani F**, Dwivedi K, Karunasaagarar K, Sharkey M, Garg P, de Koning PJH, Tóth A, Shahin Y, Johns C, Mamalakis M, Stott S, Capener D, Wood S, Metherall P, Rothman AMK, Condliffe R, Hamilton N, Wild JM, O'Regan DP, Lu H, Kiely DG, van der Geest RJ, Swift AJ. Validation of Artificial Intelligence Cardiac MRI Measurements: Relationship to Heart Catheterization and Mortality Prediction. Radiology. 2022 Jun 14:212929. doi: 10.1148/radiol.212929. Epub ahead of print. Erratum in: Radiology. 2022 Sep;304(3):E56. PMID: 35699578.

Alabed S, Shahin Y, Garg P, **Alandejani F**, Johns CS, Lewis RA, Condliffe R, Wild JM, Kiely DG, Swift AJ. Cardiac-MRI Predicts Clinical Worsening and Mortality in Pulmonary Arterial Hypertension: A Systematic Review and Meta-Analysis. JACC Cardiovasc Imaging. 2021 May;14(5):931-942. doi: 10.1016/j.jcmg.2020.08.013. Epub 2020 Sep 30. Erratum in: JACC Cardiovasc Imaging. 2021 Apr;14(4):884. PMID: 33008758; PMCID: PMC7525356.

Swift AJ, Wilson F, Cogliano M, Kendall L, **Alandejani F**, Alabed S, Hughes P, Shahin Y, Saunders L, Oram C, Capener D, Rothman A, Garg P, Johns C, Austin M, Macdonald A, Pickworth J, Hickey P, Condliffe R, Cahn A, Lawrie A, Wild JM, Kiely DG. Repeatability and sensitivity to change of non-invasive end points in PAH: the RESPIRE study. Thorax. 2021 Oct;76(10):1032-1035. doi: 10.1136/thoraxjnl-2020-216078. Epub 2021 Feb 25. PMID: 33632769; PMCID: PMC8461450.

Published papers not directly related to the thesis

Alabed S, Garg P, Johns CS, **Alandejani F**, Shahin Y, Dwivedi K, Zafar H, Wild JM, Kiely DG, Swift AJ. Cardiac Magnetic Resonance in Pulmonary Hypertension-an Update. Curr Cardiovasc Imaging Rep. 2020;13(12):30. doi: 10.1007/s12410-020-09550-2. Epub 2020 Nov 7. PMID: 33184585; PMCID: PMC7648000.

Alabed S, Saunders L, Garg P, Shahin Y, **Alandejani F**, Rolf A, Puntmann VO, Nagel E, Wild JM, Kiely DG, Swift AJ. Myocardial T1-mapping and extracellular volume in pulmonary arterial hypertension: A systematic review and meta-analysis. Magn Reson Imaging. 2021 Jun;79:66-75. doi: 10.1016/j.mri.2021.03.011. Epub 2021 Mar 18. PMID: 33745961.

Goh ZM, Balasubramanian N, Alabed S, Dwivedi K, Shahin Y, Rothman AMK, Garg P, Lawrie A, Capener D, Thompson AAR, **Alandejani F**, Wild JM, Johns CS, Lewis RA, Gosling R, Sharkey M, Condliffe R, Kiely DG, Swift AJ. Right ventricular remodelling in pulmonary arterial hypertension predicts treatment response. Heart. 2022 Aug 11;108(17):1392-1400. doi: 10.1136/heartjnl-2021-320733. PMID: 35512982; PMCID: PMC9380507.

Goh ZM, Alabed S, Shahin Y, Rothman AMK, Garg P, Lawrie A, Capener D, Thompson AAR, **Alandejani F**, Johns CS, Lewis RA, Dwivedi K, Wild JM, Condliffe R, Kiely DG, Swift AJ. Right Ventricular Adaptation Assessed Using Cardiac Magnetic Resonance Predicts Survival in Pulmonary Arterial Hypertension. JACC Cardiovasc Imaging. 2021 Jun;14(6):1271-1272. doi: 10.1016/j.jcmg.2020.10.008. Epub 2020 Nov 18. PMID: 33221232; PMCID: PMC8203554.

Shahin Y, Alabed S, Rehan Quadery S, Lewis RA, Johns C, Alkhanfar D, Sukhanenko M, **Alandejani F**, Garg P, Elliot CA, Hameed A, Charalampopoulos A, Wild JM, Condliffe R, Swift AJ, Kiely DG. CMR Measures of Left Atrial Volume Index and Right Ventricular Function Have Prognostic Value in Chronic Thromboembolic Pulmonary Hypertension. Front Med (Lausanne). 2022 Mar 14;9:840196. doi: 10.3389/fmed.2022.840196. PMID: 35360708; PMCID: PMC8964043.

Dwivedi K, Condliffe R, Sharkey M, Lewis R, Alabed S, Rajaram S, Hill C, Saunders L, Metherall P, **Alandejani F**, Alkhanfar D, Wild JM, Lu H, Kiely DG, Swift AJ. Computed tomography lung parenchymal descriptions in routine radiological reporting have diagnostic and prognostic utility in patients with idiopathic pulmonary arterial hypertension and pulmonary hypertension associated with lung disease. ERJ Open Res. 2022 Jan 24;8(1):00549-2021. doi: 10.1183/23120541.00549-2021. PMID: 35083317; PMCID: PMC8784758.

Alkhanfar D, Shahin Y, **Alandejani F**, Dwivedi K, Alabed S, Johns C, Lawrie A, Thompson AAR, Rothman AMK, Tschirren J, Uthoff JM, Hoffman E, Condliffe R, Wild JM, Kiely DG, Swift AJ. Severe pulmonary hypertension associated with lung disease is characterised by a loss of small pulmonary vessels on quantitative computed tomography. ERJ Open Res. 2022 May 16;8(2):00503-2021. doi: 10.1183/23120541.00503-2021. PMID: 35586449; PMCID: PMC9108962.

Oral presentations

Alandejani F, Hameed A, Tubman E, Alabed S, Shahin Y, Lewis RA, Dwivedi K, Mahmood A, Middleton J, Watson L, Alkhanfar D, Johns CS, Rajaram S, Garg P, Condliffe R, Elliot CA, Thompson AAR, Rothman AMK, Charalampopoulos A, Lawrie A, Wild JM, Swift AJ, Kiely DG..Cardiac MRI and risk stratification in pulmonary arterial hypertension: evaluation of ESC/ERS thresholds for right atrial area. *PVRI 2022*

Alandejani F, Hameed A, Tubman E, Alabed S, Shahin Y, Lewis RA, Dwivedi K, Mahmood A, Middleton J, Watson L, Alkhanfar D, Johns CS, Rajaram S, Garg P, Condliffe R, Elliot CA, Thompson AAR, Rothman AMK, Charalampopoulos A, Lawrie A, Wild JM, Swift AJ, Kiely DG..Cardiac MRI and risk stratification in pulmonary arterial hypertension: evaluation of ESC/ERS thresholds for right atrial area. *Sheffield PVDU 2021*

Alandejani F, Hameed A, Tubman E, Alabed S, Shahin Y, Lewis RA, Dwivedi K, Mahmood A, Middleton J, Watson L, Alkhanfar D, Johns CS, Rajaram S, Garg P, Condliffe R, Elliot CA, Thompson AAR, Rothman AMK, Charalampopoulos A, Lawrie A, Wild JM, Swift AJ, Kiely DG..Cardiac MRI and risk stratification in pulmonary arterial hypertension: evaluation of ESC/ERS thresholds for right atrial area. *University of Sheffield Medical School Annual Research Meeting 2021*

Poster presentations

Alandejani F, Alabed S, Garg P, Goh ZM, Karunasaagarar K, Sharkey M, Salehi M, Aldabbagh Z, Dwivedi K, Mamalakis M, Metherall P, Uthoff J, Johns C, Rothman A, Condliffe R, Hameed A, Charalampoplous A, Lu H, Plein S, Greenwood JP, Lawrie A, Wild JM, de Koning PJH, Kiely DG, van der Geest R, Swift AJ. Training and clinical testing of artificial intelligence derived right atrial cardiovascular magnetic resonance measurements. *ATS 2022*

Alandejani F, Alabed S, Tubman E, Shahin Y, Lewis RA, Dwivedi K, Alkhanfar D, Johns CS, Garg P, Condliffe R, Hameed A,Charalampopoulos A, Lawrie A, Wild JM, Swift AJ, Kiely DG. Cardiac MRI and risk stratification in pulmonary arterial hypertension: evaluation of ESC/ERS thresholds for right atrial area. *PVRI 2021*

Alandejani F, Tubman E, Shahin Y, Lewis RA, Dwivedi K, Alkhanfar D, Alabed S, Johns CS, Garg P, Condliffe R, Lawrie A, Wild JM, Swift AJ, Kiely DG..Cardiac MRI right atrial area measurement thresholds for risk stratification in patients with PAH. *ERS 2020*

Awards related to this thesis

A poster generated from data in Chapter 8 (“Imaging and Risk Stratification in Pulmonary Arterial Hypertension: Time to Include Right Ventricular Assessment”) has been selected among the best abstracts at the 2021 Pulmonary Vascular Research Institute.

References

Abolmaali, N., Seitz, U., Esmaeili, A., Kock, M., Radeloff, D., Ackermann, H. & Vogl, T. J. 2007. Evaluation of a resistance-based model for the quantification of pulmonary arterial hypertension using MR flow measurements. *Journal of magnetic resonance imaging : JMRI,* 26.

Alabed, S., Alandejani, F., K, D., Karunasaagarar, K., Sharkey, M., Garg, P., De Koning, P. J. H., Tóth, A., Shahin, Y., Johns, C., Mamalakis, M., Stott, S., Capener, D., Wood, S., Metherall, P., Rothman, A. M. K., Condliffe, R., Hamilton, N., Wild, J. M., O'regan, D. P., Lu, H., Kiel, Y. D. G., Van Der Geest, R. J. & Swift, A. J. 2022. Validation of Artificial Intelligence Cardiac MRI Measurements: Relationship to Heart Catheterization and Mortality Prediction. *Radiology,* 305.

Alabed, S., Shahin, Y., Garg, P., Alandejani, F., Johns, C. S., Lewis, R. A., Condliffe, R., Wild, J. M., Kiely, D. G. & Swift, A. J. 2020. Cardiac-MRI Predicts Clinical Worsening and Mortality in Pulmonary Arterial Hypertension: A Systematic Review and Meta-Analysis. *JACC. Cardiovascular imaging*.

Alandejani, F., Alabed, S., Garg, P., Goh, Z. M., Karunasaagarar, K., Sharkey, M., Salehi, M., Aldabbagh, Z., Dwivedi, K., Mamalakis, M., Metherall, P., Uthoff, J., Johns, C., Rothman, A., Condliffe, R., Hameed, A., Charalampoplous, A., Lu, H., Plein, S., Greenwood, J., Lawrie, A., Wild, J. M., De Koning, P. J. H., Kiely, D. G., Van Der Geest, R. & Swift, A. J. 2022a. Training and clinical testing of artificial intelligence derived right atrial cardiovascular magnetic resonance measurements. *Journal of cardiovascular magnetic resonance : official journal of the Society for Cardiovascular Magnetic Resonance,* 24.

Alandejani, F., Hameed, A., Tubman, E., Alabed, S., Shahin, Y., Lewis, R. A., Dwivedi, K., Mahmood, A., Middleton, J., Watson, L., Alkhanfar, D., Johns, C. S., Rajaram, S., Garg, P., Condliffe, R., Elliot, C. A., Thompson, A. A. R., Rothman, A. M. K., Charalampopoulos, A., Lawrie, A., Wild, J. M., Swift, A. J. & Kiely, D. G. 2022b. Imaging and Risk Stratification in Pulmonary Arterial Hypertension: Time to Include Right Ventricular Assessment. *Frontiers in cardiovascular medicine,* 9.

Alibay, Y., Beauchet, A., El Mahmoud, R., Brun-Ney, D., Alexandre, J. A., Benoit, M. O., Dubourg, O., Aegerter, P., Boileau, C., Jondeau, G. & Puy, H. 2004. Analytical correlation between plasma N-terminal pro-brain natriuretic peptide and brain natriuretic peptide in patients presenting with dyspnea. *Clinical Biochemistry,* 37**,** 933-936.

Anderson, J. L., Horne, B. D. & Pennell, D. J. 2005. Atrial dimensions in health and left ventricular disease using cardiovascular magnetic resonance. *J Cardiovasc Magn Reson,* 7**,** 671-5.

Andreassen, A. K., Wergeland, R., Simonsen, S., Geiran, O., Guevara, C. & Ueland, T. 2006. N-terminal pro-B-type natriuretic peptide as an indicator of disease severity in a heterogeneous

group of patients with chronic precapillary pulmonary hypertension. *American Journal of Cardiology,* 98**,** 525-529.

Anton Vonk Noordegraaf, M., Richard Channick, M., Emmanuelle Cottreel, M., David G. Kiely, M., J. Tim Marcus, P., Nicolas Martin, M., Olga Moiseeva, M., Andrew Peacock, M., Andrew J. Swift, P., Ahmed Tawakol, M., Adam Torbicki, M., Stephan Rosenkranz, M. & Nazzareno Galiè, M. 2022. The REPAIR Study: Effects of Macitentan on RV Structure and Function in Pulmonary Arterial Hypertension.

Augusto, J. B., Davies, R. H., Bhuva, A. N., Knott, K. D., Seraphim, A., Alfarih, M., Lau, C., Hughes, R. K., Lopes, L. R., Shiwani, H., Treibel, T. A., Gerber, B. L., Hamilton-Craig, C., Ntusi, N. A. B., Pontone, G., Desai, M. Y., Greenwood, J. P., Swoboda, P. P., Captur, G., Cavalcante, J., Bucciarelli-Ducci, C., Petersen, S. E., Schelbert, E., Manisty, C. & Moon, J. C. 2021. Diagnosis and risk stratification in hypertrophic cardiomyopathy using machine learning wall thickness measurement: a comparison with human test-retest performance. *Lancet Digital Health,* 3**,** E20-E28.

Austin, C., Alassas, K., Burger, C., Safford, R., Pagan, R., Duello, K., Kumar, P., Zeiger, T. & Shapiro, B. 2015. Echocardiographic Assessment of Estimated Right Atrial Pressure and Size Predicts Mortality in Pulmonary Arterial Hypertension. *Chest,* 147**,** 198-208.

Backhaus, S. J., Staab, W., Steinmetz, M., Ritter, C. O., Lotz, J., Hasenfuss, G., Schuster, A. & Kowallick, J. T. 2019. Fully automated quantification of biventricular volumes and function in cardiovascular magnetic resonance: applicability to clinical routine settings. *Journal of Cardiovascular Magnetic Resonance,* 21.

Baggen, V. J. M., Leiner, T., Post, M. C., Van Dijk, A. P., Roos-Hesselink, J. W., Boersma, E., Habets, J. & Sieswerda, G. T. 2016. Cardiac magnetic resonance findings predicting mortality in patients with pulmonary arterial hypertension: a systematic review and meta-analysis. *European Radiology,* 26**,** 3771-3780.

Bai, W., Sinclair, M., Tarroni, G., Oktay, O., Rajchl, M., Vaillant, G., Lee, A. M., Aung, N., Lukaschuk, E., Sanghvi, M. M., Zemrak, F., Fung, K., Paiva, J. M., Carapella, V., Kim, Y. J., Suzuki, H., Kainz, B., Matthews, P. M., Petersen, S. E., Piechnik, S. K., Neubauer, S., Glocker, B. & Rueckert, D. 2018. Automated cardiovascular magnetic resonance image analysis with fully convolutional networks. *Journal of Cardiovascular Magnetic Resonance,* 20.

Baillie, T. J., Sidharta, S., Steele, P. M., Worthley, S. G., Willoughby, S., Teo, K., Sanders, P., Nicholls, S. J. & Worthley, M. I. 2017a. Noninvasive Assessment of Cardiopulmonary Reserve: Toward Early Detection of Pulmonary Vascular Disease. *American Journal of Respiratory and Critical Care Medicine,* 195**,** 398-401.

Baillie, T. J., Sidharta, S., Steele, P. M., Worthley, S. G., Willoughby, S., Teo, K. R., Sanders, P., Nicholls, S. J. & Worthley, M. I. 2017b. The predictive capabilities of a novel cardiovascular magnetic resonance derived marker of cardiopulmonary reserve on established prognostic

surrogate markers in patients with pulmonary vascular disease: results of a longitudinal pilot study. *Journal of Cardiovascular Magnetic Resonance,* 19.

Basford, J. R. 2002. The Law of Laplace and its relevance to contemporary medicine and rehabilitation. *Archives of Physical Medicine and Rehabilitation,* 83**,** 1165-1170.

Bay, M., Kirk, V., Parner, J., Hassager, C., Nielsen, H., Krogsgaard, K., Trawinski, J., Boesgaard, S. & Aldershvile, J. 2003. NT-proBNP: a new diagnostic screening tool to differentiate between patients with normal and reduced left ventricular systolic function. *Heart,* 89**,** 150-4.

Beghetti, M. & Galiè, N. 2009. Eisenmenger syndrome a clinical perspective in a new therapeutic era of pulmonary arterial hypertension. *Journal of the American College of Cardiology,* 53.

Bellofiore, A. & Chesler, N. C. 2013. Methods for Measuring Right Ventricular Function and Hemodynamic Coupling with the Pulmonary Vasculature. *Annals of Biomedical Engineering,* 41**,** 1384-1398.

Benza, R., Biederman, R., Murali, S. & Gupta, H. 2008. Role of Cardiac Magnetic Resonance Imaging in the Management of Patients With Pulmonary Arterial Hypertension. *Journal of the American College of Cardiology,* 52**,** 1683-1692.

Benza, R. L., Gomberg-Maitland, M., Elliott, C. G., Farber, H. W., Foreman, A. J., Frost, A. E., Mcgoon, M. D., Pasta, D. J., Selej, M., Burger, C. D. & Frantz, R. P. 2019. Predicting Survival in Patients With Pulmonary Arterial Hypertension: The REVEAL Risk Score Calculator 2.0 and Comparison With ESC/ERS-Based Risk Assessment Strategies. *Chest,* 156.

Benza, R. L., Gomberg-Maitland, M., Miller, D. P., Frost, A., Frantz, R. P., Foreman, A. J., Badesch, D. B. & Mcgoon, M. D. 2012. The REVEAL Registry risk score calculator in patients newly diagnosed with pulmonary arterial hypertension. *Chest,* 141**,** 354-362.

Benza, R. L., Kanwar, M. K., Raina, A., Scott, J. V., Zhao, C. L., Selej, M., Elliott, C. G. & Farber, H. W. 2021. Development and Validation of an Abridged Version of the REVEAL 2.0 Risk Score Calculator, REVEAL Lite 2, for Use in Patients With Pulmonary Arterial Hypertension. *Chest,* 159.

Benza, R. L., Miller, D. P., Foreman, A. J., Frost, A. E., Badesch, D. B., Benton, W. W. & Mcgoon, M. D. 2015. Prognostic implications of serial risk score assessments in patients with pulmonary arterial hypertension: a Registry to Evaluate Early and Long-Term Pulmonary Arterial Hypertension Disease Management (REVEAL) analysis. *The Journal of heart and lung transplantation : the official publication of the International Society for Heart Transplantation,* 34.

Benza, R. L., Miller, D. P., Gomberg-Maitland, M., Frantz, R. P., Foreman, A. J., Coffey, C. S., Frost, A., Barst, R. J., Badesch, D. B., Elliott, C. G., Liou, T. G. & Mcgoon, M. D. 2010. Predicting Survival in Pulmonary Arterial Hypertension Insights From the Registry to Evaluate Early and Long-Term Pulmonary Arterial Hypertension Disease Management (REVEAL). *Circulation,* 122**,** 164-U138.

Bernard, O., Lalande, A., Zotti, C., Cervenansky, F., Yang, X., Heng, P.-A., Cetin, I., Lekadir, K., Camara, O., Gonzalez Ballester, M. A., Sanroma, G., Napel, S., Petersen, S., Tziritas, G., Grinias, E., Khened, M., Kollerathu, V. A., Krishnamurthi, G., Rohe, M.-M., Pennec, X., Sermesant, M., Isensee, F., Jaeger, P., Maier-Hein, K. H., Full, P. M., Wolf, I., Engelhardt, S., Baumgartner, C. F., Koch, L. M., Wolterink, J. M., Isgum, I., Jang, Y., Hong, Y., Patravali, J., Jain, S., Humbert, O. & Jodoin, P.-M. 2018. Deep Learning Techniques for Automatic MRI Cardiac Multi-Structures Segmentation and Diagnosis: Is the Problem Solved? *Ieee Transactions on Medical Imaging,* 37**,** 2514-2525.

Bieri, O. & Scheffler, K. 2013. Fundamentals of balanced steady state free precession MRI. *Journal of magnetic resonance imaging : JMRI,* 38.

Bland, J. M. & Altman, D. G. 1986. Statistical methods for assessing agreement between two methods of clinical measurement. *Lancet (London, England),* 1.

Blyth, K. G., Groenning, B. A., Mark, P. B., Martin, T. N., Foster, J. E., Steedman, T., Morton, J. J., Dargie, H. J. & Peacock, A. J. 2007. NT-proBNP can be used to detect right ventricular systolic dysfunction in pulmonary hypertension. *European Respiratory Journal,* 29**,** 737-744.

Bonnemains, L., Mandry, D., Marie, P. Y., Micard, E., Chen, B. L. & Vuissoz, P. A. 2012. Assessment of right ventricle volumes and function by cardiac MRI: Quantification of the regional and global interobserver variability. *Magnetic Resonance in Medicine,* 67**,** 1740-1746.

Boucly, A., Weatherald, J., Savale, L., Jais, X., Cottin, V., Prevot, G., Picard, F., De Groote, P., Jevnikar, M., Bergot, E., Chaouat, A., Chabanne, C., Bourdin, A., Parent, F., Montani, D., Simonneau, G., Humbert, M. & Sitbon, O. 2017. Risk assessment, prognosis and guideline implementation in pulmonary arterial hypertension. *European Respiratory Journal,* 50.

Boxt, L. M., Katz, J., Kolb, T., Czegledy, F. P. & Barst, R. J. 1992. Direct Quantitation Of Right And Left-Ventricular Volumes With Nuclear-Magnetic-Resonance Imaging In Patients With Primary Pulmonary-Hypertension. *Journal of the American College of Cardiology,* 19**,** 1508-1515.

Buechel, E. R. V. & Mertens, L. L. 2012. Imaging the right heart: the use of integrated multimodality imaging. *European Heart Journal,* 33**,** 949-U17.

Bustamante-Labarta, M., Perrone, S., De La Fuente, R. L., Stutzbach, P., De La Hoz, R. P., Torino, A. & Favaloro, R. 2002. Right atrial size and tricuspid regurgitation severity predict mortality or transplantation in primary pulmonary hypertension. *J Am Soc Echocardiogr,* 15**,** 1160-4.

Campo, A., Mathai, S. C., Le Pavec, J., Zaiman, A. L., Hummers, L. K., Boyce, D., Housten, T., Champion, H. C., Lechtzin, N., Wigley, F. M., Girgis, R. E. & Hassoun, P. M. 2010. Hemodynamic predictors of survival in scleroderma-related pulmonary arterial hypertension. *American journal of respiratory and critical care medicine,* 182.

Campo, A., Mathai, S. C., Le Pavec, J., Zaiman, A. L., Hummers, L. K., Boyce, D., Housten, T., Lechtzin, N., Chami, H., Girgis, R. E. & Hassoun, P. M. 2011. Outcomes of hospitalisation for

right heart failure in pulmonary arterial hypertension. *European Respiratory Journal,* 38**,** 359-367.

Chahal, H., Johnson, C., Tandri, H., Jain, A., Hundley, W. G., Barr, R. G., Kawut, S. M., Lima, J. A. C. & Bluemke, D. A. 2010. Relation of Cardiovascular Risk Factors to Right Ventricular Structure and Function as Determined by Magnetic Resonance Imaging (Results from the Multi-Ethnic Study of Atherosclerosis). *American Journal of Cardiology,* 106**,** 110-116.

Chen, C., Qin, C., Qiu, H., Tarroni, G., Duan, J., Bai, W. & Rueckert, D. 2020. Deep Learning for Cardiac Image Segmentation: A Review. *Frontiers in Cardiovascular Medicine,* 7.

Chin, K. M., Kingman, M., De Lemos, J. A., Warner, J. J., Reimold, S., Peshock, R. & Torres, F. 2008. Changes in right ventricular structure and function assessed using cardiac magnetic resonance imaging in bosentan-treated patients with pulmonary arterial hypertension. *The American journal of cardiology,* 101.

Chung, L., Liu, J., Parsons, L., Hassoun, P. M., Mcgoon, M., Badesch, D. B., Miller, D. P., Nicolls, M. R. & Zamanian, R. T. 2010. Characterization of connective tissue disease-associated pulmonary arterial hypertension from REVEAL: identifying systemic sclerosis as a unique phenotype. *Chest,* 138.

Cioffi, G., De Simone, G., Mureddu, G., Tarantini, L. & Stefenelli, C. 2007. Right atrial size and function in patients with pulmonary hypertension associated with disorders of respiratory system or hypoxemia. *Eur J Echocardiogr,* 8**,** 322-31.

Cogswell, R., Pritzker, M. & De Marco, T. 2014. Performance of the REVEAL pulmonary arterial hypertension prediction model using non-invasive and routinely measured parameters. *J Heart Lung Transplant,* 33**,** 382-7.

Condliffe, R., Kiely, D. G., Peacock, A. J., Corris, P. A., Gibbs, J. S., Vrapi, F., Das, C., Elliot, C. A., Johnson, M., Desoyza, J., Torpy, C., Goldsmith, K., Hodgkins, D., Hughes, R. J., Pepke-Zaba, J. & Coghlan, J. G. 2009. Connective tissue disease-associated pulmonary arterial hypertension in the modern treatment era. *American journal of respiratory and critical care medicine,* 179.

Condon, D. F., Nickel, N. P., Anderson, R., Mirza, S. & De Jesus Perez, V. A. 2019. The 6th World Symposium on Pulmonary Hypertension: what's old is new. *F1000Research,* 8.

Corbin, J. D., Beasley, A., Blount, M. A. & Francis, S. H. 2005. High lung PDE5: a strong basis for treating pulmonary hypertension with PDE5 inhibitors. *Biochemical and biophysical research communications,* 334.

Crandon, S., Westenberg, J. J. M., Swoboda, P. P., Fent, G. J., Foley, J. R. J., Chew, P. G., Brown, L. A. E., Saunderson, C., Al-Mohammad, A., Greenwood, J. P., Van Der Geest, R. J., Dall'armellina, E., Plein, S. & Garg, P. 2018. Impact of Age and Diastolic Function on Novel, 4D flow CMR Biomarkers of Left Ventricular Blood Flow Kinetic Energy. *Scientific Reports,* 8.

D'alto, M. & Mahadevan, V. S. 2012. Pulmonary arterial hypertension associated with congenital heart disease. *European respiratory review : an official journal of the European Respiratory Society,* 21.

Dalonzo, G. E., Barst, R. J., Ayres, S. M., Bergofsky, E. H., Brundage, B. H., Detre, K. M., Fishman, A. P., Goldring, R. M., Groves, B. M., Kernis, J. T., Levy, P. S., Pietra, G. G., Reid, L. M., Reeves, J. T., Rich, S., Vreim, C. E., Williams, G. W. & Wu, M. 1991. Survival in patients with primary pulmonary hypertension: Results from a national prospective registry. *Annals of Internal Medicine,* 115**,** 343-349.

Damman, K., Van Deursen, V. M., Navis, G., Voors, A. A., Van Veldhuisen, D. J. & Hillege, H. L. 2009. Increased Central Venous Pressure Is Associated With Impaired Renal Function and Mortality in a Broad Spectrum of Patients With Cardiovascular Disease. *Journal of the American College of Cardiology,* 53**,** 582-588.

Darsaklis, K., Dickson, M. E., Cornwell, W., 3rd, Ayers, C. R., Torres, F., Chin, K. M. & Matulevicius, S. 2016. Right atrial emptying fraction non-invasively predicts mortality in pulmonary hypertension. *Int J Cardiovasc Imaging,* 32**,** 1121-30.

De Roos, A. & Higgins, C. B. 2014. Cardiac radiology: centenary review. *Radiology,* 273**,** S142-59.

Deng, Z. M., Morse, J. H., Slager, S. L., Cuervo, N., Moore, K. J., Venetos, G., Kalachikov, S., Cayanis, E., Fischer, S. G., Barst, R. J., Hodge, S. E. & Knowles, J. A. 2000. Familial primary pulmonary hypertension (gene PPH1) is caused by mutations in the bone morphogenetic protein receptor-II gene. *American Journal of Human Genetics,* 67**,** 737-744.

Diller, G. P. & Gatzoulis, M. A. 2007. Pulmonary vascular disease in adults with congenital heart disease. *Circulation,* 115.

Dos Santos, I., Da Rocha, A. F., Nascimento, F. A. D., Neto, J. S. & Valvano, J. W. 2002. Measurement of ejection fraction with standard thermodilution catheters. *Medical Engineering & Physics,* 24**,** 325-335.

Drazner, M. H., Rame, J. E., Stevenson, L. W. & Dries, D. L. 2001. Prognostic importance of elevated jugular venous pressure and a third heart sound in patients with heart failure. *New England Journal of Medicine,* 345**,** 574-581.

Dreyer, K. J. & Geis, J. R. 2017. When Machines Think: Radiology's Next Frontier. *Radiology,* 285**,** 713-718.

Driessen, M. M., Baggen, V. J., Freling, H. G., Pieper, P. G., Van Dijk, A. P., Doevendans, P. A., Snijder, R. J., Post, M. C., Meijboom, F. J., Sieswerda, G. T., Leiner, T. & Willems, T. P. 2014. Pressure overloaded right ventricles: a multicenter study on the importance of trabeculae in RV function measured by CMR. *Int J Cardiovasc Imaging,* 30**,** 599-608.

Eschenhagen, T. 1993. G-Proteins And The Heart. *Cell Biology International,* 17**,** 723-749.

Fenster, B. E., Lasalvia, L., Schroeder, J. D., Smyser, J., Silveira, L. J., Buckner, J. K. & Brown, K. K. 2014. Cystatin C: a potential biomarker for pulmonary arterial hypertension. *Respirology (Carlton, Vic.),* 19.

Fijalkowska, A., Kurzyna, M., Torbicki, A., Szewczyk, G., Florczyk, M., Pruszczyk, P. & Szturmowicz, M. 2006. Serum N-terminal brain natriuretic peptide as a prognostic parameter in patients with pulmonary hypertension. *Chest,* 129**,** 1313-1321.

Fu, S., Ping, P., Wang, F. & Luo, L. 2018. Synthesis, secretion, function, metabolism and application of natriuretic peptides in heart failure. *Journal of biological engineering,* 12.

Fukuda, Y., Tanaka, H., Motoji, Y., Ryo, K., Sawa, T., Imanishi, J., Miyoshi, T., Mochizuki, Y., Tatsumi, K., Matsumoto, K., Shinke, T., Emoto, N. & Hirata, K.-I. 2014. Utility of combining assessment of right ventricular function and right atrial remodeling as a prognostic factor for patients with pulmonary hypertension. *International Journal of Cardiovascular Imaging,* 30**,** 1269-1277.

Fukuda, Y., Tanaka, H., Ryo-Koriyama, K., Motoji, Y., Sano, H., Shimoura, H., Ooka, J., Toki, H., Sawa, T., Mochizuki, Y., Matsumoto, K., Emoto, N. & Hirata, K.-I. 2016. Comprehensive Functional Assessment of Right-Sided Heart Using Speckle Tracking Strain for Patients with Pulmonary Hypertension. *Echocardiography-a Journal of Cardiovascular Ultrasound and Allied Techniques,* 33**,** 1001-1008.

Fuster, V., Steele, P. M., Edwards, W. D., Gersh, B. J., Mcgoon, M. D. & Frye, R. L. 1984. Primary Pulmonary-Hypertension - Natural-History And The Importance Of Thrombosis. *Circulation,* 70**,** 580-587.

Galea, N., Carbone, I., Cannata, D., Cannavale, G., Conti, B., Galea, R., Frustaci, A., Catalano, C. & Francone, M. 2013. Right ventricular cardiovascular magnetic resonance imaging: normal anatomy and spectrum of pathological findings. *Insights into imaging,* 4**,** 213-23.

Galiè, N., Channick, R. N., Frantz, R. P., Grünig, E., Jing, Z. C., Moiseeva, O., Preston, I. R., Pulido, T., Safdar, Z., Tamura, Y. & Mclaughlin, V. V. 2019. Risk stratification and medical therapy of pulmonary arterial hypertension. *The European respiratory journal,* 53.

Galiè, N. & Ghofrani, A. H. 2013. New horizons in pulmonary arterial hypertension therapies. *European respiratory review : an official journal of the European Respiratory Society,* 22.

Galiè, N., Humbert, M., Vachiery, J. L., Gibbs, S., Lang, I., Torbicki, A., Simonneau, G., Peacock, A., Vonk Noordegraaf, A., Beghetti, M., Ghofrani, A., Gomez Sanchez, M. A., Hansmann, G., Klepetko, W., Lancellotti, P., Matucci, M., Mcdonagh, T., Pierard, L. A., Trindade, P. T., M, Z. & Hoeper, M. 2015. 2015 ESC/ERS Guidelines for the diagnosis and treatment of pulmonary hypertension: The Joint Task Force for the Diagnosis and Treatment of Pulmonary Hypertension of the European Society of Cardiology (ESC) and the European Respiratory Society (ERS): Endorsed by: Association for European Paediatric and Congenital Cardiology

(AEPC), International Society for Heart and Lung Transplantation (ISHLT). *The European respiratory journal*, 46.

Galiè, N., Humbert, M., Vachiery, J. L., Gibbs, S., Lang, I., Torbicki, A., Simonneau, G., Peacock, A., Vonk Noordegraaf, A., Beghetti, M., Ghofrani, A., Gomez Sanchez, M. A., Hansmann, G., Klepetko, W., Lancellotti, P., Matucci, M., Mcdonagh, T., Pierard, L. A., Trindade, P. T., Zompatori, M. & Hoeper, M. 2016. 2015 ESC/ERS Guidelines for the diagnosis and treatment of pulmonary hypertension: The Joint Task Force for the Diagnosis and Treatment of Pulmonary Hypertension of the European Society of Cardiology (ESC) and the European Respiratory Society (ERS): Endorsed by: Association for European Paediatric and Congenital Cardiology (AEPC), International Society for Heart and Lung Transplantation (ISHLT). *European heart journal*, 37.

Galiè, N., Seeger, W., Naeije, R., Simonneau, G. & Rubin, L. J. 2004. Comparative analysis of clinical trials and evidence-based treatment algorithm in pulmonary arterial hypertension. *Journal of the American College of Cardiology*, 43.

Gan, C. T., Mccann, G. P., Marcus, J. T., Van Wolferen, S. A., Twisk, J. W., Boonstra, A., Postmus, P. E. & Vonk-Noordegraf, A. 2006. NT-proBNP reflects right ventricular structure and function in pulmonary hypertension. *European Respiratory Journal*, 28**,** 1190-1194.

García-Alvarez, A., Fernández-Friera, L., Mirelis, J. G., Sawit, S., Nair, A., Kallman, J., Fuster, V. & Sanz, J. 2011. Non-invasive estimation of pulmonary vascular resistance with cardiac magnetic resonance. *European heart journal*, 32.

Garg, P., Crandon, S., Swoboda, P. P., Fent, G. J., Foley, J. R. J., Chew, P. G., Brown, L. A. E., Vijayan, S., Hassell, M. E. C. J., Nijveldt, R., Bissell, M., Elbaz, M. S. M., Al-Mohammad, A., Westenberg, J. J. M., Greenwood, J. P., Van Der Geest, R. J., Plein, S. & Dall'armellina, E. 2018. Left ventricular blood flow kinetic energy after myocardial infarction - insights from 4D flow cardiovascular magnetic resonance. *Journal of Cardiovascular Magnetic Resonance*, 20.

Gaynor, S. L., Maniar, H. S., Bloch, J. B., Steendijk, P. & Moon, M. R. 2005a. Right atrial and ventricular adaptation to chronic right ventricular pressure overload. *Circulation*, 112**,** I212-8.

Gaynor, S. L., Maniar, H. S., Prasad, S. M., Steendijk, P. & Moon, M. R. 2005b. Reservoir and conduit function of right atrium: impact on right ventricular filling and cardiac output. *Am J Physiol Heart Circ Physiol*, 288**,** H2140-5.

Ghio, S., Mercurio, V., Fortuni, F., Forfia, P. R., Gall, H., Ghofrani, A., Mathai, S. C., Mazurek, J. A., Mukherjee, M., Richter, M., Scelsi, L., Hassoun, P. M., Tello, K. & Investigators, T. P. 2020. A comprehensive echocardiographic method for risk stratification in pulmonary arterial hypertension. *European Respiratory Journal*, 56.

Ghofrani, H. A., Galiè, N., Grimminger, F., Grünig, E., Humbert, M., Jing, Z. C., Keogh, A. M., Langleben, D., Kilama, M. O., Fritsch, A., Neuser, D. & Rubin, L. J. 2013. Riociguat for the treatment of pulmonary arterial hypertension. *The New England journal of medicine*, 369.

Goerne, H., Batra, K. & Rajiah, P. 2018. Imaging of pulmonary hypertension: an update. *Cardiovascular diagnosis and therapy,* 8.

Goh, Z. M., Alabed, S., Shahin, Y., Rothman, A. M. K., Garg, P., Lawrie, A., Capener, D., Thompson, A. A. R., Alandejani, F. A. A., Johns, C. S., Lewis, R. A., Dwivedi, K., Wild, J. M., Condliffe, R., Kiely, D. G. & Swift, A. J. 2020. Right Ventricular Adaptation Assessed Using Cardiac Magnetic Resonance Predicts Survival in Pulmonary Arterial Hypertension. *JACC. Cardiovascular imaging*.

Grothues, F., Moon, J. C., Bellenger, N. G., Smith, G. S., Klein, H. U. & Pennell, D. J. 2004. Interstudy reproducibility of right ventricular volumes, function, and mass with cardiovascular magnetic resonance. *American Heart Journal,* 147**,** 218-223.

Han, M. K., Mclaughlin, V. V., Criner, G. J. & Martinez, F. J. 2007. Pulmonary diseases and the heart. *Circulation,* 116.

Hassoun, P. M., Zamanian, R. T., Damico, R., Lechtzin, N., Khair, R., Kolb, T. M., Tedford, R. J., Hulme, O. L., Housten, T., Pisanello, C., Sato, T., Pullins, E. H., Corona-Villalobos, C. P., Zimmerman, S. L., Gashouta, M. A., Minai, O. A., Torres, F., Girgis, R. E., Chin, K. & Mathai, S. C. 2015. Ambrisentan and Tadalafil Up-front Combination Therapy in Scleroderma-associated Pulmonary Arterial Hypertension. *American journal of respiratory and critical care medicine,* 192.

Hoeper, M. M., Bogaard, H. J., Condliffe, R., Frantz, R., Khanna, D., Kurzyna, M., Langleben, D., Manes, A., Satoh, T., Torres, F., Wilkins, M. R. & Badesch, D. B. 2013. Definitions and Diagnosis of Pulmonary Hypertension. *Journal of the American College of Cardiology,* 62**,** D42-D50.

Hoeper, M. M., Humbert, M., Souza, R., Idrees, M., Kawut, S. M., Sliwa-Hahnle, K., Jing, Z. C. & Gibbs, J. S. 2016. A global view of pulmonary hypertension. *The Lancet. Respiratory medicine,* 4.

Hoeper, M. M., Kramer, T., Pan, Z., Eichstaedt, C. A., Spiesshoefer, J., Benjamin, N., Olsson, K. M., Meyer, K., Vizza, C. D., Vonk-Noordegraaf, A., Distler, O., Opitz, C., Gibbs, J. S. R., Delcroix, M., Ghofrani, H. A., Huscher, D., Pittrow, D., Rosenkranz, S. & Grünig, E. 2017. Mortality in pulmonary arterial hypertension: prediction by the 2015 European pulmonary hypertension guidelines risk stratification model. *The European respiratory journal,* 50.

Holubarsch, C., Hasenfuss, G., Schmidtschweda, S., Knorr, A., Pieske, B., Ruf, T., Fasol, R. & Just, H. 1993. Angiotensin-I And Angiotensin-Ii Exert Inotropic Effects In Atrial But Not In Ventricular Human Myocardium - An In-Vitro Study Under Physiological Experimental Conditions. *Circulation,* 88**,** 1228-1237.

Holubarsch, C., Ruf, T., Goldstein, D. J., Ashton, R. C., Nickl, W., Pieske, B., Pioch, K., Ludemann, J., Wiesner, S., Hasenfuss, G., Posival, H., Just, H. & Burkhoff, D. 1996. Existence of the

Frank-Starling mechanism in the failing human heart - Investigations on the organ, tissue, and sarcomere levels. *Circulation,* 94**,** 683-689.

Humbert, M. & Ghofrani, H. A. 2016. The molecular targets of approved treatments for pulmonary arterial hypertension. *Thorax,* 71.

Humbert, M., Kovacs, G., Hoeper, M. M., Badagliacca, R., Berger, R. M. F., Brida, M., Carlsen, J., Coats, A. J. S., Escribano-Subias, P., Ferrari, P., Ferreira, D. S., Ghofrani, H., A, Giannakoulas, G., Kiely, D. G., Mayer, E., Meszaros, G., Nagavci, B., Olsson, K. M., Pepke-Zaba, J., Quint, J. K., Rådegran, G., Simonneau, G., Sitbon, O., Tonia, T., Toshner, M., Vachiery, J. L., Vonk Noordegraaf, A., Delcroix, M. & Rosenkranz, S. 2022a. 2022 ESC/ERS Guidelines for the diagnosis and treatment of pulmonary hypertension. *The European respiratory journal*.

Humbert, M., Kovacs, G., Hoeper, M. M., Badagliacca, R., Berger, R. M. F., Brida, M., Carlsen, J., Coats, A. J. S., Escribano-Subias, P., Ferrari, P., Ferreira, D. S., Ghofrani, H. A., Giannakoulas, G., Kiely, D. G., Mayer, E., Meszaros, G., Nagavci, B., Olsson, K. M., Pepke-Zaba, J., Quint, J. K., Rådegran, G., Simonneau, G., Sitbon, O., Tonia, T., Toshner, M., Vachiery, J. L., Vonk Noordegraaf, A., Delcroix, M. & Rosenkranz, S. 2022b. 2022 ESC/ERS Guidelines for the diagnosis and treatment of pulmonary hypertension. *European heart journal,* 43.

Humbert, M., Sitbon, O., Chaouat, A., Bertocchi, M., Habib, G., Gressin, V., Yaici, A., Weitzenblum, E., Cordier, J. F., Chabot, F., Dromer, C., Pison, C., Reynaud-Gaubert, M., Haloun, A., Laurent, M., Hachulla, E., Cottin, V., Degano, B., Jais, X., Montani, D., Souza, R. & Simonneau, G. 2010a. Survival in Patients With Idiopathic, Familial, and Anorexigen-Associated Pulmonary Arterial Hypertension in the Modern Management Era. *Circulation,* 122**,** 156-163.

Humbert, M., Sitbon, O., Yaïci, A., Montani, D., O'callaghan, D. S., Jaïs, X., Parent, F., Savale, L., Natali, D., Günther, S., Chaouat, A., Chabot, F., Cordier, J. F., Habib, G., Gressin, V., Jing, Z. C., Souza, R. & Simonneau, G. 2010b. Survival in incident and prevalent cohorts of patients with pulmonary arterial hypertension. *The European respiratory journal,* 36.

Hurdman, J., Condliffe, R., Elliot, C. A., Davies, C., Hill, C., Wild, J. M., Capener, D., Sephton, P., Hamilton, N., Armstrong, I. J., Billings, C., Lawrie, A., Sabroe, I., Akil, M., O'toole, L. & Kiely, D. G. 2012. ASPIRE registry: Assessing the Spectrum of Pulmonary hypertension Identified at a REferral centre. *European Respiratory Journal,* 39**,** 945-955.

Ivanov, A., Mohamed, A., Asfour, A., Ho, J., Khan, S. A., Chen, O., Klem, I., Ramasubbu, K., Brener, S. J. & Heitner, J. F. 2017. Right atrial volume by cardiovascular magnetic resonance predicts mortality in patients with heart failure with reduced ejection fraction. *Plos One,* 12.

Jarvinen, V. M., Kupari, M. M., Hekali, P. E. & Poutanen, V. P. 1994. Right atrial MR imaging studies of cadaveric atrial casts and comparison with right and left atrial volumes and function in healthy subjects. *Radiology,* 191**,** 137-42.

Jarvinen, V. M., Kupari, M. M., Poutanen, V. P. & Hekali, P. E. 1996. Right and left atrial phasic volumetric function in mildly symptomatic dilated and hypertrophic cardiomyopathy: cine MR imaging assessment. *Radiology,* 198**,** 487-95.

Jerosch-Herold, M. & Kwong, R. Y. 2008. Magnetic Resonance Imaging in the Assessment of Ventricular Remodeling and Viability. *Curr Heart Fail Rep,* 5**,** 5-10.

Johns, C. S., Kiely, D. G., Rajaram, S., Hill, C., Thomas, S., Karunasaagarar, K., Garg, P., Hamilton, N., Solanki, R., Capener, D. A., Elliot, C., Sabroe, I., Charalamopopoulos, A., Condliffe, R., Wild, J. M. & Swift, A. J. 2019. Diagnosis of Pulmonary Hypertension with Cardiac MRI: Derivation and Validation of Regression Models. *Radiology,* 290**,** 61-68.

Katz, J., Whang, J., Boxt, L. M. & Barst, R. J. 1993. Estimation Of Right Ventricular Mass In Normal Subjects And In Patients With Primary Pulmonary-Hypertension By Nuclear-Magnetic-Resonance Imaging. *Journal of the American College of Cardiology,* 21**,** 1475-1481.

Kawut, S. M., Barr, R. G., Lima, J. A. C., Praestgaard, A., Johnson, W. C., Chahal, H., Ogunyankin, K. O., Bristow, M. R., Kizer, J. R., Tandri, H. & Bluemke, D. A. 2012. Right Ventricular Structure Is Associated With the Risk of Heart Failure and Cardiovascular Death The Multi-Ethnic Study of Atherosclerosis (MESA)-Right Ventricle Study. *Circulation,* 126**,** 1681-+.

Kawut, S. M., Horn, E. M., Berekashvili, K. K., Garofano, R. P., Goldsmith, R. L., Widlitz, A. C., Rosenzweig, E. B., Kerstein, D. & Barst, R. J. 2005. New predictors of outcome in idiopathic pulmonary arterial hypertension. *American Journal of Cardiology,* 95**,** 199-203.

Kawut, S. M., Lima, J. A. C., Barr, R. G., Chahal, H., Jain, A., Tandri, H., Praestgaard, A., Bagiella, E., Kizer, J. R., Johnson, W. C., Kronmal, R. A. & Bluemke, D. A. 2011. Sex and Race Differences in Right Ventricular Structure and Function The Multi-Ethnic Study of Atherosclerosis-Right Ventricle Study. *Circulation,* 123**,** 2542-U116.

Khan, S. S. & Rich, J. D. 2015. Novel technologies and devices for monitoring and treating pulmonary arterial hypertension. *Can J Cardiol,* 31**,** 478-88.

Kiely, D. G., Elliot, C. A., Sabroe, I. & Condliffe, R. 2013. Pulmonary hypertension: diagnosis and management. *Bmj-British Medical Journal,* 346.

Kiely, D. G., Kennedy, N. S., Pirzada, O., Batchelor, S. A., Struthers, A. D. & Lipworth, B. J. 2005. Elevated levels of natriuretic peptides in patients with pulmonary thromboembolism. *Respiratory medicine,* 99.

Kiely, D. G., Levin, D. L., Hassoun, P. M., Ivy, D., Jone, P.-N., Bwika, J., Kawut, S. M., Lordan, J., Lungu, A., Mazurek, J. A., Moledina, S., Olschewski, H., Peacock, A. J., Puri, G. D., Rahaghi, F. N., Schafer, M., Schiebler, M., Screaton, N., Tawhai, M., Van Beek, E. J. R., Vonk-Noordegraaf, A., Vandepool, R., Wort, S. J., Zhao, L., Wild, J. M., Vogel-Claussen, J. & Swift, A. J. 2019. Statement on imaging and pulmonary hypertension from the Pulmonary Vascular Research Institute (PVRI). *Pulmonary Circulation,* 9.

Klem, I., Shah, D. J., White, R. D., Pennell, D. J., Van Rossum, A. C., Regenfus, M., Sechtem, U., Schvartzman, P. R., Hunold, P., Croisille, P., Parker, M., Judd, R. M. & Kim, R. J. 2011. Prognostic Value of Routine Cardiac Magnetic Resonance Assessment of Left Ventricular Ejection Fraction and Myocardial Damage An International, Multicenter Study. *Circulation-Cardiovascular Imaging,* 4**,** 610-619.

Knight, D. S., Steeden, J. A., Moledina, S., Jones, A., Coghlan, J. G. & Muthurangu, V. 2015. Left ventricular diastolic dysfunction in pulmonary hypertension predicts functional capacity and clinical worsening: a tissue phase mapping study. *Journal of cardiovascular magnetic resonance : official journal of the Society for Cardiovascular Magnetic Resonance,* 17.

Kobirumaki-Shimozawa, F., Inoue, T., Shintani, S. A., Oyama, K., Terui, T., Minamisawa, S., Ishiwata, S. & Fukuda, N. 2014. Cardiac thin filament regulation and the Frank-Starling mechanism. *The journal of physiological sciences : JPS,* 64.

Kuwana, M., Blair, C., Takahashi, T., Langley, J. & Coghlan, J. G. 2020. Initial combination therapy of ambrisentan and tadalafil in connective tissue disease-associated pulmonary arterial hypertension (CTD-PAH) in the modified intention-to-treat population of the AMBITION study: post hoc analysis. *Annals of the rheumatic diseases,* 79.

Kylhammar, D., Kjellström, B., Hjalmarsson, C., Jansson, K., Nisell, M., Söderberg, S., Wikström, G. & Rådegran, G. 2018. A comprehensive risk stratification at early follow-up determines prognosis in pulmonary arterial hypertension. *European heart journal,* 39.

Lador, F., Soccal, P. M. & Sitbon, O. 2014. Biomarkers for the prognosis of pulmonary arterial hypertension: Holy Grail or flying circus? *The Journal of heart and lung transplantation : the official publication of the International Society for Heart Transplantation,* 33.

Launay, D., Sitbon, O., Hachulla, E., Mouthon, L., Gressin, V., Rottat, L., Clerson, P., Cordier, J.-F., Simonneau, G. & Humbert, M. 2013. Survival in systemic sclerosis-associated pulmonary arterial hypertension in the modern management era. *Annals of the rheumatic diseases,* 72.

Lee, W. T., Ling, Y., Sheares, K. K., Pepke-Zaba, J., Peacock, A. J. & Johnson, M. K. 2012. Predicting survival in pulmonary arterial hypertension in the UK. *The European respiratory journal,* 40.

Leuchte, H. H., El Nounou, M., Tuerpe, J. C., Hartmann, B., Baumgartner, R. A., Vogeser, M., Muehling, O. & Behr, J. 2007. N-terminal pro-brain natriuretic peptide and renal insufficiency as predictors of mortality in pulmonary hypertension. *Chest,* 131**,** 402-409.

Leuchte, H. H., Holzapfel, M., Baumgartner, R. A., Ding, I., Neurohr, C., Vogeser, M., Kolbe, T., Schwaiblmair, M. & Behr, J. 2004. Clinical significance of brain natriuretic peptide in primary pulmonary hypertension. *Journal of the American College of Cardiology,* 43**,** 764-770.

Lewis, R. A., Johns, C. S., Cogliano, M., Capener, D., Tubman, E., Elliot, C. A., Charalampopoulos, A., Sabroe, I., Thompson, A. A. R., Billings, C. G., Hamilton, N., Baster, K., Laud, P. J., Hickey, P. M., Middleton, J., Armstrong, I. J., Hurdman, J. A., Lawrie, A., Rothman, A. M. K., Wild, J. M., Condliffe, R., Swift, A. J. & Kiely, D. G. 2020. Identification of Cardiac Magnetic

Resonance Imaging Thresholds for Risk Stratification in Pulmonary Arterial Hypertension. *American Journal of Respiratory and Critical Care Medicine,* 201**,** 458-468.

Li, Y. D., Wang, Y. D., Ye, X. G., Kong, L. Y., Zhu, W. W. & Lu, X. Z. 2016. Clinical study of right ventricular longitudinal strain for assessing right ventricular dysfunction and hemodynamics in pulmonary hypertension. *Medicine,* 95.

Lichtblau, M., Bader, P. R., Saxer, S., Berlier, C., Schwarz, E. I., Hasler, E. D., Furian, M., Gruenig, E., Bloch, K. E. & Ulrich, S. 2020. Right Atrial Pressure During Exercise Predicts Survival in Patients With Pulmonary Hypertension. *Journal of the American Heart Association,* 9.

Ling, Y., Johnson, M. K., Kiely, D. G., Condliffe, R., Elliot, C. A., Simon, J., Gibbs, R., Howard, L. S., Pepke-Zaba, J., Sheares, K. K. K., Corriss, P. A., Fisher, A. J., Lordan, J. L., Gaine, S., Coghlan, J. G., Wort, S. J., Gatzoulis, M. A. & Peacock, A. J. 2012. Changing Demographics, Epidemiology, and Survival of Incident Pulmonary Arterial Hypertension Results from the Pulmonary Hypertension Registry of the United Kingdom and Ireland. *American Journal of Respiratory and Critical Care Medicine,* 186**,** 790-796.

Liu, K., Zhang, C., Chen, B., Li, M. & Zhang, P. 2020. Association between right atrial area measured by echocardiography and prognosis among pulmonary arterial hypertension: a systematic review and meta-analysis. *Bmj Open,* 10.

Lohani, O., Colvin, K. L. & Yeager, M. E. 2015. Biomarkers for pediatric pulmonary arterial hypertension: challenges and recommendations. *Paediatric Respiratory Reviews,* 16**,** 225-231.

Lowe, B. S., Therrien, J., Ionescu-Ittu, R., Pilote, L., Martucci, G. & Marelli, A. J. 2011. Diagnosis of pulmonary hypertension in the congenital heart disease adult population impact on outcomes. *Journal of the American College of Cardiology,* 58.

Lythgoe, M. P., Rhodes, C. J., Ghataorhe, P., Attard, M., Wharton, J. & Wilkins, M. R. 2016. Why drugs fail in clinical trials in pulmonary arterial hypertension, and strategies to succeed in the future. *Pharmacol Ther,* 164**,** 195-203.

Maceira, A. M., Cosin-Sales, J., Prasad, S. K. & Pennell, D. J. 2016. Characterization of left and right atrial function in healthy volunteers by cardiovascular magnetic resonance. *Journal of Cardiovascular Magnetic Resonance,* 18.

Maceira, A. M., Cosín-Sales, J., Roughton, M., Prasad, S. K. & Pennell, D. J. 2013. Reference right atrial dimensions and volume estimation by steady state free precession cardiovascular magnetic resonance. *Journal of cardiovascular magnetic resonance : official journal of the Society for Cardiovascular Magnetic Resonance,* 15.

Mauritz, G. J., Kind, T., Marcus, J. T., Bogaard, H. J., Van De Veerdonk, M., Postmus, P. E., Boonstra, A., Westerhof, N. & Vonk-Noordegraaf, A. 2012. Progressive Changes in Right Ventricular Geometric Shortening and Long-term Survival in Pulmonary Arterial Hypertension. *Chest,* 141**,** 935-943.

Mauritz, G. J., Rizopoulos, D., Groepenhoff, H., Tiede, H., Felix, J., Eilers, P., Bosboom, J., Postmus, P. E., Westerhof, N. & Vonk-Noordegraaf, A. 2011. Usefulness of Serial N-Terminal Pro B-Type Natriuretic Peptide Measurements for Determining Prognosis in Patients With Pulmonary Arterial Hypertension. *American Journal of Cardiology,* 108**,** 1645-1650.

Mclaughlin, V. V., Shillington, A. & Rich, S. 2002. Survival in primary pulmonary hypertension - The impact of epoprostenol therapy. *Circulation,* 106**,** 1477-1482.

Mclaughlin, V. V., Sitbon, O., Badesch, D. B., Barst, R. J., Black, C., Galle, N., Rainisio, M., Simonneau, G. & Rubin, L. J. 2005. Survival with first-line bosentan in patients with primary pulmonary hypertension. *European Respiratory Journal,* 25**,** 244-249.

Mello, M. M., Watte, G., Altmayer, S., Pallaoro, Y. L. R., Spilimbergo, F. B., Blanco, D. C., Meyer, G. M. B., Marchiori, E. & Hochhegger, B. 2019. Relationship between right atrium area and right ventricular ejection fraction on magnetic resonance imaging: comparison with other prognostic markers in patients with pulmonary arterial hypertension. *Radiologia brasileira,* 52.

Meris, A., Faletra, F., Conca, C., Klersy, C., Regoli, F., Klimusina, J., Penco, M., Pasotti, E., Pedrazzini, G. B., Moccetti, T. & Auricchio, A. 2010. Timing and Magnitude of Regional Right Ventricular Function: A Speckle Tracking-Derived Strain Study of Normal Subjects and Patients with Right Ventricular Dysfunction. *Journal of the American Society of Echocardiography,* 23**,** 823-831.

Michelakis, E. D., Tymchak, W., Noga, M., Webster, L., Wu, X. C., Lien, D., Wang, S. H., Modry, D. & Archer, S. L. 2003. Long-term treatment with oral sildenafil is safe and improves functional capacity and hemodynamics in patients with pulmonary arterial hypertension. *Circulation,* 108.

Mohiaddin, R. H. & Hasegawa, M. 1995. Measurement of atrial volumes by magnetic resonance imaging in healthy volunteers and in patients with myocardial infarction. *Eur Heart J,* 16**,** 106-11.

Mooij, C. F., De Wit, C. J., Graham, D. A., Powell, A. J. & Geva, T. 2008. Reproducibility of MRI measurements of right ventricular size and function in patients with normal and dilated ventricles. *Journal of Magnetic Resonance Imaging,* 28**,** 67-73.

Mordi, I., Bezerra, H., Carrick, D. & Tzemos, N. 2015. The Combined Incremental Prognostic Value of LVEF, Late Gadolinium Enhancement, and Global Circumferential Strain Assessed by CMR. *Jacc-Cardiovascular Imaging,* 8**,** 540-549.

Morrell, N. W., Adnot, S., Archer, S. L., Dupuis, J., Jones, P. L., Maclean, M. R., Mcmurtry, I. F., Stenmark, K. R., Thistlethwaite, P. A., Weissmann, N., Yuan, J. X. J. & Weir, E. K. 2009. Cellular and Molecular Basis of Pulmonary Arterial Hypertension. *J Am Coll Cardiol,* 54**,** S20-31.

Nacif, M. S., Zavodni, A., Kawel, N., Choi, E. Y., Lima, J. A. & Bluemke, D. A. 2012. Cardiac magnetic resonance imaging and its electrocardiographs (ECG): tips and tricks. *The international journal of cardiovascular imaging,* 28.

Nagaya, N., Nishikimi, T., Okano, Y., Uematsu, M., Satoh, T., Kyotani, S., Kuribayashi, S., Hamada, S., Kakishita, M., Nakanishi, N., Takamiya, M., Kunieda, T., Matsuo, H. & Kangawa, K. 1998. Plasma brain natriuretic peptide levels increase in proportion to the extent of right ventricular dysfunction in pulmonary hypertension. *Journal of the American College of Cardiology,* 31**,** 202-208.

Nagaya, N., Nishikimi, T., Uematsu, M., Satoh, T., Kyotani, S., Sakamaki, F., Kakishita, M., Fukushima, K., Okano, Y., Nakanishi, N., Miyatake, K. & Kangawa, K. 2000. Plasma brain natriuretic peptide as a prognostic indicator in patients with primary pulmonary hypertension. *Circulation,* 102**,** 865-870.

Nayer, J., Aggarwal, P. & Galwankar, S. 2014. Utility of point-of-care testing of natriuretic peptides (brain natriuretic peptide and n-terminal pro-brain natriuretic peptide) in the emergency department. *International journal of critical illness and injury science,* 4.

Nishimura, M., Brann, A., Chang, K. W. & Maisel, A. S. 2018. The Confounding Effects of Non-cardiac Pathologies on the Interpretation of Cardiac Biomarkers. *Current heart failure reports,* 15.

Pascall, E. & Tulloh, R. M. 2018. Pulmonary hypertension in congenital heart disease. *Future cardiology,* 14.

Peacock, A. J., Crawley, S., Mclure, L., Blyth, K. G., Vizza, C. D., Poscia, R., Francone, M., Iacucci, I., Olschewski, H., Kovacs, G., Vonk Noordegraaf, A., Marcus, J. T., Van De Veerdonk, M. C. & Oosterveer, F. P. 2014. Changes in right ventricular function measured by cardiac magnetic resonance imaging in patients receiving pulmonary arterial hypertension-targeted therapy: the EURO-MR study. *Circulation. Cardiovascular imaging,* 7.

Peacock, A. J. & Vonk Noordegraaf, A. 2013. Cardiac magnetic resonance imaging in pulmonary arterial hypertension. *European respiratory review : an official journal of the European Respiratory Society,* 22**,** 526-34.

Petersen, S. E., Aung, N., Sanghvi, M. M., Zemrak, F., Fung, K., Paiva, J. M., Francis, J. M., Khanji, M. Y., Lukaschuk, E., Lee, A. M., Carapella, V., Kim, Y. J., Leeson, P., Piechnik, S. K. & Neubauer, S. 2017. Reference ranges for cardiac structure and function using cardiovascular magnetic resonance (CMR) in Caucasians from the UK Biobank population cohort. *Journal of Cardiovascular Magnetic Resonance,* 19.

Puchalski, M. D., Williams, R. V., Askovich, B., Minich, L. L., Mart, C. & Tani, L. Y. 2007. Assessment of right ventricular size and function: echo versus magnetic resonance imaging. *Congenit Heart Dis,* 2**,** 27-31.

Pulido, T., Adzerikho, I., Channick, R. N., Delcroix, M., Galiè, N., Ghofrani, H. A., Jansa, P., Jing, Z. C., Le Brun, F. O., Mehta, S., Mittelholzer, C. M., Perchenet, L., Sastry, B. K., Sitbon, O., Souza, R., Torbicki, A., Zeng, X., Rubin, L. J. & Simonneau, G. 2013. Macitentan and

morbidity and mortality in pulmonary arterial hypertension. *The New England journal of medicine,* 369.

Qu, Y.-Y., Buckert, D., Ma, G.-S. & Rasche, V. 2021. Quantitative Assessment of Left and Right Atrial Strains Using Cardiovascular Magnetic Resonance Based Tissue Tracking. *Frontiers in Cardiovascular Medicine,* 8.

Rabinovitch, M. 2012. Molecular pathogenesis of pulmonary arterial hypertension. *J Clin Invest,* 122**,** 4306-13.

Raina, A. & Humbert, M. 2016. Risk assessment in pulmonary arterial hypertension. *European respiratory review : an official journal of the European Respiratory Society,* 25.

Ramjug, S., Hussain, N., Hurdman, J., Billings, C., Charalampopoulos, A., Elliot, C. A., Kiely, D. G., Sabroe, I., Rajaram, S., Swift, A. J. & Condliffe, R. 2017. Idiopathic and Systemic Sclerosis-Associated Pulmonary Arterial Hypertension: A Comparison of Demographic, Hemodynamic, and MRI Characteristics and Outcomes. *Chest,* 152.

Raymond, R. J., Hinderliter, A. L., Willis, P. W., Ralph, D., Caldwell, E. J., Williams, W., Ettinger, N. A., Hill, N. S., Summer, W. R., De Boisblanc, B., Schwartz, T., Koch, G., Clayton, L. M., Jobsis, M. M., Crow, J. W. & Long, W. 2002. Echo cardiographic predictors of adverse outcomes in primary pulmonary hypertension. *Journal of the American College of Cardiology,* 39**,** 1214-1219.

Rich, S., Dantzker, D. R., Ayres, S. M., Bergofsky, E. H., Brundage, B. H., Detre, K. M., Fishman, A. P., Goldring, R. M., Groves, B. M., Koerner, S. K., Levy, P. C., Reid, L. M., Vreim, C. E. & Williams, G. W. 1987. Primary Pulmonary-Hypertension - A National Prospective-Study. *Annals of Internal Medicine,* 107**,** 216-223.

Robinson, R., Valindria, V. V., Bai, W., Oktay, O., Kainz, B., Suzuki, H., Sanghvi, M. M., Aung, N., Paiva, J. M., Zemrak, F., Fung, K., Lukaschuk, E., Lee, A. M., Carapella, V., Kim, Y. J., Piechnik, S. K., Neubauer, S., Petersen, S. E., Page, C., Matthews, P. M., Rueckert, D. & Glocker, B. 2019. Automated quality control in image segmentation: application to the UK Biobank cardiovascular magnetic resonance imaging study. *Journal of Cardiovascular Magnetic Resonance,* 21.

Roca, G. Q., Campbell, P., Claggett, B., Solomon, S. D. & Shah, A. M. 2015. Right Atrial Function in Pulmonary Arterial Hypertension. *Circulation-Cardiovascular Imaging,* 8.

Rodes-Cabau, J., Taramasso, M. & O'gara, P. T. 2016. Diagnosis and treatment of tricuspid valve disease: current and future perspectives. *Lancet,* 388**,** 2431-2442.

Rodriguez-Palomares, J. F., Gavara, J., Ferreira-Gonzalez, I., Valente, F., Rios, C., Rodriguez-Garcia, J., Bonanad, C., Garcia Del Blanco, B., Minana, G., Mutuberria, M., Nunez, J., Barrabes, J., Evangelista, A., Bodi, V. & Garcia-Dorado, D. 2019. Prognostic Value of Initial Left Ventricular Remodeling in Patients With Reperfused STEMI. *Jacc-Cardiovascular Imaging,* 12**,** 2445-2456.

Rudski, L. G., Lai, W. W., Afilalo, J., Hua, L., Handschumacher, M. D., Chandrasekaran, K., Solomon, S. D., Louie, E. K. & Schiller, N. B. 2010. Guidelines for the echocardiographic assessment of the right heart in adults: a report from the American Society of Echocardiography endorsed by the European Association of Echocardiography, a registered branch of the European Society of Cardiology, and the Canadian Society of Echocardiography. *J Am Soc Echocardiogr,* 23**,** 685-713; quiz 786-8.

Ruijsink, B., Puyol-Anton, E., Oksuz, I., Sinclair, M., Bai, W., Schnabel, J. A., Razavi, R. & King, A. P. 2020. Fully Automated, Quality-Controlled Cardiac Analysis From CMR Validation and Large-Scale Application to Characterize Cardiac Function. *Jacc-Cardiovascular Imaging,* 13**,** 684-695.

Sallach, J. A., Tang, W. H. W., Borowski, A. G., Tong, W., Porter, T., Martin, M. G., Jasper, S. E., Shrestha, K., Troughton, R. W. & Klein, A. L. 2009. Right Atrial Volume Index in Chronic Systolic Heart Failure and Prognosis. *Jacc-Cardiovascular Imaging,* 2**,** 527-534.

Santaguida, P. L., Don-Wauchope, A. C., Oremus, M., Mckelvie, R., Ali, U., Hill, S. A., Balion, C., Booth, R. A., Brown, J. A., Bustamam, A., Sohel, N. & Raina, P. 2014. BNP and NT-proBNP as prognostic markers in persons with acute decompensated heart failure: a systematic review. *Heart failure reviews,* 19.

Sardanelli, F., Quarenghi, M., Di Leo, G., Boccaccini, L. & Schiavi, A. 2008. Segmentation of cardiac cine MR images of left and right ventricles: interactive semiautomated methods and manual contouring by two readers with different education and experience. *J Magn Reson Imaging,* 27**,** 785-92.

Sato, T., Tsujino, I., Ohira, H., Oyama-Manabe, N., Ito, Y. M., Yamada, A., Ikeda, D., Watanabe, T. & Nishimura, M. 2015. Right atrial volume and reservoir function are novel independent predictors of clinical worsening in patients with pulmonary hypertension. *J Heart Lung Transplant,* 34**,** 414-23.

Sato, T., Tsujino, I., Oyama-Manabe, N., Ohira, H., Ito, Y. M., Yamada, A., Ikeda, D., Watanabe, T. & Nishimura, M. 2013. Right atrial volume and phasic function in pulmonary hypertension. *Int J Cardiol,* 168**,** 420-6.

Sheffield Academic Directorate Of Respiratory Medicine. 2014. *Pulmonary Vascular Disease Unit* [Online]. Available: http://www.lungsheffield.org/clinical-services/pulmonary-vascular [Accessed Aug 2022].

Sievers, B., Addo, M., Breuckmann, F., Barkhausen, J. & Erbel, R. 2007. Reference right atrial function determined by steady-state free precession cardiovascular magnetic resonance. *J Cardiovasc Magn Reson,* 9**,** 807-14.

Simonneau, G., Galiè, N., Rubin, L. J., Langleben, D., Seeger, W., Domenighetti, G., Gibbs, S., Lebrec, D., Speich, R., Beghetti, M., Rich, S. & Fishman, A. 2004. Clinical classification of pulmonary hypertension. *Journal of the American College of Cardiology,* 43.

Simonneau, G., Gatzoulis, M. A., Adatia, I., Celermajer, D., Denton, C., Ghofrani, A., Sanchez, M. A. G., Kumar, R. K., Landzberg, M., Machado, R. F., Olschewski, H., Robbins, I. M. & Souza, R. 2013. Updated Clinical Classification of Pulmonary Hypertension. *Journal of the American College of Cardiology,* 62**,** D34-D41.

Simonneau, G., Montani, D., Celermajer, D. S., Denton, C. P., Gatzoulis, M. A., Krowka, M., Williams, P. G. & Souza, R. 2019. Haemodynamic definitions and updated clinical classification of pulmonary hypertension. *Eur Respir J,* 53.

Sitbon, O., Channick, R., Chin, K. M., Frey, A., Gaine, S., Galiè, N., Ghofrani, H. A., Hoeper, M. M., Lang, I. M., Preiss, R., Rubin, L. J., Di Scala, L., Tapson, V., Adzerikho, I., Liu, J., Moiseeva, O., Zeng, X., Simonneau, G. & Mclaughlin, V. V. 2015. Selexipag for the Treatment of Pulmonary Arterial Hypertension. *The New England journal of medicine,* 373.

Sitbon, O., Humbert, M., Nunes, H., Parent, F., Garcia, G., Herve, P., Rainisio, M. & Simonneau, G. 2002. Long-term intravenous epoprostenol infusion in primary pulmonary hypertension - Prognostic factors and survival. *Journal of the American College of Cardiology,* 40**,** 780-788.

Sitbon, O., Sattler, C., Bertoletti, L., Savale, L., Cottin, V., Jaïs, X., De Groote, P., Chaouat, A., Chabannes, C., Bergot, E., Bouvaist, H., Dauphin, C., Bourdin, A., Bauer, F., Montani, D., Humbert, M. & Simonneau, G. 2016. Initial dual oral combination therapy in pulmonary arterial hypertension. *The European respiratory journal,* 47.

Soubrier, F., Chung, W. K., Machado, R., Grunig, E., Aldred, M., Geraci, M., Loyd, J. E., Elliott, C. G., Trembath, R. C., Newman, J. H. & Humbert, M. 2013. Genetics and Genomics of Pulmonary Arterial Hypertension. *Journal of the American College of Cardiology,* 62**,** D13-D21.

Suinesiaputra, A., Bluemke, D. A., Cowan, B. R., Friedrich, M. G., Kramer, C. M., Kwong, R., Plein, S., Schulz-Menger, J., Westenberg, J. J. M., Young, A. A. & Nagel, E. 2015. Quantification of LV function and mass by cardiovascular magnetic resonance: multi-center variability and consensus contours. *Journal of Cardiovascular Magnetic Resonance,* 17**,** 63.

Suinesiaputra, A., Sanghvi, M. M., Aung, N., Paiva, J. M., Zemrak, F., Fung, K., Lukaschuk, E., Lee, A. M., Carapella, V., Kim, Y. J., Francis, J., Piechnik, S. K., Neubauer, S., Greiser, A., Jolly, M.-P., Hayes, C., Young, A. A. & Petersen, S. E. 2018. Fully-automated left ventricular mass and volume MRI analysis in the UK Biobank population cohort: evaluation of initial results. *International Journal of Cardiovascular Imaging,* 34**,** 281-291.

Swift, A. J., Capener, D., Johns, C., Hamilton, N., Rothman, A., Elliot, C., Condliffe, R., Charalampopoulos, A., Rajaram, S., Lawrie, A., Campbell, M. J., Wild, J. M. & Kiely, D. G. 2017. Magnetic Resonance Imaging in the Prognostic Evaluation of Patients with Pulmonary Arterial Hypertension. *American Journal of Respiratory and Critical Care Medicine,* 196**,** 228-239.

Swift, A. J., Rajaram, S., Campbell, M. J., Hurdman, J., Thomas, S., Capener, D., Elliot, C., Condliffe, R., Wild, J. M. & Kiely, D. G. 2014a. Prognostic Value of Cardiovascular Magnetic Resonance Imaging Measurements Corrected for Age and Sex in Idiopathic Pulmonary Arterial Hypertension. *Circulation-Cardiovascular Imaging,* 7**,** 100-106.

Swift, A. J., Rajaram, S., Condliffe, R., Capener, D., Hurdman, J., Elliot, C., Kiely, D. G. & Wild, J. M. 2012a. Pulmonary Artery Relative Area Change Detects Mild Elevations in Pulmonary Vascular Resistance and Predicts Adverse Outcome in Pulmonary Hypertension. *Investigative Radiology,* 47**,** 571-577.

Swift, A. J., Rajaram, S., Condliffe, R., Capener, D., Hurdman, J., Elliot, C. A., Wild, J. M. & Kiely, D. G. 2012b. Diagnostic accuracy of cardiovascular magnetic resonance imaging of right ventricular morphology and function in the assessment of suspected pulmonary hypertension results from the ASPIRE registry. *Journal of Cardiovascular Magnetic Resonance,* 14.

Swift, A. J., Wild, J. M., Nagle, S. K., Roldan-Alzate, A., Francois, C. J., Fain, S., Johnson, K., Capener, D., Van Beek, E. J., Kiely, D. G., Wang, K. & Schiebler, M. L. 2014b. Quantitative magnetic resonance imaging of pulmonary hypertension: a practical approach to the current state of the art. *J Thorac Imaging,* 29**,** 68-79.

Swift, A. J., Wilson, F., Cogliano, M., Kendall, L., Alandejani, F., Alabed, S., Hughes, P., Shahin, Y., Saunders, L., Oram, C., Capener, D., Rothman, A., Garg, P., Johns, C., Austin, M., Macdonald, A., Pickworth, J., Hickey, P., Condliffe, R., Cahn, A., Lawrie, A., Wild, J. M. & Kiely, D. G. 2021. Repeatability and sensitivity to change of non-invasive end points in PAH: the RESPIRE study. *Thorax,* 76.

Tao, Q., Yan, W., Wang, Y., Paiman, E. H. M., Shamonin, D. P., Garg, P., Plein, S., Huang, L., Xia, L., Sramko, M., Tintera, J., De Roos, A., Lamb, H. J. & Van Der Geest, R. J. 2019. Deep Learning-based Method for Fully Automatic Quantification of Left Ventricle Function from Cine MR Images: A Multivendor, Multicenter Study. *Radiology,* 290.

Taverne, Y. J. H. J., Sadeghi, A., Bartelds, B., Bogers, A. J. J. C. & Merkus, D. 2021. Right ventricular phenotype, function, and failure: a journey from evolution to clinics. *Heart failure reviews,* 26.

Thenappan, T., Glassner, C. & Gomberg-Maitland, M. 2012. Validation of the pulmonary hypertension connection equation for survival prediction in pulmonary arterial hypertension. *Chest,* 141.

Thenappan, T., Shah, S. J., Rich, S., Tian, L., Archer, S. L. & Gomberg-Maitland, M. 2010. Survival in pulmonary arterial hypertension: a reappraisal of the NIH risk stratification equation. *The European respiratory journal,* 35.

Thrall, J. H., Li, X., Li, Q., Cruz, C., Do, S., Dreyer, K. & Brink, J. 2018. Artificial Intelligence and Machine Learning in Radiology: Opportunities, Challenges, Pitfalls, and Criteria for Success. *Journal of the American College of Radiology,* 15**,** 504-508.

Truong, V. T., Palmer, C., Young, M., Wolking, S., Ngo, T. N. M., Sheets, B., Hausfeld, C., Ornella, A., Taylor, M. D., Zareba, K. M., Raman, S. V. & Mazur, W. 2020. Right Atrial Deformation

Using Cardiovascular Magnetic Resonance Myocardial Feature Tracking Compared with Two-Dimensional Speckle Tracking Echocardiography in Healthy Volunteers. *Scientific Reports,* 10.

Van De Veerdonk, M. C., In T Veld, A. E. H., Marcus, J. T., Westerhof, N., Heymans, M. W., Bogaard, H. J. & Vonk-Noordegraaf, A. 2017. Upfront combination therapy reduces right ventricular volumes in pulmonary arterial hypertension. *European Respiratory Journal,* 49.

Van De Veerdonk, M. C., Kind, T., Marcus, J. T., Mauritz, G. J., Heymans, M. W., Bogaard, H. J., Boonstra, A., Marques, K. M. J., Westerhof, N. & Vonk-Noordegraaf, A. 2011. Progressive Right Ventricular Dysfunction in Patients With Pulmonary Arterial Hypertension Responding to Therapy. *Journal of the American College of Cardiology,* 58**,** 2511-2519.

Van Wolferen, S. A., Marcus, J. T., Boonstra, A., Marques, K. M. J., Bronzwaer, J. G. F., Spreeuwenberg, M. D., Postmus, P. E. & Vonk-Noordegraaf, A. 2007. Prognostic value of right ventricular mass, volume, and function in idiopathic pulmonary arterial hypertension. *European Heart Journal,* 28**,** 1250-1257.

Van Wolferen, S. A., Van De Veerdonk, M. C., Mauritz, G. J., Jacobs, W., Marcus, J. T., Marques, K. M. J., Bronzwaer, J. G. F., Heymans, M. W., Boonstra, A., Postmus, P. E., Westerhof, N. & Vonk Noordegraaf, A. 2011. Clinically significant change in stroke volume in pulmonary hypertension. *Chest,* 139.

Ventetuolo, C. E., Ouyang, P., Bluemke, D. A., Tandri, H., Barr, R. G., Bagiella, E., Cappola, A. R., Bristow, M. R., Johnson, C., Kronmal, R. A., Kizer, J. R., Lima, J. A. C. & Kawut, S. M. 2011. Sex Hormones Are Associated with Right Ventricular Structure and Function The MESA-Right Ventricle Study. *American Journal of Respiratory and Critical Care Medicine,* 183**,** 659-667.

Vonk-Noordegraaf, A. & Souza, R. 2012. Cardiac magnetic resonance imaging: what can it add to our knowledge of the right ventricle in pulmonary arterial hypertension? *Am J Cardiol,* 110**,** 25s-31s.

Weil, J., Eschenhagen, T., Hirt, S., Magnussen, O., Mittmann, C., Remmers, U. & Scholz, H. 1998. Preserved Frank-Starling mechanism in human end stage heart failure. *Cardiovascular Research,* 37**,** 541-548.

Wensel, R., Opitz, C. F., Anker, S. D., Winkler, J., Hoffken, G., Kleber, F. X., Sharma, R., Hummel, M., Hetzer, R. & Ewert, R. 2002. Assessment of survival in patients with primary pulmonary hypertension importance of cardiopulmonary exercise testing. *Circulation,* 106**,** 319-324.

Wharton, J., Strange, J. W., Møller, G. M., Growcott, E. J., Ren, X., Franklyn, A. P., Phillips, S. C. & Wilkins, M. R. 2005. Antiproliferative effects of phosphodiesterase type 5 inhibition in human pulmonary artery cells. *American journal of respiratory and critical care medicine,* 172.

Wood, P. 1958. The Eisenmenger syndrome or pulmonary hypertension with reversed central shunt. *British medical journal,* 2.

Xie, E., Yu, R., Ambale-Venkatesh, B., Bakhshi, H., Heckbert, S. R., Soliman, E. Z., Bluemke, D. A., Kawut, S. M., Wu, C. O., Nazarian, S. & Lima, J. A. C. 2020. Association of right atrial structure with incident atrial fibrillation: a longitudinal cohort cardiovascular magnetic resonance study from the Multi-Ethnic Study of Atherosclerosis (MESA). *Journal of Cardiovascular Magnetic Resonance,* 22.

Yuan, J. X., Aldinger, A. M., Juhaszova, M., Wang, J., Conte, J. V., Jr., Gaine, S. P., Orens, J. B. & Rubin, L. J. 1998. Dysfunctional voltage-gated K+ channels in pulmonary artery smooth muscle cells of patients with primary pulmonary hypertension. *Circulation,* 98**,** 1400-6.

Zanatta, E., Polito, P., Famoso, G., Larosa, M., Zorzi, E. D., Scarpieri, E., Cozzi, F. & Doria, A. 2019. Pulmonary arterial hypertension in connective tissue disorders: Pathophysiology and treatment. *Experimental biology and medicine,* 244.